Department of Physics and Astronomy

University of Heidelberg

Diploma thesis

in Physics

submitted by

Jennifer Schober

born in Miltenberg

- 2011 -

The Small-Scale Dynamo: Amplification of Magnetic Fields in the Early Universe

This diploma thesis has been carried out by Jennifer Schober

at the

Institut für Theoretische Astrophysik

under the supervision of

Prof. Dr. Ralf Klessen

To my parents.

Der kleinskalige Dynamo:
Verstärkung von Magnetfeldern im Frühen Universum

In dieser Arbeit untersuchen wir den kleinskaligen Dynamo - einen Mechanismus, durch den schwache magnetische Saatfelder rasch verstärkt werden können, indem turbulente kinetische Energie in magnetische Energie umgewandelt wird. Der kleinskalige Dynamo wird in einer Theorie von Kazantsev beschrieben, die empfindlich von der Art der Turbulenz abhängt. Wir schlagen ein Model für verschiedene Turbulenztypen vor und benutzen die Kazantsev-Theorie, um Eigenschaften des kleinskaligen Dynamos zu bestimmen. Mit unserem Model finden wir, dass die kritische magnetische Reynoldszahl, die für das Wirken des kleinskaligen Dynamos überschritten werden muss, zwischen 110 und 2700 liegt. Weiterhin leiten wir her, dass die Wachstumrate des kleinskaligen Magnetfeldes stark von der hydrodynamischen Reynoldszahl Re abhängt. Im Grenzfall unendlich großer magnetischer Prandtlzahlen skaliert die Wachstumrate Γ zwischen $\Gamma \propto Re^{1/2}$ und $\Gamma \propto Re^{1/3}$ für die unterschiedlichen Turbulenztypen. Für niedrigere magnetische Prandtlzahlen nimmt die Wachstumsrate des kleinskaligen Dynamos ab. Wir wenden unser Model auf Magnetfelder während der Entstehung der ersten Sterne an. Dafür schätzen wir mit Hilfe eines Ein-Zonen-Chemiecodes die typischen Eigenschaften des primordialen Gases ab. Das resultierende kleinskalige Magnetfeld erreicht nahezu instantan die Sättigung, weshalb wir erwarten, dass es während der primordialen Sternentstehung dynamisch wichtig ist.

The Small-Scale Dynamo:
Amplification of Magnetic Fields in the Early Universe

In this work we explore the small-scale dynamo - a mechanism which may rapidly amplify a week magnetic seed field by converting turbulent kinetic energy into magnetic energy. The small-scale dynamo is described by a theory of Kazantsev, which depends crucially on the nature of turbulence. We propose a model for different types of turbulence and use the Kazantsev theory to determine properties of the small-scale dynamo. With our model we find that the critical magnetic Reynolds number, which needs to be exceeded for small-scale dynamo action, lies between 110 and 2700. Furthermore, we show that the growth rate of the small-scale magnetic field depends strongly on the hydrodynamical Reynolds number Re. In the limit of infinite magnetic Prandtl numbers the growth rate Γ scales between $\Gamma \propto Re^{1/2}$ and $\Gamma \propto Re^{1/3}$ for different types of turbulence. For decreasing magnetic Prandtl number, the growth rate of the small-scale dynamo decreases. We apply our model to the magnetic fields in the formation of the first stars. For this we estimate the typical quantities of primordial gas by using a one-zone chemistry code. The resulting small-scale magnetic field reaches its saturation value almost instantly and thus we expect it to be dynamically important in primordial star formation.

Contents

1 Introduction

1.1 The Magnetised Universe

Magnetic fields are observed in the whole Universe [1]. Our own planet, the Earth, has, like other planets, a magnetic dipole field. The magnetic field strength on the surface is about 0.5 G [1] (1 G $\approx 10^{-4}$ T). This field holds as a protective shield for the life on Earth, as it keeps a large fraction of the dangerous cosmic radiation from arriving at the surface. The main part of this radiation comes from the Sun, which itself provides a magnetic field of up to 4000 G on the surface [2]. The field of the Sun goes through a cycle of twenty-two years. At its maximum, many sun spots, which are cooler spots on the surface caused by magnetic fluxes, can be observed. These fluxes can carry plasma and then appear at the rid of the Sun as enormous prominences. There also exist observations of magnetic fields of other stars. Magnetic fields lead to interesting effects especially at the beginning and the end of the life of a star. There is observational and theoretical evidence that protostars, i.e. stars were just born, often have jets induced by strong magnetic fields. These jets are outflows of material, which determine the "final" mass of the star. Stars with a mass between 1.46 $M_\odot$ and 3 $M_\odot$ end their lives as neutron stars. These objects are known to have extremely strong magnetic fields of about 10^{12} G. A special class of neutron stars, the magnetars, reach even field strength up to 10^{15} G [3]. On larger scales, observations show coherent magnetic fields of galaxies. The magnetic field of our Milky Way has a strength of roughly 6 μG in the solar neighborhood approximating equipartition of magnetic fields, cosmic rays and thermal energy. In the center of active galaxies strong magnetic fields can lead to the creation of galactical jets. For example in the active galaxy M 87 accretion onto the central supermassive black hole leads to a huge jet with a length of roughly 2 kpc [4] (1 pc $\approx 3.1 \times 10^{18}$ cm). These jets strongly influence the host galaxy and the intergalactic medium.
Our imaginary journey through the Universe has shown that magnetic fields play important roles in many astrophysical objects (see also Table 1.1). In this work we try to explain a possible origin of these magnetic fields.

Object	Magnetic Field Strength
Earth (surface) [1]	≈ 0.5 G
Jupiter (surface) [1]	≈ 10 G
Sun (strong sun spots) [2]	$\approx 4 \times 10^3$ G
white dwarf (if strongly magnetised) [1]	$\approx 10^7$ G
neutron star [3]	$\approx 10^{12}$ G
magnetar [3]	$\approx 10^{15}$ G
Milky Way (solar neighborhood) [5]	$\approx 6 \times 10^{-6}$ G
Milky Way (at 3 kpc radius) [5]	$\approx 10 \times 10^{-6}$ G

Table 1.1: Compilation of magnetic field strength in different astrophysical objects.

1.2 The Problem of the First Magnetic Fields

The origin of magnetic fields has been a mystery for a long time. Today there are different theories suggesting how weak magnetic seed fields have been generated. Most of theses generation mechanisms take place in the very early Universe, i.e. during inflation or certain phase transitions. But there are also astrophysical mechanisms, which can take place in the present-day Universe. For example the Biermann-battery produces magnetic fields in a plasma with a temperature gradient.
The remaining problem is that theses generation mechanisms only produce very weak magnetic field strengths. They are many orders of magnitude below the observed field strengths in stars and other astrophysical objects described above.
This contradiction between observations and theory is the main motivation for this work. We suggest that very week magnetic seed fields have been amplified exponentially by the small-scales dynamo. This is a process, by that kinetic energy from turbulence is converted into magnetic energy.
With an initially weak seed field this amplification process could have already worked in the early Universe during the formation of the first stars, because primordial halos were very turbulent [6]. Dynamically important magnetic fields would have influenced the primordial star formation strongly.

1.3 Outline of this Work

In order to describe the small-scale dynamo, we present the basics of ideal hydrodynamics in Chapter 2. We summarise the assumptions of this theory and derive the main equations, the continuity equation, the Navier-Stokes equation and the energy equation.
Chapter 3 is on turbulence. Although there is currently no theory that describes turbulence in all details, there are some models handling this topic. We introduce the concept of the hydrodynamical Reynolds number and the statistical theory developed by Taylor. In this chapter we also present our model for the correlation function of the turbulent velocity field, which depends on the different types of turbulence.
The next chapter, Chapter 4, is on electrodynamics. The basic equations for describing the electromagnetic field are the Maxwell equations. We present the Lorentz force, the force acting on charged particles in an electromagnetic field, and the energy conservation equation of this field. Furthermore, we show the equation that connects the electromagnetic field and matter, Ohms law.
In Chapter 5 hydrodynamics and electrodynamics are combined to the theory of magnetohydrodynamics (MHD). The equations of MHD are the same as for hydrodynamics with some additional terms and one additional equation, the induction equation. We also summarise the most important effects of non-ideal MHD.
Chapter 6 treats magnetic fields in the Universe. In the first section we present a selection of important observations of magnetic fields, in the present-day as well as in the high-redshifted Universe. In the second section we introduce theories describing the fundamental origin of these fields. There are many different generation scenarios postulated in the literature, but they typically result in very low magnetic field strengths. The observed field strengths cannot be explained by these theories alone. Thus, there need to be processes that amplify magnetic fields, which we list up and describe phenomenologically in the last section of this chapter.
Magnetohydrodynamical dynamos are one possibility to amplify the weak magnetic seed fields. The theory of dynamos is presented in Chapter 7. We give derivations for the main equations of the two different types of dynamos: the large-scale dynamo and the small-scale dynamo. The small-scale dynamo, on which we focus in this work, is described by the so-called Kazantsev theory.
In Chapter 8 we use our model for different types of turbulence to calculate properties of the small-scale dynamo. We use the quantum-mechanical WKB-approximation to solve the evolution equation of the small-scale dynamo, the Kazantsev equation. The validity of the WKB-approximation is tested in detail in the first section. In the next section we calculate the critical magnetic Reynolds number that needs to be exceeded for small-scale dynamo action. Furthermore, we determine the growth rate of the small-scale magnetic field. In the limit of large magnetic Prandtl numbers, which is the ratio of the magnetic to the hydrodynamic Reynolds number, an analytical solution can be found. We also give numerical results for large, but finite

magnetic Prandtl numbers.
We apply our results of the small-scale dynamo in Chapter 9 to primordial star formation. For that we estimate typical quantities in primordial gas using a one-zone chemical code. This way we can calculate the magnetic Reynolds number and check if it is larger than the critical value. We determine the growth rate of the small-scale magnetic field in primordial gas. Finally, we calculate the magnetic field strength as a function of the density.
We close our work with a summary of the main results and implications for primordial star formation.

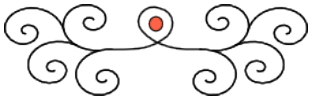

2 Basic Formalism of Hydrodynamics

2.1 Why do we use Hydrodynamics in Astrophysics?

It is not obvious that we can think of fluids in astrophysical problems. In our imagination a fluid is something dense like water, which has a particle density of 10^{22} cm^{-3} under standard conditions. In comparison to that, for example, the interstellar medium (ISM) has a density of only a few particles per cm^{-3}. Why can this be treated as a fluid?
The answer to this problem lies in the definition of a fluid. A fluid is an object build of many particle, which collide in a high frequency. In these collisions "information", i.e. momentum and energy, is exchanged and the fluid acts locally as a unit.
Now on a scale of a few cm, which is the typical extension a glass of water, the mean free path[1] of a water molecule is about 10^{-10} cm. Compared to the extension of the glass this is very short. The ratio between the length scale of the system "water glass" and the mean free path is extremely high. We find such a high ratio also in the ISM. Here the typical lengthscale is 1 pc = 10^{18} cm and the mean free path of the particles is 10^{13} cm. This implies that the particles interact highly frequently and we can treat the ISM as a fluid.

2.2 Describing Fluids

Hydrodynamics is the theory of fluid motions. To describe the dynamics of gases and fluids there are, in principle, two different ways: the Eulerian and the Lagrangian point of view.
In the Eulerian point of view, the time differentiation of a given quantity Q is taken with respect to a fixed point. We will denote Eulerian time derivations from now on with $\partial/\partial t$.
In the Lagrangian point of view, on the other hand, one takes the time differentiation associated with a certain fluid element, which is moving with the fluid velocity $\mathbf{v}$ (A bold letter represents a vector: $\mathbf{v} \equiv \vec{v}$.). The Lagrangian time differentiation,

[1] The mean free path is the typical way a particle travels between two collisions.

denoted by d/dt, is defined as

$$\begin{aligned}\frac{\mathrm{d}Q}{\mathrm{d}t} &= \lim_{\delta t\to 0}\frac{Q(\mathbf{x}+\mathbf{v}\delta t, t+\delta t)-Q(\mathbf{x},t)}{\delta t}\\ &\approx \lim_{\delta t\to 0}\frac{Q(\mathbf{x},t)+\delta t\frac{\partial Q}{\partial t}+\delta t\mathbf{v}\cdot\nabla Q-Q(\mathbf{x},t)}{\delta t}\\ &= \frac{\partial Q}{\partial t}+\mathbf{v}\cdot\nabla Q. \end{aligned} \tag{2.1}$$

In the second line we applied a first order Taylor expansion. Equation (2.1) connects the Lagrangian and the Eulerian point of view.

2.3 Derivation of the Equations of Hydrodynamics

Three differential equations build the mathematical framework of hydrodynamics. The *continuity equation* describes the time evolution of the density, the *Navier-Stokes equation* the evolution of the momentum and the *energy equation* governs the time evolution of the energy.
In this chapter we want to illustrate the derivation of these equations by using the Boltzmann equation and explain their meanings. For this purpose we mainly follow the book of Choudhuri [7].

2.3.1 The Boltzmann Equation

For a complete description of the state of a fluid, one has to predict the position and the velocity of every single fluid particle at every time. For a typical molecular cloud with about 10^{63} particles this is impossible. Thus, a statistical ansatz is necessary.
If our fluid consists of N particles we have to consider a (6+1)-dimensional coordinate space (3 coordinates for the position, 3 for the velocity vector and one for the time). In this space we can introduce a distribution function

$$f(\mathbf{x},\mathbf{u},t)\equiv\lim_{\delta V\to 0}\frac{\delta N}{\delta V}. \tag{2.2}$$

The volume in this limit needs to be small compared to the extension of the points in space, but still large enough to contain many particles.
If we now consider a fluid, in which the particles do not interact with each other, the time derivation of the distribution function in our (6+1)-dimensional space along any trajectory needs to vanish,

$$\begin{aligned}\frac{\mathrm{D}f}{\mathrm{D}t} &= 0\\ \Leftrightarrow \frac{\partial f}{\partial t}+\dot{\mathbf{x}}\cdot\nabla f+\dot{\mathbf{u}}\cdot\nabla_{\mathbf{u}} f &= 0, \end{aligned} \tag{2.3}$$

where

$$\nabla_{\mathbf{u}} \equiv \frac{\partial}{\partial u_{\mathrm{x}}}\mathbf{e}_{\mathrm{x}} + \frac{\partial}{\partial u_{\mathrm{y}}}\mathbf{e}_{\mathrm{y}} + \frac{\partial}{\partial u_{\mathrm{z}}}\mathbf{e}_{\mathrm{z}}. \tag{2.4}$$

Equation (2.3) tells us how the distribution function evolves in time. As we call a fluid without particle interaction collisionless, equation (2.3) is called the *collisionless Boltzmann equation.*

Now let us go one step further and consider the more realistic case of a fluid, in which the particles interact with each other. Due to collisions particles can change their velocities. This means that a particle, which has a velocity $\mathbf{u}$ before a collision, can change its velocity leading to a decrease of the distribution function $f(\mathbf{x}, \mathbf{u}, t)$. On the other hand, a particle with an initially different velocity can be changed $\mathbf{u}$ due to a collision, which increases $f(\mathbf{x}, \mathbf{u}, t)$. So the general form of the evolution of $f(\mathbf{x}, \mathbf{u}, t)$ is

$$\frac{\mathrm{D}f}{\mathrm{D}t}\mathrm{d}x^3\mathrm{d}u^3 = C_{\mathrm{in}} - C_{\mathrm{out}}, \tag{2.5}$$

where C_{in} and C_{out} describe the amount of particles changing their velocity to and from $\mathbf{u}$.

This two quantities can be determined for example for a dilute gas, in which only binary collisions take place. Choudhuri [7] finds for this special case

$$C_{\mathrm{in}} = \mathrm{d}x^3\mathrm{d}u^3 \int \mathrm{d}\tilde{u}^3 \int \mathrm{d}\Omega\sigma(\mathbf{u}, \tilde{\mathbf{u}}|\mathbf{u}', \tilde{\mathbf{u}}')\,|\mathbf{u} - \tilde{\mathbf{u}}|\, f(\mathbf{x}, \mathbf{u}', t) f(\mathbf{x}, \tilde{\mathbf{u}}', t), \tag{2.6}$$

$$C_{\mathrm{out}} = \mathrm{d}x^3\mathrm{d}u^3 \int \mathrm{d}\tilde{u}^3 \int \mathrm{d}\Omega\sigma(\mathbf{u}, \tilde{\mathbf{u}}|\mathbf{u}', \tilde{\mathbf{u}}')\,|\mathbf{u} - \tilde{\mathbf{u}}|\, f(\mathbf{x}, \mathbf{u}, t) f(\mathbf{x}, \tilde{\mathbf{u}}, t). \tag{2.7}$$

In the above expressions $\mathbf{u}$ and $\tilde{\mathbf{u}}$ are the velocities of the two particles before the collision, $\mathbf{u}'$ and $\tilde{\mathbf{u}}'$ afterwards, Ω is the scattering angle and $\sigma(\mathbf{u}, \tilde{\mathbf{u}}|\mathbf{u}', \tilde{\mathbf{u}})$ the cross section for the collision. The full *Boltzmann equation* follows as

$$\begin{aligned} \frac{\partial f}{\partial t} + \dot{\mathbf{x}} \cdot \nabla f + \dot{\mathbf{u}} \cdot \nabla_{\mathbf{u}} f \;\; = \;\; & \int \mathrm{d}\tilde{u}^3 \int \mathrm{d}\Omega\sigma(\Omega)\,|\mathbf{u} - \tilde{\mathbf{u}}| \cdot \\ & \left(f(\mathbf{x}, \mathbf{u}', t) f(\mathbf{x}, \tilde{\mathbf{u}}', t) - f(\mathbf{x}, \mathbf{u}, t) f(\mathbf{x}, \tilde{\mathbf{u}}, t)\right). \end{aligned} \tag{2.8}$$

This equation tells us how the distribution function of the gas changes in time.

2.3.2 The Moment Equations

Now let us consider a quantity χ that is conserved in a binary collision, i.e.

$$\chi + \tilde{\chi} = \chi' + \tilde{\chi}', \tag{2.9}$$

where the $'$ denotes a later time. If we multiply the Boltzmann equation with this quantity χ and integrate over d^3u we have

$$\begin{aligned} \int \mathrm{d}^3u \chi \frac{\mathrm{D}f}{\mathrm{D}t} \;\; = \;\; & \int \mathrm{d}^3u \int \mathrm{d}^3\tilde{u} \int \mathrm{d}\Omega\sigma(\Omega)|\mathbf{u} - \tilde{\mathbf{u}}| \cdot \\ & \left(f(\mathbf{x}, \mathbf{u}', t) f(\mathbf{x}, \tilde{\mathbf{u}}', t) - f(\mathbf{x}, \mathbf{u}, t) f(\mathbf{x}, \tilde{\mathbf{u}}, t)\right) \chi. \end{aligned} \tag{2.10}$$

One can show that the right hand side equals zero [7]. Thus, we are left with

$$\int \mathrm{d}^3u\chi \left(\frac{\partial f}{\partial t} + u_\mathrm{i} \frac{\partial f}{\partial x_\mathrm{i}} + \frac{F_\mathrm{i}}{m} \frac{\partial f}{\partial u_\mathrm{i}} \right) = 0, \tag{2.11}$$

where we have used equation (2.3) and the relations $\dot{\mathbf{x}} = \mathbf{u}$ and $\dot{\mathbf{u}} = \mathbf{F}/m$ with $\mathbf{F}$ being the acting force and the mass of the particle m. We can rewrite this as

$$\frac{\partial}{\partial t} \int \mathrm{d}^3u\chi f + \frac{\partial}{\partial x_\mathrm{i}} \int \mathrm{d}^3u\chi u_\mathrm{i} f - \int \mathrm{d}^3u u_\mathrm{i} f \frac{\partial \chi}{\partial x_\mathrm{i}} - \frac{1}{m} \int \mathrm{d}^3u \frac{\partial \chi}{\partial u_\mathrm{i}} F_\mathrm{i} f \\ - \frac{1}{m} \int \mathrm{d}^3u\chi \frac{\partial F_\mathrm{i}}{\partial u_\mathrm{i}} f = 0. \tag{2.12}$$

This equation simplifies, if we introduce the definition of the average. Given a quantity Q we define its average $\langle Q \rangle$ by

$$\langle Q \rangle \equiv \frac{1}{n} \int \mathrm{d}^3u Q f, \tag{2.13}$$

where the number density per unit volume is

$$n \equiv \int \mathrm{d}^3u f. \tag{2.14}$$

Using this definition we can modify equation (2.12) and end up with

$$\boxed{\frac{\partial}{\partial t} \left(n \langle \chi \rangle \right) + \frac{\partial}{\partial x_\mathrm{i}} \left(n \langle u_\mathrm{i} \chi \rangle \right) - n \left\langle u_\mathrm{i} \frac{\partial \chi}{\partial x_\mathrm{i}} \right\rangle - \frac{n}{m} \left\langle F_\mathrm{i} \frac{\partial \chi}{\partial u_\mathrm{i}} \right\rangle - \frac{n}{m} \left\langle \frac{\partial F_\mathrm{i}}{\partial u_\mathrm{i}} \chi \right\rangle = 0}. \tag{2.15}$$

This is the so-called *conservation equation*, which tells us how the volume density $n \langle \chi \rangle$ of a conserved quantity χ changes in time. This equation is of crucial importance for hydrodynamics. We will see that evaluating it for the conserved quantities in a fluid, the mass, the momentum and the energy, will give us the three central equations of hydrodynamics.
Now let us start with substituting the particle mass m, which is conserved in a binary collision, into the conservation equation (2.15). The value of the mass does not depend on the position of the particle nor its velocity (in the non-relativistic limit at least). If we additionally consider the force $\mathbf{F}$ to be independent of velocity, we end up with

$$\frac{\partial}{\partial t} \left(nm \right) + \frac{\partial}{\partial x_\mathrm{i}} \left(nm \langle u_\mathrm{i} \rangle \right) = 0. \tag{2.16}$$

We used that $\langle m \rangle = m$, as we consider for simplicity a fluid made of particles having all the same mass. By introducing the mass density

$$\rho \equiv nm \tag{2.17}$$

and the average velocity

$$\mathbf{v} \equiv \langle \mathbf{u} \rangle \tag{2.18}$$

we obtain for equation (2.16)

$$\begin{aligned} \frac{\partial \rho}{\partial t} + \frac{\partial}{\partial x_\mathrm{i}} (\rho v_\mathrm{i}) &= 0 \\ \Rightarrow \frac{\partial \rho}{\partial t} + \nabla (\rho \mathbf{v}) &= 0. \end{aligned} \tag{2.19}$$

This is the first moment of the Boltzmann equation and also known as the *continuity equation*.
For deriving the second moment equation we substitute χ in (2.15) by a momentum mu_j. This leads to

$$\begin{aligned} \frac{\partial}{\partial t} (nm \langle u_\mathrm{j} \rangle) + \frac{\partial}{\partial x_\mathrm{i}} (nm \langle u_\mathrm{i} u_\mathrm{j} \rangle) - n \langle F_\mathrm{i} \delta_\mathrm{ij} \rangle &= 0 \\ \Rightarrow \frac{\partial}{\partial t} (\rho v_\mathrm{j}) + \frac{\partial}{\partial x_\mathrm{i}} (\rho \langle u_\mathrm{i} u_\mathrm{j} \rangle) - \frac{\rho}{m} F_\mathrm{j} &= 0. \end{aligned} \tag{2.20}$$

We can simplify this further by defining a tensor

$$\begin{aligned} P_\mathrm{ij} &\equiv nm \langle (u_\mathrm{i} - v_\mathrm{i})(u_\mathrm{j} - v_\mathrm{j}) \rangle \\ &= nm (\langle u_\mathrm{i} u_\mathrm{j} \rangle - v_\mathrm{i} v_\mathrm{j}) . \end{aligned} \tag{2.21}$$

With P_ij we can put equation (2.20) into the form

$$\frac{\partial}{\partial t} (\rho v_\mathrm{j}) + \frac{\partial}{\partial x_\mathrm{i}} (\rho v_\mathrm{i} v_\mathrm{j}) = \frac{\rho}{m} F_\mathrm{j} - \frac{\partial P_\mathrm{ij}}{\partial x_\mathrm{i}}. \tag{2.22}$$

Using the continuity equation (2.19) we can simplify the left hand side and get

$$\rho \left(\frac{\partial v_\mathrm{j}}{\partial t} + v_\mathrm{i} \frac{\partial v_\mathrm{j}}{\partial x_\mathrm{i}} \right) = \frac{\rho}{m} F_\mathrm{j} - \frac{\partial P_\mathrm{ij}}{\partial x_\mathrm{i}}. \tag{2.23}$$

At last we calculate the third moment of the conservation equation. We assume that the translational kinetic energy $1/2m|\mathbf{u} - \mathbf{v}|^2$ is a conserved quantity in a monoatomic gas. Substituting this quantity into the conservation equation (2.15), we get

$$\frac{\partial}{\partial t} (\rho \epsilon) + \frac{\partial}{\partial x_\mathrm{i}} (\rho \epsilon v_\mathrm{i}) + \frac{\partial q_\mathrm{i}}{\partial x_\mathrm{i}} + P_\mathrm{ij} \Lambda_\mathrm{ij} = 0, \tag{2.24}$$

with the internal energy per unit mass

$$\epsilon = \frac{1}{2} \left\langle |\mathbf{u} - \mathbf{v}|^2 \right\rangle , \tag{2.25}$$

the energy flux

$$\epsilon = \frac{1}{2}\rho \left\langle (\mathbf{u}-\mathbf{v}) \left|\mathbf{u}+\mathbf{v}\right|^2 \right\rangle, \tag{2.26}$$

and

$$\Lambda_{\mathrm{ij}} = \frac{1}{2}\left(\frac{\partial v_{\mathrm{i}}}{\partial x_{\mathrm{j}}} - \frac{\partial v_{\mathrm{j}}}{\partial x_{\mathrm{i}}}\right). \tag{2.27}$$

We can simplify this by using of the continuity equation and end up with

$$\rho\left(\frac{\partial \epsilon}{\partial t} + v_{\mathrm{i}}\frac{\partial \epsilon}{\partial x_{\mathrm{i}}}\right) + \frac{\partial q_{\mathrm{i}}}{\partial x_{\mathrm{i}}} + P_{\mathrm{ij}}\Lambda_{\mathrm{ij}} = 0. \tag{2.28}$$

The moment equations describe the evolution of the conserved quantities in a fluid. However, the equations (2.20), (2.23) and (2.28) are not a dynamical theory, because we have, in total, 5 individual equations including 14 variables.

2.3.3 The Equations of Hydrodynamics

In the last section we derived the three momentum equations by inserting the conserved quantities of an idealised fluid into the Boltzmann equation. If we want to develop to a full dynamical theory, we have to reduce the number of free variables. We will see that this can be done, when we assume a system that is fluid-like, i.e. has many collisions between the particles. A system with many collisions is in zero-order approximation Maxwell-Boltzmann distributed with

$$f(\mathbf{x},\mathbf{u},t) = n(\mathbf{x},t)\left(\frac{m}{2\pi kT(\mathbf{x},t)}\right)^{3/2} \exp\left(-\frac{m\left(\mathbf{u}-\mathbf{v}(\mathbf{x},t)\right)^2}{2kT(\mathbf{x},t)}\right). \tag{2.29}$$

With this distribution function we can calculate the quantities P_{ij}, $\mathbf{q}$, ϵ and $P_{\mathrm{ij}}\Lambda_{\mathrm{ij}}$. We find after some algebra

$$\begin{aligned} P_{\mathrm{ij}} &= p\delta_{\mathrm{ij}}, && (2.30)\\ \mathbf{q} &= 0, && (2.31)\\ \epsilon &= \frac{3}{2}\frac{kT}{m}, && (2.32)\\ P_{\mathrm{ij}}\Lambda_{\mathrm{ij}} &= p\nabla\cdot\mathbf{v}, && (2.33) \end{aligned}$$

with

$$p = nkT. \tag{2.34}$$

If we put this expressions into the momentum equations from the last section, we end up with the hydrodynamic equations. We present the results in the next paragraphs, where we also add additional terms, which come from transport phenomena, that we have not discussed here (see [7]).

Continuity Equation

The first conserved quantity we considered in the last section was the mass. We ended up with the so-called continuity equation

$$\boxed{\frac{\partial \rho}{\partial t} + \nabla \cdot (\rho \mathbf{v}) = 0}. \tag{2.35}$$

This equation describes how the mass or better the density is conserved in a fluid. If the density changes in a fluid element in time, there needs to be a flux $\rho\mathbf{v}$ through the surface of this fluid element such that no mass gets lost. This argument becomes clear by looking at the integral form of the continuity equation,

$$\frac{\partial}{\partial t} \int_{\mathrm{V}} \rho \mathrm{d}V = - \int_{\mathrm{V}} \nabla \cdot (\rho \mathbf{v}) \mathrm{d}V = - \int_{\partial \mathrm{V}} \rho \mathbf{v} \mathrm{d}\mathbf{f}, \tag{2.36}$$

where we used Gauss' theorem in the last transformation. The left-hand side of the equation above is the change of the mass $\int \rho \mathrm{d}V$ and the right-hand side the material flux through the surface of the fluid element.
An important special case are fluids of constant density in time. For these holds in general

$$\nabla \cdot (\rho \mathbf{v}) = 0. \tag{2.37}$$

If the density is also constant in space, we have

$$\nabla \cdot \mathbf{v} = 0. \tag{2.38}$$

We speak of an incompressible fluid in this case.

Navier-Stokes Equation

The Navier-Stokes equation, which follows from further modifications of the conservation of momentum (2.23), reads

$$\boxed{\rho \left(\frac{\partial \mathbf{v}}{\partial t} + (\mathbf{v} \cdot \nabla) \mathbf{v} \right) = -\nabla p + n\mathbf{F} + \mu \left(\nabla^2 \mathbf{v} + \frac{1}{3} \nabla \left(\nabla \cdot \mathbf{v} \right) \right)}. \tag{2.39}$$

Here μ is the dynamical viscosity. Also common is the kinetic viscosity, which is defined as $\nu \equiv \mu / \rho$. The Navier-Stokes equation describes the conservation of momentum in a fluid, i.e. it is an equation of motion. All appearing forces are collected on the right-hand side of (2.39). The first term on the right hand-side is the pressure force, the second term represents the external forces like gravity or the Coriolis force and the last term represents forces caused by viscosity, which is the inner friction of the fluid.
For the special case of an incompressible fluid, the term including $\nabla \cdot \mathbf{v}$ vanishes.

The Navier-Stokes equation simplifies in the special case of negligible viscosity ($\mu = 0$). It then reduces to the Euler equation

$$\frac{\partial \mathbf{v}}{\partial t} + (\mathbf{v} \cdot \nabla)\mathbf{v} = -\frac{1}{\rho}\nabla p + \frac{1}{m}\mathbf{F}. \tag{2.40}$$

This equation is much easier to solve than (2.39), as it does not contain derivatives of high order any more and thus requires less boundary conditions.

Energy Equation

The conservation of energy gives us the last hydrodynamical equation. Modification of equation (2.28) results in an equation for the energy density ϵ

$$\boxed{\rho\left(\frac{\partial \epsilon}{\partial t} + (\mathbf{v} \cdot \nabla)\,\epsilon\right) = \nabla \cdot (K \nabla T) - p \nabla \cdot \mathbf{v}}, \tag{2.41}$$

where K is the coefficient of thermal conductivity.

Equation of State

To close our system of equations we need one additional equation, the equation of state. The equation of state relates the pressure p to another variable of state, for example the temperature T.

$$\boxed{p = p(T)} \tag{2.42}$$

For an ideal gas the equation of state is the ideal gas law

$$p = nkT, \tag{2.43}$$

with the Boltzmann constant k.

The hydrodynamic equations, the continuity equation (2.35), the Navier-Stokes equation (2.39) and the energy equation (2.41), together with the equation of state (2.42) form a full dynamical theory. They contain 6 variables, the density ρ, the velocity $\mathbf{v}$ with three components, the pressure p and the internal energy ϵ. But two of these variables are related due to the equation of state, which leaves us with 5 independent variables. Those variables are determined by the 5 hydrodynamical equations.

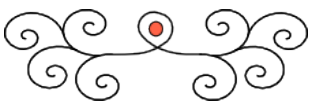

3 Turbulence

"*When I meet God, I am going to ask him two questions: Why relativity? And why turbulence? I really believe he will have an answer for the first.*"
(This quotation is accredited to Werner Heisenberg.[1])

3.1 Describing Turbulence

Chaotic motion is called turbulence. The description of chaos has alway been a problem and there is, until today, no complete theoretical description of that topic. Thus, turbulence is one of the last major mysteries in classical physics. In this section we give the common approaches of handling turbulence.

3.1.1 Concept of the Reynolds Number

The appearance of turbulence in a flow depends crucially on properties like the flow velocity, the geometry and its chemical composition. The latter determines the viscosity ν. Fluids with high viscosity, like for example honey, are only turbulent when the velocity is very high. Fluids with vanishing viscosity can become turbulent easily.
In order to find a dimensionless quantity that tells if a flow is turbulent or not, we have to make the Navier-Stokes equation (2.39) dimensionless. The curl of the Navier-Stokes equation is

$$\frac{\partial \omega}{\partial t} = \nabla \times (\mathbf{v} \times \omega) + \nu \nabla^2 \omega, \tag{3.1}$$

where $\omega \equiv \nabla \times v$ is called *vorticity*. The term with the conservative force $\mathbf{F}$ in (2.39) vanishes. Also the term with the pressure gradient vanishes in the case of incompressible fluids.
The upper equation becomes dimensionless, if we express all quantities through the typical length L, time T and velocity V of the system. Hence we substitute $\mathbf{x} = L\,\tilde{\mathbf{x}}$, $\mathbf{v} = V\,\tilde{\mathbf{v}}$, $\mathbf{t} = T\,\tilde{\mathbf{t}}$, $\omega = V/L\,\tilde{\omega}$ and $\nabla = 1/L\,\tilde{\nabla}$ into (3.1) and get

$$\frac{\partial \tilde{\omega}}{\partial \tilde{t}} = \tilde{\nabla} \times (\tilde{\mathbf{v}} \times \tilde{\omega}) + \frac{\nu}{VL} \tilde{\nabla}^2 \tilde{\omega}. \tag{3.2}$$

The prefactor of the last term is labeled

$$\boxed{\frac{\nu}{VL} \equiv \frac{1}{Re}}, \tag{3.3}$$

[1] http://scienceworld.wolfram.com/biography/Heisenberg.html, 11/9/2011

with the *hydrodynamical Reynolds number Re*. If *Re* is high the viscosity is low and the first term on the RHS of (3.2) overwhelms. This term creates vorticity and the flow is very turbulent. A flow with Reynolds number higher than about one thousand is referred to be turbulent. For smaller *Re* the second term of (3.2) is the important one. As this term is the dissipation term, the vorticity is dissipated. The flow is then called *laminar*.

3.1.2 Statistical Description by Taylor

A statistical description of turbulence starts with decomposing the velocity field $\mathbf{v}$ in a mean field $\langle \mathbf{v} \rangle$ and a turbulent component $\delta\mathbf{v}$:

$$\mathbf{v} = \langle \mathbf{v} \rangle + \delta\mathbf{v}. \tag{3.4}$$

Following the work of Taylor [8] we model the spatial appearance of turbulence via the two-point correlation function. The correlation of two turbulent velocity components at the positions $\mathbf{r}_1$ and $\mathbf{r}_2$ at the times t and s for a Gaussian random velocity field with zero mean, which is isotropic, homogeneous and δ-correlated in time, is given as

$$\boxed{\langle \delta v_i(\mathbf{r}_1, t) \delta v_j(\mathbf{r}_2, s) \rangle = T_{ij}(r)\delta(t-s)}. \tag{3.5}$$

$T_{ij}(r)$ is the two-point correlation function with $r \equiv |\mathbf{r}_1 - \mathbf{r}_2|$. It was shown by Bachelor [9] that the correlation function can be divided into a transversal part T_N and a longitudinal part T_L,

$$\boxed{T_{ij}(r) = \left(\delta_{ij} - \frac{r_i r_j}{r^2}\right) T_\mathrm{N}(r) + \frac{r_i r_j}{r^2} T_\mathrm{L}(r) + C(r)\epsilon_{\mathrm{ijk}} r^\mathrm{k}}. \tag{3.6}$$

The last term including $C(r)$, refers to the effect of helicity.
In the special case of a divergence-free turbulent velocity field (div $\delta\mathbf{v} = 0$), characteristic of incompressible fluids, one can easily show that

$$\frac{\partial}{\partial x_\mathrm{i}} T_{ij}(r) = 0. \tag{3.7}$$

From this it follows that

$$\frac{\partial}{\partial x_\mathrm{i}} \left(r_\mathrm{i} r_\mathrm{j} T_{ij}(r)\right) = T_{ij}(r) \frac{\partial}{\partial x_\mathrm{i}} \left(r_\mathrm{i} r_\mathrm{j}\right) \tag{3.8}$$

and hence the transversal correlation function is connected to the longitudinal one via

$$T_\mathrm{N}(r) = \frac{1}{2r} \frac{\mathrm{d}}{\mathrm{d}r} \left(r^2 T_\mathrm{L}(r)\right). \tag{3.9}$$

For the other extreme case, an irrotational turbulent velocity field (rot $\delta\mathbf{v} = 0$), as expected for purely shock-dominated flows, we find in a similar way as above the relation

$$T_\mathrm{L}(r) = r \frac{\mathrm{d}T_\mathrm{N}(r)}{\mathrm{d}r} + T_\mathrm{N}(r). \tag{3.10}$$

3.2 Turbulence Picture of Kolmogorov

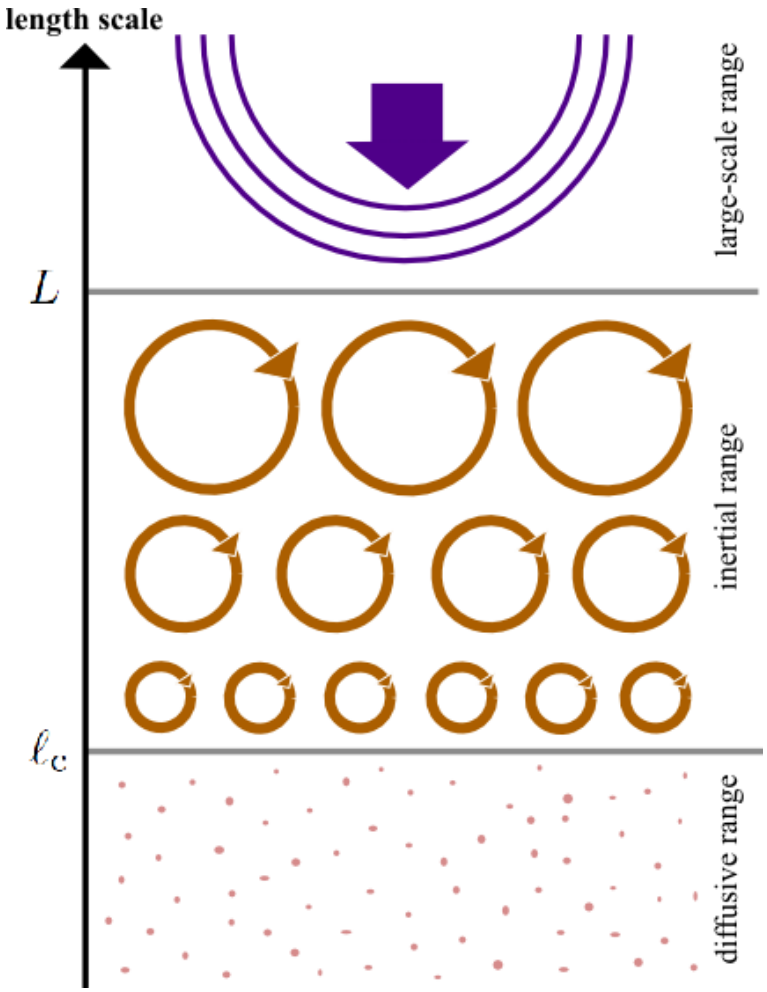

Figure 3.1: The different scales of turbulence in the picture of Kolmogorov.

Kolmogorov [10] described in 1941 the very different behavior of turbulence on different scales (see Figure 3.1) by dimensional analysis. Below a scale L turbulent eddies of a maximal length L appear. These cascade into smaller and smaller eddies. Kolmogorov assumed that the kinetic energy flux stays constant during this process. By this *kinetic energy cascade* the kinetic energy is transported onto smaller and smaller scales. The range, where this eddy decay takes place is called the *inertial range*. The decay of eddies ends at the so-called *cut-off scale* ℓ_c, where the Reynolds number becomes unity. Here the fluid is, per definition, not turbulent any more and microscopic diffusion gets important. Below ℓ_c the kinetic energy is converted into heat.
The assumption of a constant kinetic energy flux $\dot{E}_{kin}$ in the inertial range of the

turbulence leads to

$$\begin{aligned} E_{\text{kin}} &\propto v^2 \\ \Rightarrow \dot{E_{\text{kin}}} &\propto 2v\dot{v} \propto \frac{v^2}{t} = \frac{v^2 v}{\ell} \equiv const \\ \Rightarrow v &\propto \ell^{1/3}, \end{aligned} \tag{3.11}$$

where E_{kin} is the kinetic energy, v is the velocity, t the time and ℓ the length. The $\dot{}$ denotes the time derivation. Thus, Kolmogorov turbulence is characterised in the inertial range via the relation between the length of the a turbulent fluctuation ℓ and the velocity v on that scale.
With this we can calculate the Reynolds number on the cut-off scale of turbulence.

$$Re(\ell_{\text{c}}) = \frac{v_{\text{c}}\ell_{\text{c}}}{\nu} = \frac{VL}{\nu}\frac{v_{\text{c}}\ell_{\text{c}}}{VL} = Re\frac{v_{\text{c}}\ell_{\text{c}}}{VL} = Re\frac{\ell_{\text{c}}^{4/3}}{L^{4/3}}, \tag{3.12}$$

where we have defined $Re \equiv Re(L)$ and in the last step used $v_{\text{c}} \propto \ell_{\text{c}}^{1/3}$ and $V \propto L^{1/3}$. However, the cut-off scale is defined as the scale below that there is no turbulence and so the Reynolds number at this scale is just one. This leads to

$$\begin{aligned} Re(\ell_{\text{c}}) &= 1 \\ \Rightarrow Re\frac{\ell_{\text{c}}^{4/3}}{L^{4/3}} &= 1 \\ \Leftrightarrow \ell_{\text{c}} &= LRe^{-3/4}. \end{aligned} \tag{3.13}$$

3.3 Burgers-Turbulence

The counterpart to the incompressible turbulence of Kolmogorov is the extremely compressible turbulence. The latter is very important in the astrophysical context. Here we often find high Mach numbers[2], which means that astrophysical gases are highly compressible. In cold molecular clouds the Mach number can be around 50 [11].
In 1948 Burgers described this extreme case by assuming that the momentum flux in the inertial range is constant [12]. This leads to

$$\begin{aligned} p &\propto v \\ \Rightarrow \dot{p} &\propto \dot{v} \propto \frac{v}{t} = \frac{v^2}{\ell} \equiv const \\ \Rightarrow v &\propto \ell^{1/2}, \end{aligned} \tag{3.14}$$

where p is the momentum.
The cut-off scale in Burgers turbulence is

$$\ell_{\text{c}} = LRe^{-2/3}. \tag{3.15}$$

[2]The Mach number is defined by the ratio of the velocity and the sound speed in the medium.

3.4 Model for a General Type of Turbulence

We analyse the case of general turbulence types, i.e. turbulence with arbitrary compressibility. We can describe them with the relation between the velocity $v(\ell)$ and the size ℓ of a turbulent fluctuation,

$$\boxed{v(\ell) \propto \ell^{\vartheta}}. \tag{3.16}$$

The power-law index ϑ varies for the different types. It has its minimum value of $\vartheta = 1/3$ for Kolmogorov theory [10], i.e. incompressible turbulence. For Burgers turbulence [12], i.e. highly compressible turbulence, ϑ has its maximum value of $1/2$ [13]. With this relation we can determine the cut-off scale of the turbulence for a general exponent ϑ.

$$\begin{aligned} Re(\ell_\mathrm{c}) &= \frac{v_\mathrm{c}\ell_\mathrm{c}}{\nu} = \frac{VL}{\nu}\frac{v_\mathrm{c}\ell_\mathrm{c}}{VL} = Re\frac{v_\mathrm{c}\ell_\mathrm{c}}{VL} = Re\frac{\ell_\mathrm{c}^{\vartheta+1}}{L^{\vartheta+1}} \equiv 1 \\ \Rightarrow \ell_\mathrm{c} &= LRe^{-1/(1+\vartheta)}. \end{aligned} \tag{3.17}$$

With relation (3.16) we are able to model the correlation function of the turbulent velocity field, which provides of statistical description of turbulence. The correlation tensor T_ij has per definition the same unit as a diffusion coefficient. Thus, modeling this tensor starts with the ansatz $T_\mathrm{ij} \propto v\ell$, which is in the inertial range $T_\mathrm{ij} \propto \ell^{1+\vartheta}$. At first we construct a model for the longitudinal correlation function of the turbulent velocity field $T_\mathrm{L}(r)$. We assume the correlation function in the inertial range to be [14, 15]

$$T_\mathrm{L}(r) = \frac{VL}{3}\left(1 - (r/L)^{\vartheta+1}\right). \tag{3.18}$$

The prefactor, VL, fixes the unit, which should be the same as for a diffusivity. V and L are the velocity and the length scale of the largest eddies. On the diffusive scale the correlation function should be steadily continued and satisfy the condition that its derivative $T_\mathrm{L}'(0)$ vanishes at $r = 0$. This is accomplished for example for $T_\mathrm{L} \propto r^2$. The exact form of T_L in the diffusive range does not effect the results crucially [15]. Furthermore, we expect no correlation on scales larger than the largest eddies, thus T_L should vanish there.
Taken all together, we can set up a general turbulence model for the longitudinal correlation function on the different length scales as follows

$$\boxed{T_\mathrm{L}(r) = \begin{cases} \frac{VL}{3}\left(1 - Re^{(1-\vartheta)/(1+\vartheta)}\left(\frac{r}{L}\right)^2\right) & 0 < r < \ell_\mathrm{c} \\ \frac{VL}{3}\left(1 - \left(\frac{r}{L}\right)^{\vartheta+1}\right) & \ell_\mathrm{c} < r < L \\ 0 & L < r, \end{cases}} \tag{3.19}$$

where $\ell_\mathrm{c} = L\ Re^{-1/(\vartheta+1)}$ denotes the cut-off scale of the turbulence and L the length of the largest eddies. The hydrodynamic Reynolds number Re is defined as VL/ν

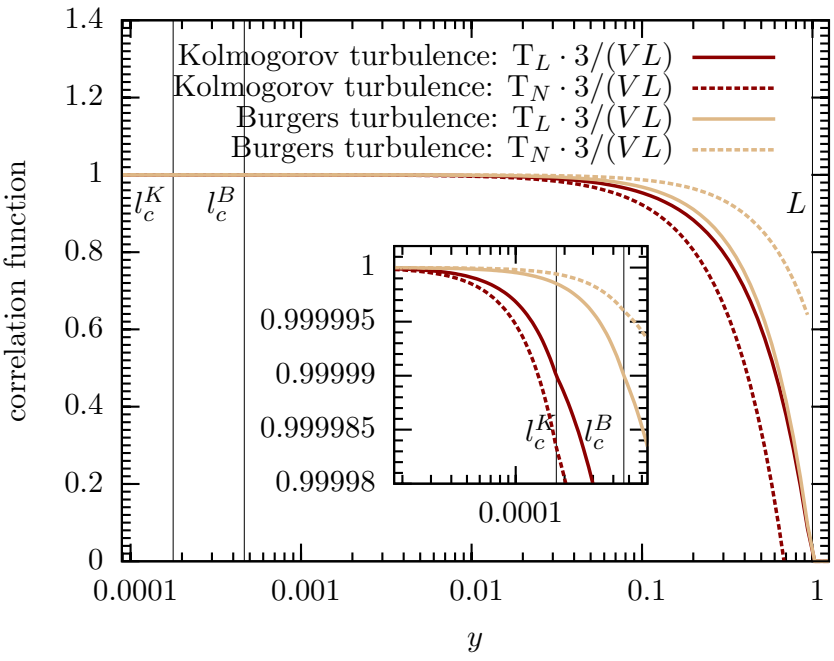

Figure 3.2: The longitudinal and transversal correlation function, T_L and T_N, depending on the dimensionless parameter $y \equiv r/L$ for Kolmogorov ($\vartheta = 1/3$) and Burgers turbulence ($\vartheta = 1/2$). We choose a fixed Reynolds number of 10^5. The vertical lines indicate the cut-off scale of the turbulence ℓ_c and the largest scale of the eddies L. Notice that the cut-off scale for Kolmogorov turbulence ($\ell_\mathrm{c}^\mathrm{K} = Re^{-3/4}L$) is different from the one for Burgers turbulence ($\ell_\mathrm{c}^\mathrm{B} = Re^{-2/3}L$). In the middle one can see a zoom of the dissipative range.

with the typical velocity of the largest eddies V and the viscosity of the gas ν.

The transversal correlation functions T_N for a divergence-free, i.e. Kolmogorov turbulence, and for an irrotational turbulent velocity field, i.e. Burgers turbulence, can be derived from the relations (3.9) and (3.10). Note, however, that a turbulent velocity field that is divergence free (or irrotational) in the initial range does not have to be this in the diffusive range. We find for the extreme cases in the inertial range ($\ell_\mathrm{c} < r < L$)

$$T_\mathrm{N}^\mathrm{K}(r) = \frac{VL}{3}\left(1 - \frac{5}{3}\left(\frac{r}{L}\right)^{4/3}\right), \tag{3.20}$$

$$T_\mathrm{N}^\mathrm{B}(r) = \frac{VL}{3}\left(1 - \frac{2}{5}\left(\frac{r}{L}\right)^{3/2}\right). \tag{3.21}$$

In order to find a general expression for T_N we make the ansatz

$$T_\mathrm{N}(r) = \frac{VL}{3}\left(1 - t(\vartheta)\left(\frac{r}{L}\right)^{\vartheta+1}\right) \tag{3.22}$$

where we assume a linear interpolation between $T_{\mathrm{N}}^{\mathrm{K}}$ and $T_{\mathrm{N}}^{\mathrm{B}}$ with $t(\vartheta) = a - b\vartheta$. With equations (3.20) and (3.21) we find that $a = 21/5$ and $b = 38/5$. Furthermore, we find the small-scale transversal correlation, i.e. $0 < r < \ell_{\mathrm{c}}$, by steady continuation. So we end up with the following model for the transversal correlation function for a general slope of the turbulent velocity spectrum:

$$\boxed{T_{\mathrm{N}}(r) = \begin{cases} \frac{VL}{3}\left(1 - t(\vartheta) Re^{(1-\vartheta)/(1+\vartheta)} \left(\frac{r}{L}\right)^2\right) & 0 < r < \ell_{\mathrm{c}} \\ \frac{VL}{3}\left(1 - t(\vartheta) \left(\frac{r}{L}\right)^{\vartheta+1}\right) & \ell_{\mathrm{c}} < r < L \\ 0 & L < r, \end{cases}} \tag{3.23}$$

with $t(\vartheta) = (21 - 38\vartheta)/5$.
The longitudinal and transversal correlation functions depend on the dimensionless parameter $y \equiv r/L$ as shown in Figure 3.2 for Kolmogorov and Burgers turbulence. We choose here a fixed hydrodynamical Reynolds number of 10^5. In Figure 3.2 we also show a zoom into the dissipative range ($0 < r < \ell_{\mathrm{c}}$).

3.5 Turbulence in Astrophysics

Turbulence is a ubiquitous phenomenon in the Universe. For example the outer layers of the Sun are turbulent. In stars regions with large temperature gradients become unstable and, thus, turbulent. We then speak of convection. Hot blobs of gas rise up until they give their thermal energy to the environment. Then the cool blobs sink again, because they have a larger density. This behavior is described in the "mixing length theory" (see for example [16]). Fortunately, the stellar structure seems not to depend on the details of turbulence.
Observations show that spectra of giant molecular clouds in the Milky Way and nearby galaxies have significant non-thermal line widths [17]. This is a signature of supersonic, i.e. highly compressible, turbulence [18].
The main driving mechanisms of this turbulence are thought to be supernovae [11]. Korpi et al. [19] simulated a galactic disk with randomly distributed supernova explosions. They find that the first explosions give rise to density fluctuations in the interstellar medium. The shock wave of a new supernova propagates through this clumpy medium, while its velocity changes with changing density. This way vorticity is generated.
Moreover, Klessen and Hennebelle [20] and Federrath et al. [21] show that the accretion process during a gravitational collapse itself leads generally to turbulence. This is a very important driving mechanism for turbulence, as accretion appears in many different astrophysical objects. The presence of turbulence affects star formation in these molecular clouds, as the turbulent pressure works against the collapse to a star [11, 22].

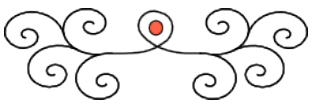

4 Electromagnetism

4.1 Maxwell's Equations

In the 19th century Maxwell developed the theoretical basis of electromagnetism. He described the electromagnetic field with a set of four linear coupled differential equations, which are known as the *Maxwell equations*.
In this chapter, we derive the Maxwell equations, which determine the electric field $\mathbf{E}$ and the magnetic field $\mathbf{B}$[1] from fundamental laws of electrodynamics.[2]

4.1.1 Basic Laws of the Electric Field

The electric flux Φ appearing from an arbitrary distribution of charge $\rho(\mathbf{x})$ with total charge Q is given as

$$\Phi = \int_{\partial \mathrm{V}} \mathbf{E}\ \mathrm{d}\mathbf{f} = \int_{\partial \mathrm{V}} \int_{\mathrm{V}} \rho(\mathbf{x'}) \frac{\mathbf{r}^3}{r}\ \mathrm{d}^3x' \mathrm{d}\mathbf{f} = 4\pi \int_{\mathrm{V}} \rho(\mathbf{x'})\ \mathrm{d}^3x' = 4\pi Q, \tag{4.1}$$

where we have used Coulombs law for the electric field $\mathbf{E}$. The second step in this calculation can be rewritten with Gauss' theorem, which leads to

$$\int_{\partial \mathrm{V}} \mathbf{E}\ \mathrm{d}\mathbf{f} = \int_{\partial \mathrm{V}} \mathrm{div}\mathbf{E}\ \mathrm{d}V = 4\pi \int_{\mathrm{V}} \rho(\mathbf{x'})\ \mathrm{d}V. \tag{4.2}$$

The relation

$$\boxed{\mathrm{div}\mathbf{E} = 4\pi\rho(\mathbf{x})} \tag{4.3}$$

is the first Maxwell equation.
The second Maxwell equation can be derived from the Faradays law of induction, which says that the electric voltage is proportional to the change of the magnetic flux,

$$\int_{\mathrm{c}} \mathbf{E}\ \mathrm{d}s = -\frac{1}{c}\frac{\mathrm{d}}{\mathrm{d}t} \int_{\partial \mathrm{V}} \mathbf{B}\ \mathrm{d}\mathbf{f}. \tag{4.4}$$

[1] In this work, we will call $\mathbf{B}$ the magnetic field strength. Officially $\mathbf{B}$ is called the magnetic induction and $\mathbf{B}/\mu$ is the magnetic field strength. However, in cgs-units the magnetic permeability μ equals 1 and $\mathbf{B}$ and $\mathbf{H}$ are the same.

[2] We will use here Gaussian/cgs units, which are typical for theoretical works. During developing the electromagnetic equations one is free to choose a few parameters which then give rise to different units like cgs or SI (see Table B.1).

With Stokes' theorem we find

$$\int_{\partial \mathrm{V}} \mathrm{rot}\mathbf{E}\ \mathrm{d}\mathbf{f} = -\frac{1}{c}\int_{\partial \mathrm{V}} \frac{\partial \mathbf{B}}{\partial t}\ \mathrm{d}\mathbf{f} \tag{4.5}$$

Thus, we find the second Maxwell equation

$$\boxed{\mathrm{rot}\mathbf{E} + \frac{1}{c}\frac{\partial \mathbf{B}}{\partial \mathrm{t}} = 0}. \tag{4.6}$$

4.1.2 Basic Laws of the Magnetic Field

The derivation of the divergence of the magnetic field is simple, when we use our experience that there are no magnetic charges. So the magnetic flux through a closed area always vanishes,

$$\int_{\partial \mathrm{V}} \mathbf{B}\ \mathrm{d}\mathbf{f} = \int_{\mathrm{V}} \mathrm{div}\mathbf{B}\ \mathrm{d}V = 0, \tag{4.7}$$

and we find the third Maxwell equation

$$\boxed{\mathrm{div}\mathbf{B} = 0}. \tag{4.8}$$

For the last Maxwell equation we have to rewrite Ampere's law, which is given as

$$\oint_{\mathrm{c}} \mathbf{B}\ \mathrm{d}\mathbf{x} = \frac{4\pi}{c} I, \tag{4.9}$$

where $I = \int_{\partial \mathrm{V}} \mathbf{j}\mathrm{d}\mathbf{f}$ is the electric current. With Stokes law we find

$$\oint_{\mathrm{c}} \mathbf{B}\ \mathrm{d}\mathbf{x} = \int_{\partial \mathrm{V}} \mathrm{rot}\mathbf{B}\ \mathrm{d}V = \int_{\partial \mathrm{V}} \frac{4\pi}{c}\mathbf{j}\ \mathrm{d}\mathbf{f}. \tag{4.10}$$

The equation

$$\mathrm{rot}\mathbf{B} = \frac{4\pi}{\mathrm{c}}\mathbf{j} \tag{4.11}$$

does not fulfill the continuity equation for the charge. For this reason an additional term, the Maxwells displacement current $c^{-1}\partial\mathbf{E}/\partial\mathrm{t}$, needs to be included. Thus, we end up with the fourth Maxwell equation

$$\boxed{\mathrm{rot}\mathbf{B} - \frac{1}{c}\frac{\partial \mathbf{E}}{\partial \mathrm{t}} = \frac{4\pi}{\mathrm{c}}\mathbf{j}}. \tag{4.12}$$

We have found four equations that describe the divergence and the rotation of the electric and the magnetic field. According to the *fundamental theorem of vector analysis* these equations determine the electromagnetic field completely as long as $\mathbf{E}$ and $\mathbf{B}$ decrease fast enough for large distances.
Obviously, one can collect the Maxwell equations into to groups. Equations (4.6) and (4.8) are source-free and therefore are also called *homogeneous* and equations (4.3) and (4.12), which include the distribution of matter in space ρ and the distribution of the current $\mathbf{j}$, depend on a source and are called *inhomogeneous* equations.

4.2 Gauging of the Electromagnetic Field

From the homogeneous equations one can construct general electric potentials [23]. The vanishing divergence of the magnetic field says that there should exist a vector field $\mathbf{A}$ known as *vector potential* with

$$\text{rot } \mathbf{A} \equiv \mathbf{B}. \tag{4.13}$$

Due to the properties of the rotation operator the magnetic field is invariant under the gauge transformation

$$\mathbf{A} \to \mathbf{A}' = \mathbf{A} + \nabla\chi. \tag{4.14}$$

By putting rot $\mathbf{A} = \mathbf{B}$ into the second homogeneous equation we find

$$\text{rot } (\mathbf{E} + \frac{1}{c}\dot{\mathbf{A}}) = 0,$$

where the dot over the vector potential denotes the time derivation. This leads directly to the definition of an *electric potential* ϕ,

$$-\text{grad } \phi \equiv \mathbf{E} + \frac{1}{c}\dot{\mathbf{A}}. \tag{4.15}$$

Now one can show that the electric field is invariant under following gauge transformation,

$$\phi \to \phi' = \phi - \frac{1}{c}\frac{d}{dt}\chi. \tag{4.16}$$

4.3 Lorentz Force

A charged particle moving in an electromagnetic field is deflected. The equation for describing the movement of a particle with charge q and velocity $\dot{\mathbf{x}}$ in an electromagnetic field can be derived in the Lagrangian formalism of electrodynamics. The resulting equation of motion with the momentum $\mathbf{p}$ is

$$\frac{\mathrm{d}\mathbf{p}}{\mathrm{d}t} = q\left(\mathbf{E}(\mathbf{x},t) + \frac{1}{c}\dot{\mathbf{x}} \times \mathbf{B}(\mathbf{x},t)\right). \tag{4.17}$$

The force

$$\boxed{\mathbf{F}_\mathrm{L}(\mathbf{x},t) = q\left(\mathbf{E}(\mathbf{x},t) + \frac{1}{c}\dot{\mathbf{x}} \times \mathbf{B}(\mathbf{x},t)\right)}. \tag{4.18}$$

is known as the *Lorentz force*. Notice that the term including the E-field is parallel to the force $\mathbf{F}_\mathrm{L}$, while the term including the B-field is perpendicular to $\mathbf{F}_\mathrm{L}$. This tells us that the magnetic field never exerts any work.

4.4 Energy in the Electromagnetic Field

In order to determine the energy of the electromagnetic field we look at the power it exerts on a test particle with charge q,

$$P = \mathbf{F}_\mathrm{L} \cdot \mathbf{v} = q\mathbf{E} \cdot \mathbf{v} = \int_\mathrm{V} \mathbf{j} \cdot \mathbf{E} \, \mathrm{d}^3x. \tag{4.19}$$

Substituting $\mathbf{j}$ by the Maxwell equation (4.12) leads to

$$P = -\frac{1}{4\pi}\left(\frac{1}{2}\int \frac{\mathrm{d}}{\mathrm{d}t}\left(B^2 + E^2\right) \, \mathrm{d}^3x - c\int_{\partial\mathrm{V}} (\mathbf{B} \times \mathbf{E}) \, \mathrm{d}\mathbf{f}\right). \tag{4.20}$$

Thus, the law of energy conservation for the electromagnetic field is

$$\boxed{-\mathbf{j} \cdot \mathbf{E} = \frac{1}{8\pi}\frac{\mathrm{d}}{\mathrm{d}t}\left(B^2 + E^2\right) + \frac{c}{4\pi}\mathrm{div}\,(\mathbf{B} \times \mathbf{E})}. \tag{4.21}$$

This law tells us that the kinetic energy particles lose in a volume V, $\mathbf{j} \cdot \mathbf{E}$, goes either in the energy of the electromagnetic field, $1/(8\pi)\,(B^2 + E^2)$, or streams out of the volume, $c/(4\pi)\ \mathrm{div}\,(\mathbf{B} \times \mathbf{E})$.

4.5 Ohm's Law

We have seen in the last section that charged particles get deflected and accelerated in a electromagnetic field. Thus, we can conclude that the electric current, which is a collection of many moving charged particles, is connected to the Lorentz force. Typically the electric current density is proportional to the force density $\mathbf{F}/q$ that is acting,

$$\mathbf{j}(\mathbf{x}, t) = \sigma\frac{\mathbf{F}}{q}, \tag{4.22}$$

where the proportional factor σ is labeled the electric conductivity. One can show that

$$\sigma = \frac{n_\mathrm{e} e^2 \tau_\mathrm{ei}}{m_\mathrm{e}}, \tag{4.23}$$

where m_e and n_e are the mass and the density of the electrons, e their charge and τ_ei the collision time. As the force that acts in the electromagnetic field is the Lorentz force, we get

$$\boxed{\mathbf{j}(\mathbf{x}, t) = \sigma\left(\mathbf{E}(\mathbf{x}, t) + \frac{1}{c}\dot{\mathbf{x}} \times \mathbf{B}(\mathbf{x}, t)\right)}. \tag{4.24}$$

The upper equation is known as *Ohm's law*, which describes the coupling between the electromagnetic field and matter.

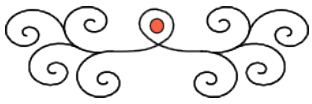

5 Expansion of Hydrodynamics to Magnetohydrodynamics

In order to model astrophysical objects more realistically we have to include electromagnetic fields. As we have seen in the introduction, magnetic fields and charged particles are ubiquitous in the Universe. The combination of hydrodynamics with of electrodynamics leads us to the theory of magnetohydrodynamics (MHD).
Besides the two thermodynamical variables, the density ρ and the internal energy ϵ, and the velocity of the gas $\mathbf{v}$, we now have to include the magnetic field $\mathbf{B}$ in our equations[1]. This also means that we need one additional equation to have a fully dynamical theory.

5.1 The Equations of Magnetohydrodynamics

5.1.1 Continuity Equation

The equation, which describes the density evolution, stays the same, if we include the magnetic field,

$$\boxed{\frac{\partial \rho}{\partial t} + \nabla \cdot (\rho \mathbf{v}) = 0}. \tag{5.1}$$

The density is obviously still a conserved quantity in the presence of an electromagnetic field.

5.1.2 Momentum Equation

The Navier-Stokes equation describes the evolution of the momentum in hydrodynamics. It relates all the forces that appear in a system. If now a magnetic field flows though our plasma, we have to consider an additional magnetic body force. The Lorentz force for a continuous system is $1/c\ \mathbf{j} \times \mathbf{B}$. Thus, we have to include the term

$$\frac{1}{c\rho}\mathbf{j} \times \mathbf{B} = \frac{1}{4\pi\rho} (\nabla \times \mathbf{B}) \times \mathbf{B} = \frac{(\mathbf{B} \cdot \nabla)\, \mathbf{B}}{4\pi\rho} - \frac{1}{\rho}\nabla \frac{B^2}{8\pi}, \tag{5.2}$$

[1] It is enough to include either the magnetic field or the electric field in our equations, because those fields are not independent.

where we have used Amperes law. Altogether, in magnetohydrodynamics we have to use the momentum equation

$$\boxed{\frac{\partial \mathbf{v}}{\partial t} + (\mathbf{v}\cdot\nabla)\mathbf{v} = -\frac{1}{\rho}\nabla\left(p + \frac{B^2}{8\pi}\right) + \frac{1}{m}\mathbf{F} + \frac{(\mathbf{B}\cdot\nabla)\,\mathbf{B}}{4\pi\rho} + \frac{\mu}{\rho}\nabla^2\mathbf{v}}. \tag{5.3}$$

One can easily see, that the magnetic field leads to an magnetic pressure $B^2/(8\pi)$. Furthermore, one can show, that the second term including $\mathbf{B}$ is responsible for a tension along the magnetic field lines (see [7]).

5.1.3 Energy Equation

The equation of the internal energy is in magnetohydrodynamics almost the same as it is in hydrodynamics,

$$\boxed{\rho\left(\frac{\partial \epsilon}{\partial t} + \mathbf{v}\cdot\nabla\epsilon\right) = \nabla\cdot(K\nabla T) + \frac{j^2}{\sigma} - p\nabla\cdot\mathbf{v}}. \tag{5.4}$$

We only have one additional term, j^2/σ, which takes care of the *Ohmic heating*.

5.1.4 Induction Equation

As mentioned earlier in this chapter, we have to find an additional equation for the theory of MHD, because there are now four independent variables. We need an equation describing the magnetic field $\mathbf{B}$, which we can derive from the Maxwell equations and Ohm's law.
By combination of the law of Faraday (4.6) with Ohm's law (4.24) we can eliminate the electric field $\mathbf{E}$,

$$\frac{1}{c}\frac{\partial \mathbf{B}}{\partial t} = -\nabla\times\left(\frac{\mathbf{j}}{\sigma} - \mathbf{v}\times\mathbf{B}\right). \tag{5.5}$$

When we neglect Maxwell's displacement current $c^{-1}\partial\mathbf{E}/\partial t$ in Ampere's law (4.12) and substitute the current density $\mathbf{j}$ into the upper equation we get the *induction equation*

$$\boxed{\frac{\partial \mathbf{B}}{\partial t} = \nabla\times(\mathbf{v}\times\mathbf{B} - \eta\nabla\times\mathbf{B})}, \tag{5.6}$$

where we have defined the magnetic diffusivity as

$$\eta \equiv \frac{c^2}{4\pi\sigma}. \tag{5.7}$$

We can make the induction equation dimensionless by introducing the typical quantities of our system B, L, V and T. With $\mathbf{B} = B\tilde{\mathbf{B}}$, $\nabla = 1/L\tilde{\nabla}$, $\mathbf{v} = V\tilde{\mathbf{v}}$ and $\mathbf{t} = T\tilde{\mathbf{t}}$ we get

$$\frac{\partial \tilde{\mathbf{B}}}{\partial t} = \tilde{\nabla} \times \left(\tilde{\mathbf{v}} \times \tilde{\mathbf{B}} - \frac{1}{Rm} \nabla \times \tilde{\mathbf{B}} \right). \tag{5.8}$$

We defined here the *magnetic Reynolds number*

$$\boxed{Rm \equiv \frac{VL}{\eta}}, \tag{5.9}$$

which is an indicator for the importance of the two terms on the RHS. The limit of $Rm \ll 1$ leads to a diffusion equation. In this case the magnetic field can only decay. The other limit, $Rm \gg 1$, is the limit of perfect conduction, where the electric conductivity $\sigma \gg 1$. Only in this case the magnetic field can increase.

5.2 Ideal Magnetohydrodynamics

We speak of ideal MHD, if several conditions are fulfilled:

1. In an ionised gas the collision rate between ions and neutrals needs to be very high. This makes sure, that the neutral and the charged particles are coupled perfectly and behave as one fluid. If there is for example a strong external magnetic field the whole fluid feels the Lorentz force and not only the ions.

2. The viscosity needs to vanish ($\nu \to 0$).

3. The electric conductivity needs to be infinite ($\sigma \to \infty$), while the resistivity vanishes ($\eta \propto 1/\sigma \to 0$). Because of this ideal MHD is also known as non-resistive MHD. The magnetic Reynolds number also is infinite in this limit ($Rm \propto 1/\eta \to \infty$).

Thus, in ideal magnetohydrodynamics the induction equation becomes

$$\frac{\partial \mathbf{B}}{\partial t} = \nabla \times (\mathbf{v} \times \mathbf{B}). \tag{5.10}$$

It can be shown, that the equation $\partial \mathbf{Q}/\partial t = \nabla \times (\mathbf{v} \times \mathbf{Q})$ for an arbitrary vector field Q, can be written as $\mathrm{d}/\mathrm{d}t \int_{\partial \mathrm{V}} \mathbf{Q} \mathrm{d}\mathbf{f} = 0$ [7]. Hence we get

$$\frac{\mathrm{d}}{\mathrm{d}t} \int_{\partial \mathrm{V}} \mathbf{B} \ \mathrm{d}\mathbf{f} = 0. \tag{5.11}$$

Note, that here the Lagrangian time derivation appears. This means that we follow the moving fluid elements, while determine the variation in time. Thus, the magnetic field is frozen in the fluid, which is also known as *Alvén's theorem of flux freezing* [24]. However, the flux freezing only takes place, as long as the magnetic field is weak. With increasing magnetic energy, magnetic back reactions become more important and at some point the neutrals will not follow the magnetic field any more.

5.3 Effects of Non-Ideal Magnetohydrodynamics

Non-ideal magnetohydrodynamics is also called resistive MHD, as here the resistivity does not vanish. This opens a way for magnetic field decay. For very high resistivity η, the induction equation becomes

$$\frac{\partial \mathbf{B}}{\partial t} = -\eta \nabla \times (\nabla \times \mathbf{B}), \tag{5.12}$$

which is, due to the freedom of divergence of the magnetic field (4.8) equivalent to

$$\frac{\partial \mathbf{B}}{\partial t} = \eta \nabla^2 \mathbf{B}. \tag{5.13}$$

The upper equation is a diffusion equation, which only has solutions in which the magnetic field decays. The dissipation of the magnetic energy has a typical timescale of L^2/η, where L is the length of the system.
Furthermore, in non-ideal MHD the plasma may not act as one fluid anymore. At certain conditions, like in the presence of strong magnetic fields, the charged particles can react different then the neutrals. The drift between ions and neutral is called *ambipolar diffusion*.

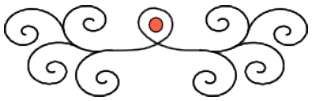

6 Magnetic Fields in the Universe

6.1 Observations of Magnetic Fields

6.1.1 Present-Day Universe

In the present-day Universe magnetic fields can be observed with different more or less direct methodes [25, 26]. The most intuitive way to measure the magnetic field strength is using the Zeemann effect. With Zeemann splitting of radio spectral lines one can measure the strength of relatively strong fields, like for example in stellar objects.
Another powerful tool for observing magnetic fields is synchrotron radiation. This non-thermal radiation appears, when charged particles with high energy move in magnetic fields. By measuring the intensity of synchrotron radiation the magnetic field strength can be estimated. This radiation can also be polarised. It gets linearly polarised due to extinction by enlongated dust grains in the line of sight, which is called the *Davis-Greenstein effect*. Optical light can also get polarised by scattering and not distinguished from polarisation by dust grains. This is why infrared or sub-millimeter measurements are used to detect magnetic fields. Polarisation is used to determine the direction of the magnetic field in the plane of the sky. It indicates an ordered field structure, which has been genereted for example by a large-scale dynamo. Observations find the strongest polarised synchrotron radiation in galaxies in the interarm region 10-15 μG and in the radio halo of edge-on galaxies. In galaxies also unpolarised synchrotron radiation is found, interpreted as a turbulent magnetic field generated by the small-scale dynamo. This has been observed in the spiral arms and bars of galaxies with a strength of 20-30 μG and in central starburst regions with 50-100 μG [26].
A third important method to detect magnetic fields is Faraday rotation, which describes the rotation of the polarisation vector in a magnetised thermal plasma. With this method the strength and the direction of the magnetic field in the line-of sight can be determined.
With the upper methods the magnetic field of the Milky Way can be determined. Using the total synchrotron emission at 408 MHz (from survey of Haslam et al. [27]) Beuermann et al. [28] find a field strength of 6 ± 2 μG locally and 10 ± 3 μG at 3 kpc galactic radius. The structure of magnetic fields can be observed easier in other galaxies. Observations show, generally, that the spatial structure of the magnetic field in spiral galaxies follows the spiral arms. For example, in Figure 6.1 the face-on galaxy M 51 is shown. Moreover, observations confirm that magnetic fields in galaxies are dynamically important, as they have an energy density up to

ten times higher than the thermal energy density of the ionised gas.
Recent studies confirm that magnetic fields can not only be found within galaxies, but also in the intergalactic medium. Neronov & Vovk [29] find, using gamma-ray observations of the intergalactic medium, a lower limit of $B_0 \approx 10^{-16}$ G (see also [30, 31]). This might be indicative of an early generation scenario, if its was not generated by outflows of galaxies or the Biermann battery. However, they neglected certain plasma instabilities in their derivation, which could change the results.

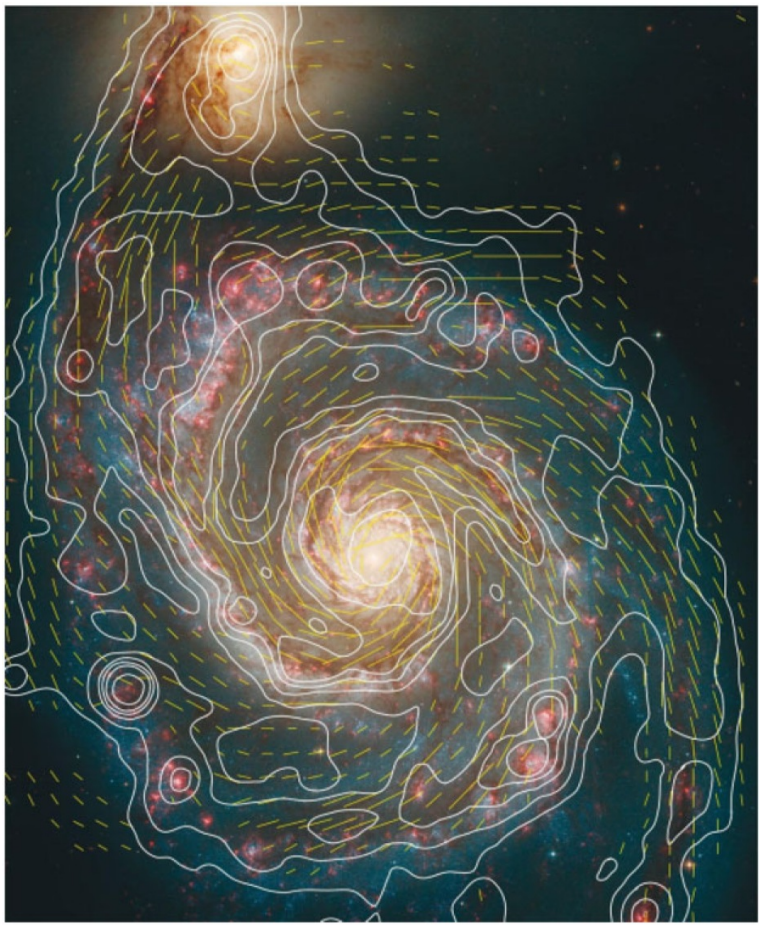

Figure 6.1: The magnetic field of the spiral galaxy M 51. The contours indicate the total radio emission, the yellow lines show the magnetic field vectors. These observations come from the VLA and Effelsberg telescopes at a wavelength of 6 cm [32] and an optical image from the Hubble space telescope. (Copyright: MPIfR Bonn and *Hubble Heritage Team*, Graphics: *Sterne und Weltraum*)

6.1.2 Early Universe

Naturally it is much more difficult to make predictions of magnetic fields in the early Universe. Observations suggest that magnetic fields have been space-filling already in the early Universe. Until today we only have upper limits for the very early Universe, but no direct observations showing the presence of magnetic fields.
Yamazaki et al. [33] derive an upper limit of the magnetic field strength from the cosmic microwave background (CMB) temperature anisotropy. They predict that the magnetic field strength at a present scale of 1 Mpc.
Primordial nucleosynthesis provides additional constraints on the magnetic field strength. Grasso and Rubinstein [34] find that the magnetic field needs to have been less than $10^{11} - 10^{12}$ G at a temperature of 10^9 K. This corresponds to a comoving field strength of $1 - 10$ μG.
Moreover, Schleicher and Miniati [35] present a method to derive the magnetic field strength in the reionisation epoch (redshift $z > 6$). They show that the upper halo mass is set by the magnetic pressure and conclude, by using data from the reionisation epoch, that the co-moving magnetic field strength is $B_0 \lesssim 3$ nG (see also [36]).
Kronberg et al. [37] observed the Faraday rotation of high-redshift quasars out to $z \approx 3.7$. They find that the Universe becomes increasingly "Faraday-opaque" for sources beyond $z \approx 2$, which indicates that galaxies at these redshifts were significantly magnetised.
Hints towards high-redshift ($z \approx 1.3$) magnetic fields in galaxies come from the study of Bernet et al. [38]. They used high resolution spectra from normal galaxies and observed a magnetic field strength of a few microgauss, which is of the same order as present-day magnetic fields.

6.2 Generation of Magnetic Seed Fields

The last section shows that the Universe is strongly magnetised. Magnetic fields are even observed in the space between galaxies. But where do these fields come from? There is no possibility to explain the generation of magnetic seed fields from the standard MHD-equations (Section 5). In the induction equation (5.6) every term contains the magnetic field strength $\mathbf{B}$. Thus starting with a zero magnetic field will never create a non-zero field.

6.2.1 Field Generation in the Early Universe

There are different theories that describe the origin of primordial magnetic fields. The first seed fields could already have been produced during inflation. Turner and Widrow [39] find that a magnetic field $B_0 \approx 10^{-25}$–10^{-1} nG on a scale of 1 Mpc can be produced when the conformal invariance is broken.
Following Sigl et al. [40], there is also a possibility to create a magnetic field during first-oder phase transitions in the very early Universe. They predict a field strength

$B_0 \approx 10^{-20}$ nG from the electroweak phase transition and $B_0 \approx 10^{-11}$ nG from the QCD phase transition on a scale of 10 Mpc.
Miniati and Bell [41] suggest that cosmic rays generated magnetic fields in the early Universe. Cosmic rays, which are charged particles with relativistic velocities, were emitted from supernova explosions of the first stars. They act like an electric current and, thus, there is a return current in the cold plasma. This leads to Ohmic heating of the gas, from which a rotational component of the electric field develops. By Faraday's induction law a magnetic field is generated. Miniati and Bell [41] find that cosmic ray propagation can produce a magnetic field of 10^{-8}–10^{-7} nG, until the intergalactic medium is reionised.
The generation mechanisms of magnetic fields in the very early Universe lead only to very low field strengths. We can use these results as a lower limit.

6.2.2 Biermann Battery

Besides a cosmological origin of magnetic fields there are so-called battery mechanisms, which can continuously work in the Universe. We have seen, that the normal induction equation (5.6) provides no way of creating a magnetic field. Every term of this equation includes $\mathbf{B}$ and thus $\mathbf{B} = 0$ is a valid solution. However, we have so far used the one-fluid approximation for magnetohydrodynamics, which means, that we assumed that there is only one charged species. We will see that additional terms will appear in our equations if we go one step further and use a two-fluid approximation, including two different charged species.
We consider a partially ionised hydrogen gas, which consists of electrons, protons and neutrals. In the two-fluid approximation the generalised Ohm's law reads [42]

$$\mathbf{E} + \mathbf{v}_\mathrm{i} \times \mathbf{B} = \frac{\mathbf{j}}{\sigma} - \frac{\nabla p_\mathrm{e}}{e n_\mathrm{e}} + \frac{1}{e n_\mathrm{e}} \mathbf{j} \times \mathbf{B} + \frac{m_\mathrm{e}}{e^2} \frac{\partial}{\partial t} \left(\frac{\mathbf{j}}{n_\mathrm{e}} \right). \tag{6.1}$$

The first term on the right hand side refers to the classical Ohm's law with the current density $\mathbf{j}$ and the electric conductivity $\sigma = n_\mathrm{e} e^2 \tau_\mathrm{ei} / m_\mathrm{e}$. Here m_e and n_e are the mass and the density of the electrons, e their charge and τ_ei the collision time. The second term, which includes the gradient of the electronic pressure, is called the Biermann term. We will see that this term provides us a way of creating magnetic fields, if it has a curl. The third term on the right hand side refers to the Hall effect and the fourth one is the inertial term. The last terms are usually very small and we ignore them from now on.
Deriving the induction equation in the same way like we did in Section 5.1, but now using the generalised Ohm's law, gets us [42]

$$\frac{\partial \mathbf{B}}{\partial t} = \nabla \times (v_\mathrm{i} \times \mathbf{B}) - \frac{\eta}{4\pi} \nabla \times (\nabla \times \mathbf{B}) - \frac{ck}{e} \frac{\nabla n_\mathrm{e}}{n_\mathrm{e}} \times \nabla T, \tag{6.2}$$

where we used $p_\mathrm{e} = n_\mathrm{e} k T$. This generalised induction equation has, compared to equation (5.6), one new term $ck/(en_\mathrm{e}) \nabla n_\mathrm{e} \times \nabla T$. Note, that it is independent of the

magnetic field **B**. Thus, this source term can generate a field, if there is a pressure and a temperature gradient that are not parallel.
The descriptive explanation of this generation mechanism uses the fact that our two charged species have very different masses, i.e. $m_\mathrm{e} \ll m_\mathrm{p}$. If there is a pressure gradient in the plasma the particles become accelerated. The electrons are more strongly accelerated than the protons, because they have a smaller mass. This leads to separation of charge and an electric field is generated. If now the electron density n_e is constant in space the electric field is static. But a spatial dependence of n_e gives rise to an electric current and thus to the generation of a magnetic field [43, 44].
Let us now estimate how strong the fields produced by the Biermann battery are [44]. In a system that is formed by gravity, the energy that can be transformed into the magnetic energy is the gravitational energy. The typical timescale on which the magnetic field is generated is then the free-fall time $T_\mathrm{ff} = 1/\sqrt{Gmn}$, where G is the gravitational constant, m the mean partial mass and n the particle number density. From the generalised induction equation (6.2) we get

$$\frac{\mathbf{B}}{T_\mathrm{ff}} \approx \frac{ck}{e}\frac{\frac{1}{L}n_\mathrm{e}}{n_\mathrm{e}}\frac{1}{L}T = \frac{ckT}{L^2 e}. \tag{6.3}$$

The typical lengthscale of a gravitationally formed system is the Jeans length, hence we set $L \approx \sqrt{\gamma kT/(Gm^2 n)}$. Here k is Boltzmann's constant and T the temperature. Thus, we find

$$\mathbf{B} \approx \frac{c\sqrt{G}m^{3/2}}{\gamma e}\sqrt{n}. \tag{6.4}$$

For the typical intergalactic medium with $\gamma \approx 1.4$, $m \approx 1.75 m_\mathrm{u}$ and $n \approx 1\mathrm{cm}^{-3}$ [45] the Biermann battery can generate a magnetic field of roughly 10^{-21}G.
On the numerical side, there are a number of magnetohydrodynamical simulations including the Biermann battery effect. For example Xu et el. [46] explored primordial star formation with a self-consistent three-dimensional adaptive mesh refinement simulation. They find that the Biermann battery is most important in the early evolution of a primordial halo. The generated magnetic field gets amplified further in the collapse through gravitational compression. Xu et al. find a peak magnetic field strength of 10^{-19} G at a redshift of 17.55.

6.2.3 Additional Generation Mechanisms

There are more generation mechanisms of magnetic fields suggested in literature.
For example Schlickeiser and Shukla [47] find that magnetic fields can be produced in the intergalactic medium through Weibel instability, which arises from an electron temperature anisotropy. This instability appears in interpenetrating electron-ion flows with high Mach numbers. Schlickeiser and Shukla predict that flows develop in large-scale structure evolution and can give rise to a magnetic field strength of maximal 10^{-7} G.

Shukla et al. [48] suggest another way of generating magnetic seed fields in very dense astrophysical plasmas like white dwarfs or neutron stars. They show that the ponderomotive force[1] of large-amplitude electromagnetic waves in a quantum plasma with streaming degenerate electrons can generate a magnetic field.

6.3 Amplification of Magnetic Fields

In this section we present the four most important mechanisms to amplify weak magnetic seed field in a collapsing cloud.
At first, and most intuitively, a magnetic field which is perfectly coupled to the gas becomes stronger due to gravitational compression, as here simply the field lines get closer. Another mechanism is the magnetorotational instability, which takes place in magnetised accretion disks. An amplification can also take place through the action of so-called dynamos, where we differentiate between a small-scale dynamo, which can only act on preexisting seed magnetic fields, and a large-scale dynamo appearing in protostellar and galactic disks.

6.3.1 Amplification due to Gravitational Collapse

When the magnetic field follows the motion of the plasma, i.e. the magnetic flux is frozen into the fluid (see Section 5.2), it can be amplified when the density increases. We present here a derivation from the book on plasma physics of Frank-Kamenezki [49]. A mathematical treatment of this amplification by gravitational compression starts with the continuity and the induction equation, as these describe the evolution of the density and the magnetic field strength. In the Lagrangian notation, they are

$$\begin{aligned} \frac{\mathrm{d}\rho}{\mathrm{d}t} &= -\rho\nabla\cdot\mathbf{v}, \\ \frac{\mathrm{d}\mathbf{B}}{\mathrm{d}t} &= (\mathbf{B}\cdot\nabla)\,\mathbf{v} - \mathbf{B}\,(\nabla\cdot\mathbf{v})\,. \end{aligned} \tag{6.5}$$

Elimination of $\nabla\cdot\mathbf{v}$ leads to

$$\begin{aligned} \frac{\mathrm{d}\mathbf{B}}{\mathrm{d}t} &= (\mathbf{B}\cdot\nabla)\,\mathbf{v} + \frac{\mathbf{B}}{\rho}\frac{\mathrm{d}\rho}{\mathrm{d}t} \\ \Leftrightarrow \frac{\mathrm{d}}{\mathrm{d}t}\left(\frac{\mathbf{B}}{\rho}\right) &= \left(\frac{\mathbf{B}}{\rho}\cdot\nabla\right)\mathbf{v}. \end{aligned} \tag{6.6}$$

Now let us imagine what happens to a field line, when the plasma is compressed arbitrarily and the field is frozen into the matter. We consider two fluid elements and connect them through a fluid line $\mathbf{l}$. If these elements have the velocities $\mathbf{v}_1$ and $\mathbf{v}_2$, the length of the fluid line $\mathbf{l}$ changes as

$$\frac{\mathrm{d}\mathbf{l}}{\mathrm{d}t} = (\mathbf{v}_2 - \mathbf{v}_1)_l, \tag{6.7}$$

[1] The ponderomotive force is the force that acts in an inhomogeneous oscillating electromagnetic field on charged particles.

where the index l indicates the protection of the velocities on the fluid line. For an infinitesimal fluid line $\delta\mathbf{l}$ this expression becomes

$$\frac{\mathrm{d}\delta\mathbf{l}}{\mathrm{d}t} = (\delta\mathbf{l}\nabla)\mathbf{v}. \tag{6.8}$$

By comparing the upper equation with equation (6.6), we directly find

$$\frac{B}{\rho} \propto \delta l. \tag{6.9}$$

This means that the ratio of the magnetic field strength over the density changes proportional to the length of the fluid line. We can consider some special cases of this result. When the compression of the fluid, for example, is perpendicular to the magnetic field lines, the length of the field line δl does not change (see Figure 6.2). With $\delta l = const$, we find

$$B \propto \rho. \tag{6.10}$$

In this case the magnetic field strength increases proportional to the density, because the magnetic field lines get closer together.
When, on the other hand, the compression takes place parallel to the field lines, the single fluid lines get shorter, but the distance between the fluid lines does not change (see Figure 6.2). In this change δl changes inversely proportional to ρ, and we find

$$B = const. \tag{6.11}$$

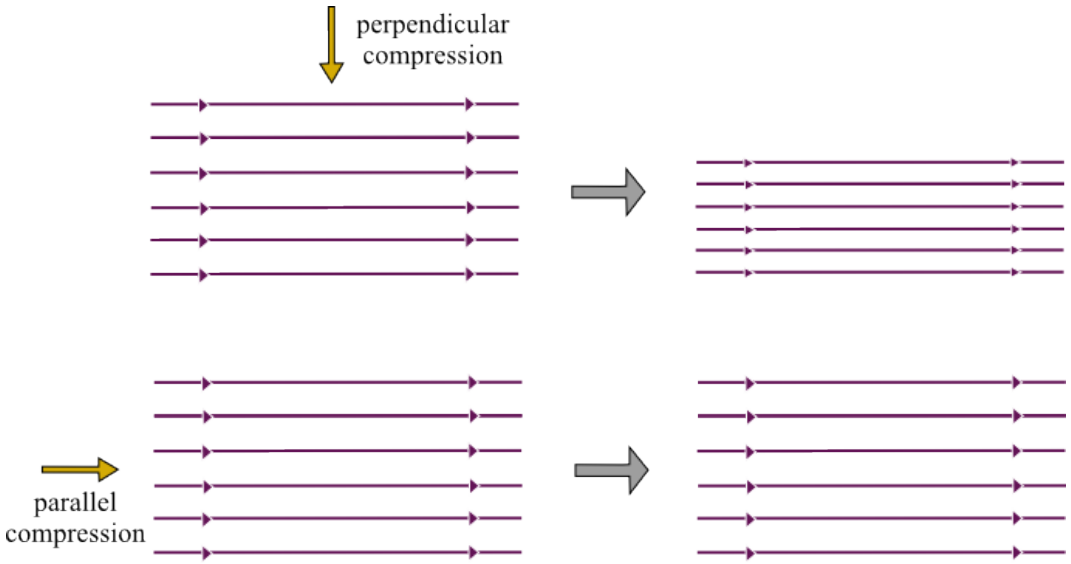

Figure 6.2: Compression of magnetic field lines. In the upper picture the field lines are compressed perpendicular, which results in a compaction of the field lines and thus to an amplification of the field strength. The lower picture shows parallel compression, which has no effect on the magnetic field strength.

In astrophysics the most important case is spherical compression, where $\rho \propto \delta l^{-3}$. With equation (6.9) we find for this case

$$B \propto \rho^{2/3}. \tag{6.12}$$

The effect of magnetic field amplification due to gravitational compression is also seen in numerical simulations. Xu et al. [46] find in their simulation of Population III star formation, besides the field generation due to the Biermann battery, an amplification of the field roughly proportional to $\rho^{2/3}$. Also Federrath et al. [21] test the amplification due to spherical compression in their MHD simulations. They start with a weak field in z-direction and analyse the magnetic field strength during the collapse. The field grows less than proportional to $\rho^{2/3}$ at the beginning, as here the field is not isotropic. Due to the collapse, the field lines get stretched and the typical hour-glass shape is generated (see Figure 6.3). Then the field becomes isotropic and grows almost[2] proportional to $\rho^{2/3}$.

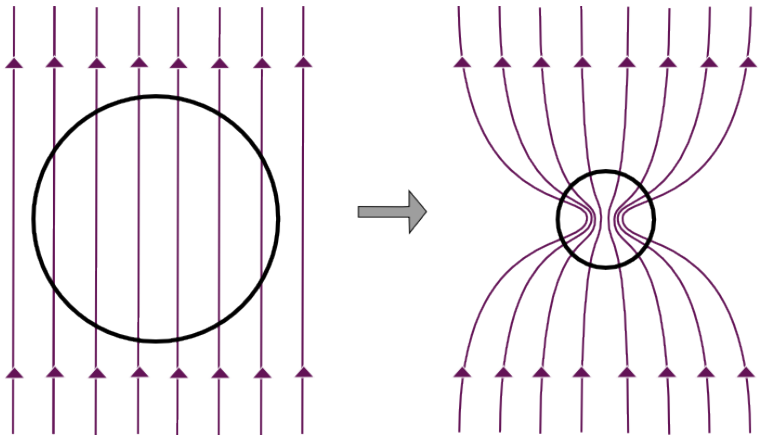

Figure 6.3: The typical hour-glass shape of the magnetic field resulting from a collapsing sphere. The left picture shows the initial condition of a magnetic field in z-direction. This field is not isotropic. In the later stages of the collapse the field becomes more and more isotropic (see right picture). Then the magnetic field gets amplified proportional to $\rho^{2/3}$.

In the astrophysical context we find often a spherical collapse for example during the formation of a galaxy. We want to estimate the typical timescale for amplifying a Biermann seed field of $B_1 = 10^{-20}$ G by gravitational compression to $B_2 = 10^{-6}$ G, which is observed in the Milky Way. In spherical compression we have

$$B_1 \rho_1^{-2/3} = B_2 \rho_2^{-2/3}, \tag{6.13}$$

[2]However, Federrath et al. [21] find in a test of the ideal MHD-approximation small derivations from $B \propto \rho^{2/3}$, which depend on the resolution of the simulation. This is caused by non-ideal magnetohydrodynamical effects due to small numerical diffusivity.

where we take $\rho_2 = 10^{-24}$ g as the density of the Milky Way. The galaxy formed from the collapse of a cloud with density ρ_1 within the free-fall time $T = 1/\sqrt{G\rho_1}$. Thus, we find

$$\begin{aligned} B_1 G^{2/3} T^{4/3} &= B_2 \rho_2^{-2/3} \\ \Leftrightarrow T &= \left(\frac{B_2}{B_1}\right)^{3/4} \frac{1}{\sqrt{G\rho_2}}. \end{aligned} \tag{6.14}$$

For our example we find a typical timescale for amplification by gravitational compression of 10^{18} years, which is many orders higer than the Hubble time. We thus conclude that gravitational compression alone can not explain the high magnetic fields observed in galaxies.

6.3.2 Magnetorotational Instability

An effect that leads to amplification of magnetic fields in accretion discs is magnetorotational instability (MRI).
The magnetorotational instability, which was first found by Velikhov [50] in 1959 and later generalised by Chandrasekhar [51], solves an important problem of accretion. In accretion discs the particles follow Kepler orbits. This means that the inner particles have a larger angular velocity Ω than the outer particles ($\Omega \propto r^{-3/2}$). In ideal hydrodynamics there is no cause for particles to move to the central object. Different ideas, like the effect of viscosity or turbulence, tried to explain how particles could lose angular momentum and get accreted [52]. But simulations show that those effects are not important enough.
Balbus & Hawley [53] showed in 1991 that a weak magnetic field can lead to an instability in an astrophysical accretion disk. The condition for this instability is, that the angular velocity needs to decrease with increasing radius. This is the case for Keplerian motion like in accretion disk. If the magnetic flux is frozen in the gas, it gets twisted up due to this differential rotation. The field lines get tangled and the magnetic energy increases in the inner part of the disk. By this the inner parts slow down and the angular momentum is transported to the outer parts. So the inner parts can move further inside and accretion takes place.

6.3.3 Magnetohydrodynamical Dynamos - Phenomenologically

Under special physical conditions, flows of magnetised fluids can amplify magnetic seed fields by converting kinetic energy into magnetic energy. These processes are called *magnetohydrodynamical dynamos*. It turns out that dynamos amplify the magnetic energy exponentially until they are saturated. One has to distinguish two different types of dynamos: the *large-scale dynamo*, which is excited by large-scale motions, and the *small-scale dynamo*, which is excited by turbulence on very small scales.

In this section we provide a phenomenological description of the magnetohydrodynamical dynamos.

The Large-Scale Dynamo The magnetic field of the Sun has been observed for the first time by Hale in 1908 [54]. He discovered the Zeemann effect of H-alpha lines in Sun spots. Later he showed that the sunspots on the two hemispheres have different polarities [55]. Moreover, the whole magnetic activity seemed to change periodicly within a time of 22 years (see "butterfly-diagramm" by Maunder [56]). With this observations many questions appeared and a theory that aims to describe the magnetism of the Sun, would need to explain all these observed effects. In 1955 Parker [57, 58] published the first physical interpretation of magnetic field in the Sun. Today that mechanism is referred to as the *alpha-omega dynamo*. The systematic mathematical desciription of this large-scale dynamo was formulated in 1966 by Steenbeck, Krause and Rädler [59] (see Chaper 7).

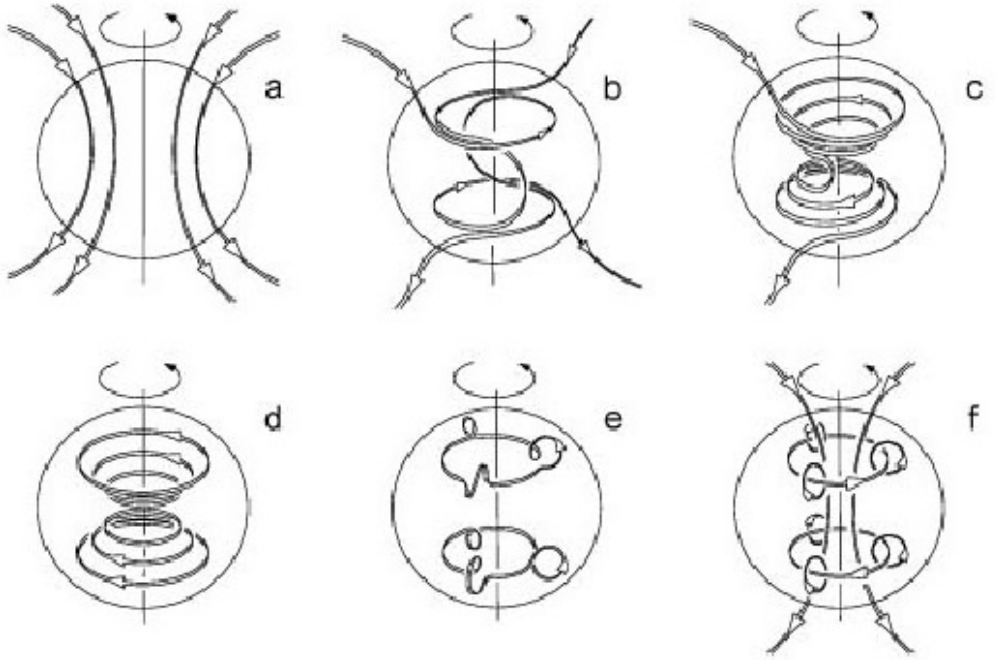

Figure 6.4: The $\alpha\Omega$-mechanism as a toy model for the large-scale dynamo [60].

We want to describe the $\alpha\Omega$-dynamo, as it takes place for example in the Sun, qualitatively [7]. We divide the magnetic field into a toroidal field $B_\phi \mathbf{e}_\phi$ and a poloidal field $B_\mathrm{r}\mathbf{e}_\mathrm{r} + B_\theta \mathbf{e}_\theta$. Now let us assume we have an inital poloidal field for instance from gravitational compression during the formation of the Sun. This poloidal field is shown in part (a) of Figure 6.4. As the Sun rotates differentially, i.e. it rotates faster on the equator than on the poles, the poloidal field lines get

stretched on the sphere (see (b) in Figure 6.4). Note that we assume here flux freezing. By this stretching a torodial magnetic field component is generated. The torodial field lines become denser and denser (part (c)) until a full toroidal field is created by magnetic reconnection (part (d)). There is still a poloidal component, of course, but this is omitted now in the figure for simplicity. However, if there is no mechanism that generates a poloidal field it will decay away at some point and thus also the production of the toroidal field will stop. Parker solved this problem by including the convective motions inside the Sun [57]. He assumed that, with partial flux freezing, the field lines of the torodial field are stretched (see (e)). As this takes place in a rotating system, the Coriolis force leads to vorticity of the field lines and a poloidal field is build up again (see part (f) of Figure 6.4).

The Small-Scale Dynamo The small-scale dynamo, also called "turbulent dynamo" or "fluctuation dynamo", converts turbulent kinetic energy into magnetic energy. The turbulent motions lead to a winding of the magnetic field lines and compact them. This way the magnetic field energy is amplified.

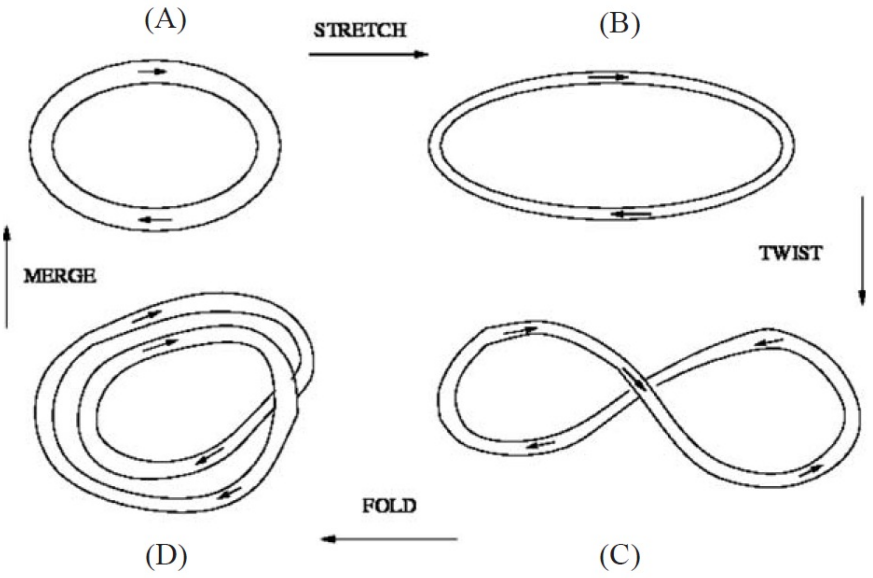

Figure 6.5: The "stretch-twist-fold"-mechanism as a toy model for the small-scale dynamo [61].

For a physical interpretation it is useful to take the *stretch-twist-fold dynamo* as a toy-model of the turbulent dynamo [61, 62]. Figure 6.5 shows the principle mechanism. In this picture we think of a magnetic flux rope that gets stretched due to turbulent motions as indicated in the transition from picture (A) to (B). This motion decreases the cross section of the flux rope A. If we assume that the magnetic

flux $B \cdot A$ is frozen into the gas, then the magnetic field increases during this process, because the magnetic flux is a conserved quantity. In step (C) the flux rope is twisted and then folded in step (D). In the end, the two parts of the flux rope merge again (step (D) to (A)) and result in a flux rope with the same appearance as the one at the beginning, but the magnetic field strength has increased. This process works best in a purely rotational turbulent velocity field. Therefore, we expect the dynamo to be more easily excited in Kolmogorov turbulence rather than in Burgers turbulence.
In this picture the magnetic energy is amplified fastest on small-scales, i.e. on the scales of the smallest turbulent eddies. Smaller turbulent eddies have smaller turnover times and thus the field lines are tangled up faster.

7 Theoretical Description of Magnetohyrodynamical Dynamos

In this chapter we present the most important steps for the theoretical treatment of magnetohydrodynamical dynamos following Subramanian [15]. We distinguish the mean magnetic field $\langle \mathbf{B} \rangle$ and the fluctuating field $\delta\mathbf{B}$. The total field can be written as

$$\mathbf{B} = \langle \mathbf{B} \rangle + \delta\mathbf{B}. \tag{7.1}$$

In the following derivation we include the effect of ambipolar diffusion (see Section 5.3). For that we start with generalising the induction equation. We will end with a theory for the large-scale dynamo describing the evolution of $\langle \mathbf{B} \rangle$ and a theory for the small scale dynamo describing the evolution of the fluctuating field $\delta\mathbf{B}$.

7.1 Induction Equation with Ambipolar Diffusion

Astrophysical plasmas are often only partially ionised. If there is a magnetic field in such a plasma, only the ions feel a force. Hence, we have to be careful when using the magnetohydrodynamical equations. The induction equation, which is the most important equation for describing dynamos, contains the velocity of the ions $\mathbf{v}_\mathrm{i}$,

$$\frac{\partial \mathbf{B}}{\partial t} = \nabla \times \mathbf{v}_\mathrm{i} \times \mathbf{B} - \eta \nabla \times \nabla \times \mathbf{B}, \tag{7.2}$$

with the magnetic diffusivity

$$\eta \equiv \frac{c^2}{4\pi\sigma}. \tag{7.3}$$

But often we know only the velocity of the whole gas, which is, for gases with a low degree of ionisation, in sum the velocity of the neutrals $\mathbf{v}_\mathrm{n}$. When the magnetic field is strong enough the Lorentz force acts on the ions and leads to a drift between the ions and the neutrals. This effect is called *ambipolar drift* (described in Section 5.3).
Now let us assume that the Lorentz force acting only on the ions, is balanced by the friction between ions and neutrals, which affects both species. This is a good approximation, if the ion-neutral collisions are rapid enough. Then we have a force equilibrium

$$\mathbf{F}_\mathrm{f,i} + \mathbf{F}_\mathrm{f,n} = \mathbf{F}_\mathrm{L}. \tag{7.4}$$

The force due to friction for a particle with mass m and velocity $\mathbf{v}$ is in general

$$\mathbf{F}_\mathrm{f} = m\frac{\mathrm{d}\mathbf{v}}{\mathrm{d}t} \approx m\nu_\mathrm{ni}\mathbf{v}, \tag{7.5}$$

where we have approximated the time derivation of the velocity by the product of velocity and collision frequency ν_in.
The Lorentz force (4.18), which acts on a particle with charge q in a magnetic field, can be combined with the Maxwell equation (4.12) in order to substitute the particle velocity $\mathbf{v}$

$$\mathbf{F}_\mathrm{L} = \frac{q}{c}\mathbf{v}\times\mathbf{B} = \frac{V}{4\pi}(\nabla\times\mathbf{B})\times\mathbf{B}. \tag{7.6}$$

Here we have used the definition of the current density $\mathbf{j} = q/V\mathbf{v}$, where V is the volume.
Substituting the friction and the Lorentz force into equation (7.4) gives us

$$\begin{aligned} m_\mathrm{i}\nu_\mathrm{ni}\mathbf{v}_\mathrm{i} - m_\mathrm{n}\nu_\mathrm{ni}\mathbf{v}_\mathrm{n} &= \frac{V}{4\pi}(\nabla\times\mathbf{B})\times\mathbf{B} \\ \Rightarrow \rho_\mathrm{i}\nu_\mathrm{ni}(\mathbf{v}_\mathrm{i}-\mathbf{v}_\mathrm{n}) &= \frac{1}{4\pi}(\nabla\times\mathbf{B})\times\mathbf{B} \\ \Leftrightarrow \mathbf{v}_\mathrm{i} &= \frac{1}{4\pi\rho_\mathrm{i}\nu_\mathrm{ni}}(\nabla\times\mathbf{B})\times\mathbf{B} + \mathbf{v}_\mathrm{n} \\ &= a(\nabla\times\mathbf{B})\times\mathbf{B} + \mathbf{v}_\mathrm{n}, \end{aligned} \tag{7.7}$$

where we have assumed that the masses of the ions and the neutrals are almost equal ($m_\mathrm{i} \approx m_\mathrm{n}$) and defined a mass density of the ions $\rho_\mathrm{i} = m_\mathrm{i}/V$. Furthermore, we have introduced a coefficient a with

$$a \equiv \frac{1}{4\pi\rho_\mathrm{i}\nu_\mathrm{ni}}. \tag{7.8}$$

If the collision rate between the neutrals and the ions ν_ni is very high, the two fluids are coupled very well and we have ideal MHD. In this case the coefficient a vanishes and from equation (7.7) it follows that the velocity of the ions equals the velocity of the neutrals. If the collision rate is low the velocities of ions and neutrals are different, leading to ambipolar diffusion.
Substituting the velocity of the ions into (7.2) gives an induction equation, which takes the ambipolar diffusion into account

$$\frac{\partial\mathbf{B}}{\partial t} = \nabla\times\left(\mathbf{v}_\mathrm{n}\times\mathbf{B} - a((\nabla\times\mathbf{B})\times\mathbf{B})\times\mathbf{B} - \eta\nabla\times\mathbf{B}\right). \tag{7.9}$$

We will use this induction equation, which is generalised for ambipolar diffusion, to determine the evolution equation for the magnetohydrodynamical dynamos.

7.2 Large-Scale Dynamo: Time Evolution of the Mean Field

The initial point of our analysis is the induction equation, which describes the evolution of the total magnetic field in time. An iterative solution to the first order in a timestep δt of equation (7.9) gives us

$$\mathbf{B}(\mathbf{x},\delta t) = \mathbf{B}(\mathbf{x},0)+\delta t\eta\nabla^2\mathbf{B}(\mathbf{x},0)+\int_0^{\delta t} \mathrm{d}t\nabla\times\mathbf{D}_1(\mathbf{x},t)+\int_0^{\delta t}\mathrm{d}t\int_0^{\delta t}\mathrm{d}s\nabla\times\mathbf{D}_2(\mathbf{x},t,s) \tag{7.10}$$

with

$$\mathbf{D}_1(\mathbf{x},t) = \mathbf{v}_\mathrm{i}(\mathbf{x},t)\times\mathbf{B}(\mathbf{x},0) \tag{7.11}$$

$$\mathbf{D}_2(\mathbf{x},t,s) = \delta\mathbf{v}(\mathbf{x},t)\times[\nabla\times(\delta\mathbf{v}(\mathbf{x},s)\times\mathbf{B}(\mathbf{x},0))] \tag{7.12}$$

Taking the ensamble average of the fluctuating velocity field $\delta\mathbf{v}$ over equation (7.10) and simultaneously taking the limit of $\delta t\to 0$ leads to

$$\frac{\partial\langle\mathbf{B}\rangle}{\partial t} = \nabla\times[\langle\mathbf{v}\rangle\times\langle\mathbf{B}\rangle + 2C(0)\langle\mathbf{B}\rangle - (\eta+T_\mathrm{L}(0))\nabla\times\langle\mathbf{B}\rangle]+\langle\nabla\times\mathbf{v}_\mathrm{D}\times\mathbf{B}\rangle\,. \tag{7.13}$$

$T_\mathrm{L}(r)$ is the longitudinal part of the correlation function of the turbulent velocity field $\delta\mathbf{v}$ and $C(r)$ corresponds to helicity (see Section 3.1.2). Furthermore, we have defined the drift velocity $\mathbf{v}_\mathrm{D}\equiv\mathbf{v}_\mathrm{i}-\mathbf{v}_\mathrm{n}$.
Now let us assume that the magnetic fluctuation field $\delta\mathbf{B}$ is, like the velocity field, a homogeneous, isotropic Gaussian random field with zero mean. Then we can write the correlation function as

$$\langle\delta B_i(\mathbf{x},t)\delta B_j(\mathbf{y},t)\rangle = M_\mathrm{ij}(r,t) \tag{7.14}$$

with the two-point correlation function

$$M_\mathrm{ij}(r,t) = \left(\delta_\mathrm{ij}-\frac{r_\mathrm{i}r_\mathrm{j}}{r^2}\right)M_\mathrm{N}(r)+\frac{r_\mathrm{i}r_\mathrm{j}}{r^2}M_\mathrm{L}(r)+H(r)\epsilon_\mathrm{ijk}r^\mathrm{k}. \tag{7.15}$$

As the magnetic field is divergence free, we can derive a relation between the transverse and the longitudinal correlation function,

$$M_\mathrm{N} = \frac{1}{2r}\frac{\partial}{\partial r}\left(r^2M_\mathrm{L}(r)\right), \tag{7.16}$$

where we have used that $(r_ir_j/r^2)M_{ij}=M_\mathrm{L}$ and $(r_i/r_j)M_{ij}=M_\mathrm{N}$. We can use this to simplify equation (7.13), for which we get after a some algebra

$$\frac{\partial\mathbf{B}_0}{\partial t} = \nabla\times[\mathbf{v}_0\times\mathbf{B}_0+\alpha_\mathrm{eff}\mathbf{B}_0-\eta_\mathrm{eff}\nabla\times\mathbf{B}_0], \tag{7.17}$$

where we have defined the effective parameters

$$\alpha_{\text{eff}} = 2C(0) - 4aH(0,t) + a(\mathbf{B}_0 \cdot \nabla \times \mathbf{B}_0), \tag{7.18}$$

$$\eta_{\text{eff}} = \eta + T_{\text{L}}(0) + 2aM_{\text{L}}(0,t) + a\mathbf{B}_0^2. \tag{7.19}$$

The evolution equation of the mean magnetic field (7.17) looks very similar to the induction equation. The only difference is that the two effective parameters α_{eff} and η_{eff} appear. The term including α_{eff} is responsible for the alpha effect of the large-scale dynamo (see alpha-omega dynamo in Section 6.3.3). The last term in (7.17) is a diffusion term. The effective parameter η_{eff} contains, besides the usual magnetic diffusivity η, a turbulent diffusivity $T_{\text{L}}(0)$ and terms including from ambipolar diffusion coefficient.

7.3 Small-Scale Dynamo: Time Evolution of Magnetic Fluctuations

In 1968 Kazantsev developed a theory for describing the time evolution of the fluctuating magnetic energy. He found that the field grows due to turbulent motions of a conducting fluid [63]. The mechanism of converting kinetic energy into magnetic energy in this way is known as the turbulent or small-scale dynamo.
In this section we describe the Kazantsev theory following the formalism proposed by Brandenburg and Subramanian [61] and Subramanian [15]. For simplicity we ignore from now on the effects due to helicity, i.e. $C(r) = 0$, and ambipolar diffusion, i.e. $a = 0$.

7.3.1 Kazantsev Theory

In the last section we have introduced the correlation function of the fluctuating magnetic field $\langle \delta B_i \delta B_j \rangle$ in equation (7.14). The time derivative of this is

$$\begin{aligned}
\frac{\partial M_{ij}}{\partial t} &= \frac{\partial}{\partial t}\left(\langle \delta B_i \delta B_j \rangle\right) \\
&= \frac{\partial}{\partial t}\left(\langle B_i B_j \rangle - \langle B_i \rangle \langle B_j \rangle\right) \\
&= \left\langle \frac{\partial B_i}{\partial t} B_j \right\rangle + \left\langle B_i \frac{\partial B_j}{\partial t} \right\rangle - \frac{\partial}{\partial t}\left(\langle B_i \rangle \langle B_j \rangle\right)
\end{aligned} \tag{7.20}$$

In the upper equation we can substitute the induction equation

$$\frac{\partial \mathbf{B}}{\partial t} = \nabla \times \mathbf{v} \times \mathbf{B} - \eta \nabla \times \nabla \times \mathbf{B}, \tag{7.21}$$

where $\eta \equiv c^2/(4\pi\sigma)$ is the magnetic diffusivity with the speed of light c and the electrical conductivity σ, and the evolution equation of the magnetic mean field

(7.17). After a lengthy derivation (see [61]) this leads to

$$\frac{\partial M_{\mathrm{L}}}{\partial t} = 2\kappa_{\mathrm{diff}} M_{\mathrm{L}}'' + 2\left(\frac{4\kappa_{\mathrm{diff}}}{r} + \kappa_{\mathrm{diff}}'\right) M_{\mathrm{L}}' + \frac{4}{r}\left(\frac{T_{\mathrm{N}}}{r} - \frac{T_{\mathrm{L}}}{r} - T_{\mathrm{N}}' - T_{\mathrm{L}}'\right) M_{\mathrm{L}} \quad (7.22)$$

with

$$\kappa_{\mathrm{diff}}(r) = \eta + T_{\mathrm{L}}(0) - T_{\mathrm{L}}(r). \quad (7.23)$$

The $'$ denotes differentiation with respect to r. The diffusion of the magnetic correlations, κ_{diff}, contains besides the magnetic diffusivity η the scale-dependent turbulent diffusion $T_{\mathrm{L}}(0) - T_{\mathrm{L}}(r)$.
With the solution of equation (7.22) we can calculate also M_{N} by using relation (7.16) and so find the total correlation function of the magnetic field fluctuations M_{ij}. We note that this quantity is proportional to the energy density of the magnetic field $B^2/(8\pi)$.
In order to separate the time from the spatial coordinates we use the ansatz

$$M_{\mathrm{L}}(r,t) \equiv \frac{1}{r^2\sqrt{\kappa_{\mathrm{diff}}}}\psi(r)\mathrm{e}^{2\Gamma t}. \quad (7.24)$$

The factor Γ in the exponential function is called the growth rate of the small-scale dynamo. Substituting this ansatz in equation (7.22) gives us

$$\boxed{-\kappa_{\mathrm{diff}}(r)\frac{\mathrm{d}^2\psi(r)}{\mathrm{d}^2 r} + U\psi(r) = -\Gamma\psi(r)}. \quad (7.25)$$

This is the *Kazantsev equation*. It formally looks like the quantum-mechanical Schrödinger equation with a "mass" $\hbar^2/(2\kappa_{\mathrm{diff}})$ and the "potential"

$$U(r) \equiv \frac{\kappa_{\mathrm{diff}}''}{2} - \frac{(\kappa_{\mathrm{diff}}')^2}{4\kappa_{\mathrm{diff}}} + \frac{2\kappa_{\mathrm{diff}}}{r^2} + \frac{2T_{\mathrm{N}}'}{r} + \frac{2(T_{\mathrm{L}} - T_{\mathrm{N}} + \kappa_{\mathrm{diff}})}{r^2}. \quad (7.26)$$

It describes the *kinematic limit*, because U is independent of the time.

7.3.2 WKB-Approximation

We can use common methods from quantum mechanics, like the WKB-approximation, to solve the Kazantsev equation (7.25). WKB stands for Wentzel, Kramers and Brillouin, who developed this method in 1926 [64].

Solution of the Kazantsev Equation in WKB-Approximation In order to use the standard WKB-method, we have to make some substitutions. Let us first introduce a new radial coordinate x by defining $r \equiv \mathrm{e}^x$. This leads to

$$\frac{\kappa_{\mathrm{diff}}(x)}{\mathrm{e}^x}\frac{\mathrm{d}}{\mathrm{d}x}\left(\frac{1}{\mathrm{e}^x}\frac{\mathrm{d}\psi(x)}{\mathrm{d}x}\right) - (\Gamma + U(x))\,\psi(x) = 0. \quad (7.27)$$

Next we eliminate the first derivative terms through the substitution

$$\psi(x) \equiv \mathrm{e}^{x/2}\theta(x), \tag{7.28}$$

to obtain

$$\frac{\mathrm{d}^2\theta(x)}{\mathrm{d}x^2} + p(x)\theta(x) = 0, \tag{7.29}$$

with the definition

$$p(x) \equiv -\frac{(\Gamma + U(x))\mathrm{e}^{2x}}{\kappa_{\mathrm{diff}}(x)} - \frac{1}{4}. \tag{7.30}$$

The WKB-solutions of this equations are linear combinations of

$$\theta(x) = \frac{1}{p^{1/4}}\exp\left(\pm i \int \sqrt{p(x')}\mathrm{d}x'\right). \tag{7.31}$$

The boundary conditions for $\psi(r)$ and $\theta(x)$ are

$$\begin{aligned} \psi(r) &\xrightarrow{r\to 0,\infty} 0 \\ \Rightarrow \theta(x) &\xrightarrow{r\to\pm\infty} 0. \end{aligned} \tag{7.32}$$

We can make some predictions about the shape of the function $\theta(x)$. For very small x ($x \to -\infty$), $p(x)$ goes to $-1/4 < 0$, which leads to exponentially growing and decaying solutions of θ. In the other limit ($x \to \infty$), $p(x) \to -\Gamma/\eta\ \mathrm{e}^{2x}$, so we have growing mode solutions only for positive Γ. The boundary conditions require that θ grows exponentially for $x \to -\infty$ and decay exponentially at $x \to \infty$. In order to arrange this, $p(x)$ must go through zero, so $U(x)$ needs to become negative for some r. From now on we label the roots of $U(x)$ as x_1 and $x_2 > x_1$. As $U(r)$ gets negative for some r, $p(r)$ gets positive for certain values of r. This means that we have oscillatory solutions for $x_1 < x < x_2$. The conditions for the eigenvalues Γ in this case is [65]

$$\boxed{\int_{x_1}^{x_2} \sqrt{p(x')}\mathrm{d}x' = \frac{2n+1}{2}\pi} \tag{7.33}$$

for different excitation levels $n \in \mathbb{N}$. In this work we concentrate on the lowest mode $n = 0$.

Validity of the WKB-Approximation in General In order to find the limits in which the WKB-method leads to valid solutions of the Kazantsev equation, we derive the differential equation that is solved exactly by

$$\theta(x) = \frac{1}{p^{1/4}}\exp\left(\pm i \int_{x_1}^{x_2} \sqrt{p(x')}\mathrm{d}x'\right). \tag{7.34}$$

The second derivative of $\theta(x)$ with respect to x can be written as

$$\theta''(x) + \left(1 + \frac{p''}{4p^2} - \frac{3}{16}\frac{(p')^2}{p^3}\right) p\theta(x) = 0, \tag{7.35}$$

where now $'$ denotes $\mathrm{d}/\mathrm{d}x$. This equation results in the Kazantsev equation (7.29) if

$$|f(x)| \ll 1, \tag{7.36}$$

with

$$f(x) \equiv \frac{p''}{4p^2} - \frac{3}{16}\frac{(p')^2}{p^3}. \tag{7.37}$$

We use this result in the next section to check in which range of parameters the WKB-method produces accurate results of the Kazantsev equation.

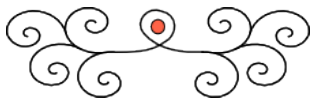

8 Small-Scale Dynamo with Different Turbulence Models

In this section we use our model of the turbulent velocity correlation function (3.19) and (3.23) as the input for the Kazantsev theory. We solve the Kazantsev equation in order to get the characteristic properties of the small-scale dynamo. For this we use the WKB-method which gives a good approximative solution for large magnetic Prandtl numbers. In fact, in the limit of infinite magnetic Prandtl numbers the WKB-approximation is an exact solution of the Kazantsev equation.
In this section, we closely follow Schober et al. [66].

8.1 Validity of the WKB-Approximation

The WKB-method is only an approximate solution of the Kazantsev equation. We derived condition (7.36), $|f| \ll 1$, for which the WKB-method is valid in order to find solutions. In z-space, f reads

$$f(z) \equiv \frac{z^2 p''(z) + 2zp'(z)}{4p(z)^2} - \frac{3}{16}\frac{(zp'(z))^2}{p(z)^3}. \tag{8.1}$$

However, we have seen that the magnetic field is amplified strongest on the scale $\ell_c(z) = \sqrt{Pm/3}$, as here the potential U has its minimum. So we analyse $f(z, \Gamma)$ on this scale and get a dependency of the Prandtl number Pm. Hence we label $f(\ell_c, \Gamma) \equiv f(Pm, \Gamma)$.
One can show that the $f(Pm, \Gamma)$ vanishes in the limit of large Prandtl numbers for all Γ and all turbulence types,

$$\lim_{Pm\to\infty} f(Pm, \Gamma) = 0. \tag{8.2}$$

This means that the WKB-method is very good in the limit of large magnetic Prandtl numbers.

8.1.1 Validity of the WKB-Approximation for Kolmogorov Turbulence

In order to check also lower Prandtl numbers we plot $f(Pm, \bar{\Gamma})$ for different normalised growth rates

$$\boxed{\bar{\Gamma} \equiv \frac{L}{V}\Gamma}. \tag{8.3}$$

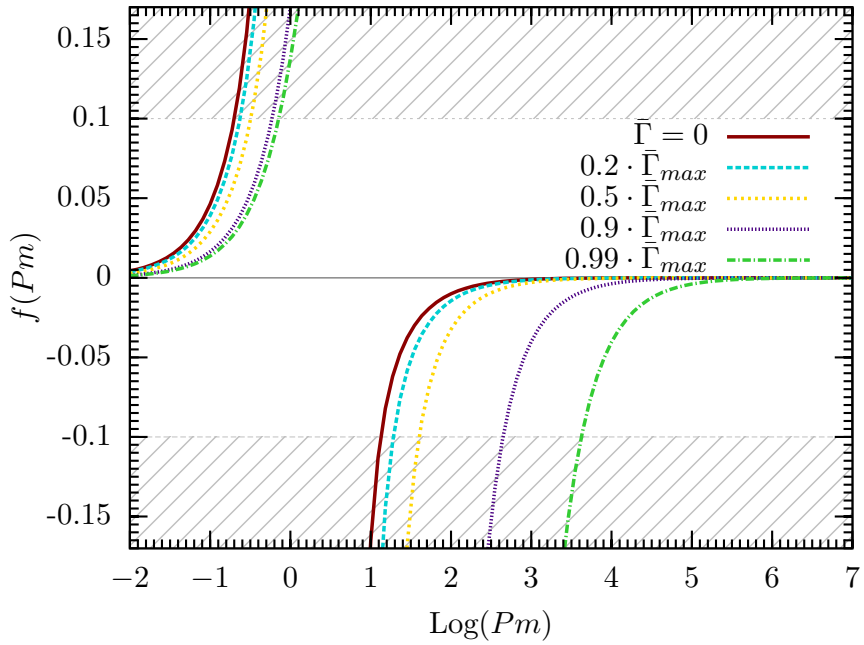

Figure 8.1: The function $f(Pm, \bar{\Gamma})$ for different values of the normalised growth rate for Kolmogorov turbulence. $\bar{\Gamma}_{\max}$ is the normalised growth rate in the limit of infinite magnetic Prandtl numbers, $\bar{\Gamma}_{\max} = 37/36\ Re^{1/2}$. The WKB-approximation is valid within the non-hatched area, i.e., for $|f(Pm, \Gamma)| < 0.1$.

and Kolmogorov turbulence in Figure 8.1. However, one can show that $f(Pm, \bar{\Gamma})$ does not depend on the Reynolds number for Kolmogorov turbulence. So we choose values for $\bar{\Gamma}$ between 0 and the maximal value $\bar{\Gamma}_{\max}$ for the plot in Figure 8.1, where $\bar{\Gamma}_{\max}$ is the value for an infinite Prandtl number and depends on the Reynolds number. One can see that the critical Prandtl number for the WKB-approximation gets larger with increasing normalised growth rate.
To make a more quantitative estimate of the critical Prandtl number we hatched the area above $f(Pm, \bar{\Gamma}) = 0.1$ and below $f(Pm, \bar{\Gamma}) = -0.1$. When f is not in this area, its absolute value is smaller than ten percent. We take this as a threshold for our approximation.
We find that our method is applicable in the case of $\bar{\Gamma} = 0$ for

$$Pm \gtrsim 13. \tag{8.4}$$

For higher normalised growth rates the critical Prandtl number increases.

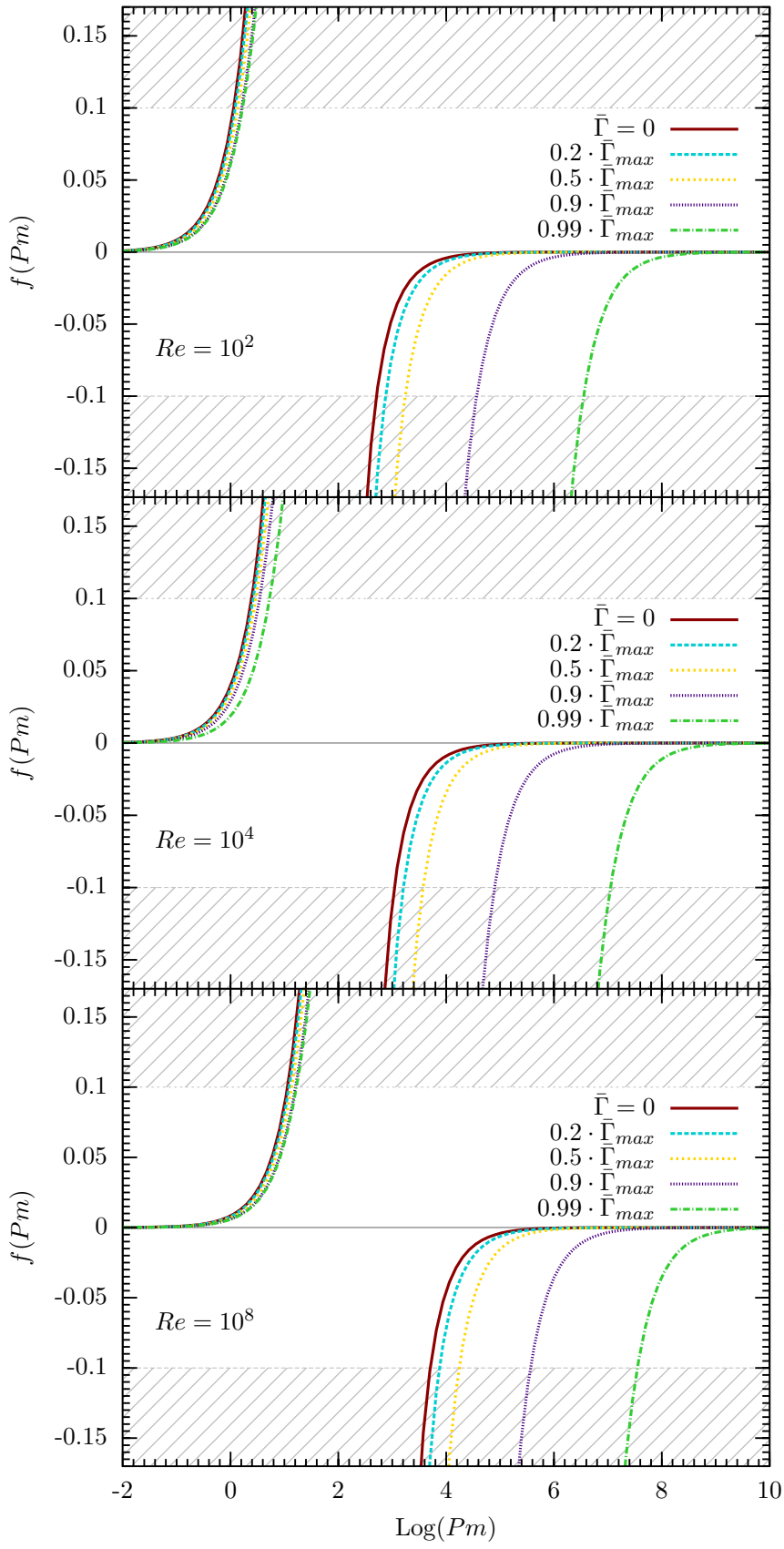
0.15
0.1
0.05
0
-0.05
-0.1
-0.15
$f(Pm)$
$\bar{\Gamma} = 0$
$0.2 \cdot \bar{\Gamma}_{max}$
$0.5 \cdot \bar{\Gamma}_{max}$
$0.9 \cdot \bar{\Gamma}_{max}$
$0.99 \cdot \bar{\Gamma}_{max}$
$Re = 10^2$
$Re = 10^4$
$Re = 10^8$
-2
0
2
4
6
8
10
$\mathrm{Log}(Pm)$

8.1.2 Validity of the WKB-Approximation for Burgers Turbulence

We can analyse of the validity of the WKB-solutions for Burgers turbulence in the same way as for Kolmogorov turbulence using (7.36).
However, we find that the function f given in (8.1) now not only depends on the normalised growth rate $\bar{\Gamma}$ and the Prandtl number Pm, but also on the Reynolds number Re. The result is shown in Figure 8.2, where we plot f against the Prandtl number for different Reynolds numbers and different normalised growth rates.
We again determine the critical Prandtl number for the WKB-method for the a vanishing normalised growth rate. For our different values of the Reynolds number we get the following critical Prandtl numbers at vanishing growth rate

$$Pm(Re = 10^2) \gtrsim 500, \tag{8.5}$$
$$Pm(Re = 10^4) \gtrsim 1100, \tag{8.6}$$
$$Pm(Re = 10^8) \gtrsim 5100. \tag{8.7}$$

8.2 Critical Magnetic Reynolds Number for Small-Scale Dynamo Action

8.2.1 Derivation of the Critical Magnetic Reynolds Number

Intuitively, one expects that the high magnetic diffusivity for very low magnetic Reynolds numbers prevents the amplification of the magnetic field. Even higher diffusivity eventually results in a net decrease of the field strength. In this section we calculate a critical magnetic Reynolds number Rm_{crit} for small-scale dynamo action. To accomplish this we set the growth in our equations zero.
It should be noted that we use the inertial range ($\ell_{\mathrm{c}} < r < L$) for determining Rm_{crit} as the potential in this range is always negative and for that we have a positive growth rate (see Figure 8.3). In this range with our turbulence spectrum (see equations (3.19) and (3.23)) and $\Gamma = 0$ we get for the p-function (7.30)

$$p(y) = \frac{-9/4 - a(\vartheta) Rm_{\mathrm{crit}} y^{\vartheta+1} + b(\vartheta) Rm_{\mathrm{crit}}^2 y^{2(\vartheta+1)}}{\left(1 + \frac{1}{3} Rm_{\mathrm{crit}} y^{\vartheta+1}\right)^2} \tag{8.8}$$

Figure 8.2 *(facing page)*: The function $f(Pm, \bar{\Gamma})$ for fixed Reynolds numbers and different values of the normalised growth rate for Burgers turbulence. Notice that in the limit $Pm \to \infty$ the normalised growth rates are $\bar{\Gamma} = 0.85$ for $Re = 10^2$, $\bar{\Gamma} = 3.95$ for $Re = 10^4$ and $\bar{\Gamma} = 85.1$ for $Re = 10^8$. The WKB-approximation is valid within the non-hatched area, i.e., for $f(Pm, \bar{\Gamma}) < 0.1$.

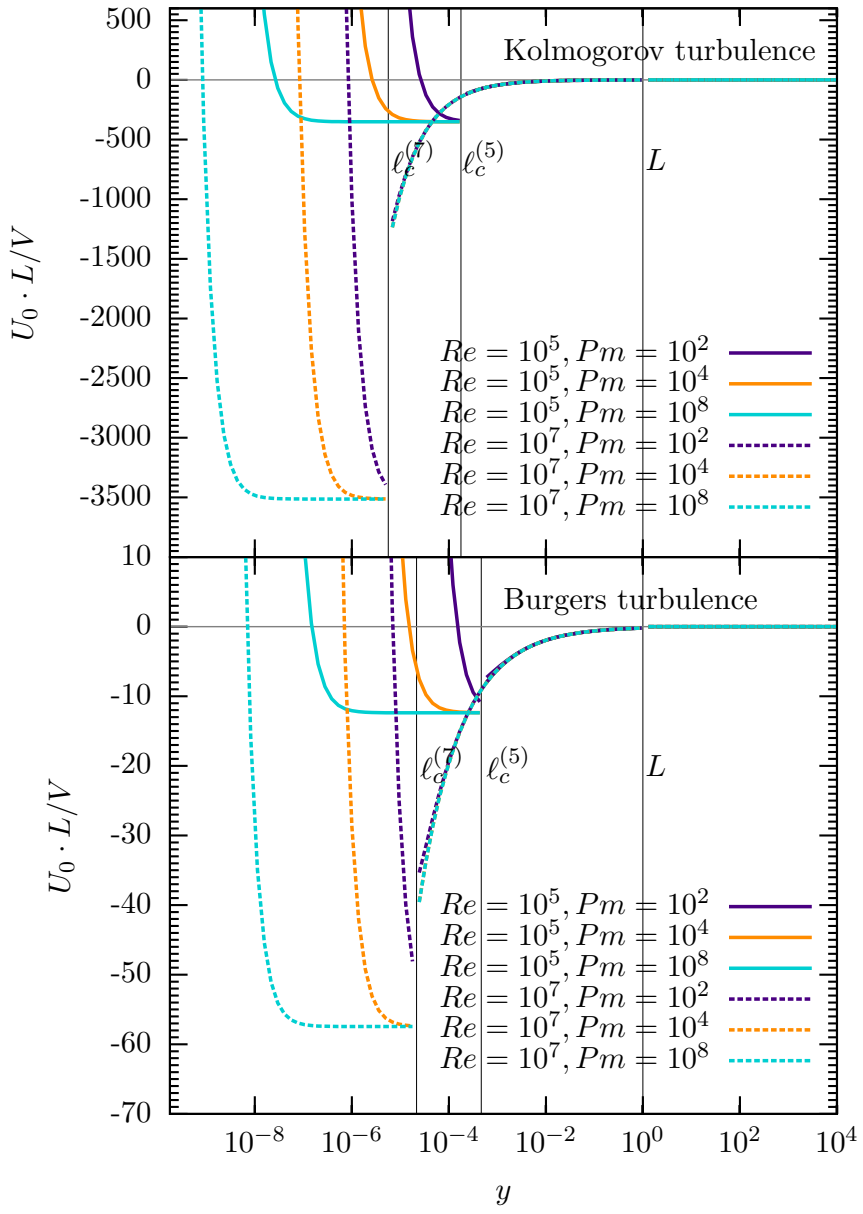

Figure 8.3: The potential depending on the dimensionless parameter $y \equiv r/L$ for Kolmogorov ($\vartheta = 1/3$) and Burgers turbulence ($\vartheta = 1/2$). We choose two different Reynolds numbers, $Re = 10^5$ and $Re = 10^7$, and different Prandtl numbers, $Pm = 10^2$, $Pm = 10^4$ and $Pm = 10^8$. The cut-off scale ℓ_c depends on the turbulence model and the Reynolds number. For Kolmogorov turbulence $\ell_c = Re^{-3/4}L$, for Burgers turbulence $\ell_c = Re^{-2/3}L$. A Reynolds number 10^x is indicated in the cut-off scale as $\ell_c^{(x)}$.

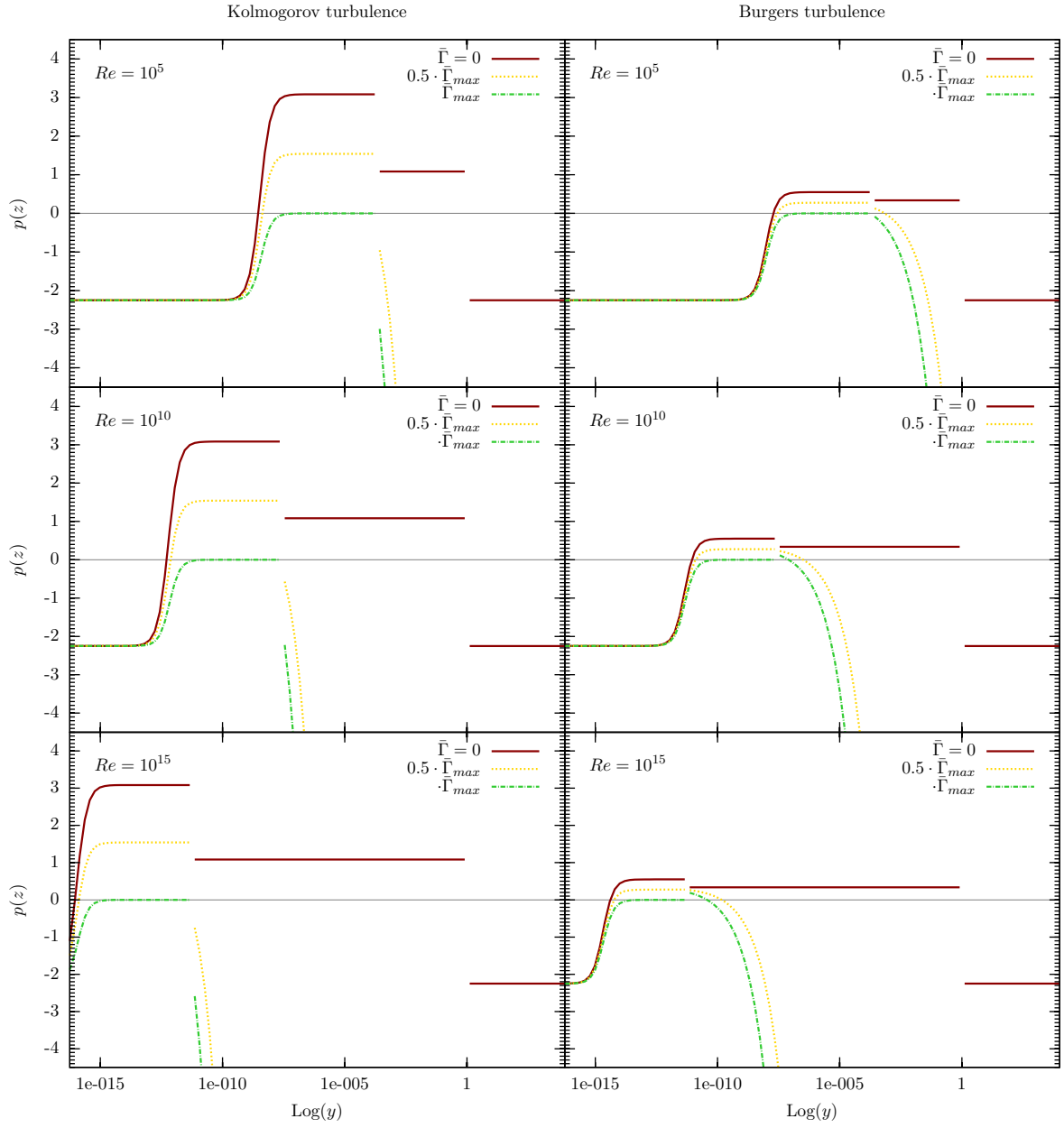

Figure 8.4: The p-function for a magnetic Prandtl number of 10^{10} as a function of the dimensionless parameter $y \equiv r/L$ for Kolmogorov ($\vartheta = 1/3$) and Burgers turbulence ($\vartheta = 1/2$). We set here $L = 1$ and choose three different Reynolds numbers, $Re = 10^5$, $Re = 10^{10}$ and $Re = 10^{15}$. The cut-off scale ℓ_c depends on the turbulence model and the Reynolds number. For Kolmogorov turbulence $\ell_c = Re^{-3/4}L$, for Burgers turbulence $\ell_c = Re^{-2/3}L$.

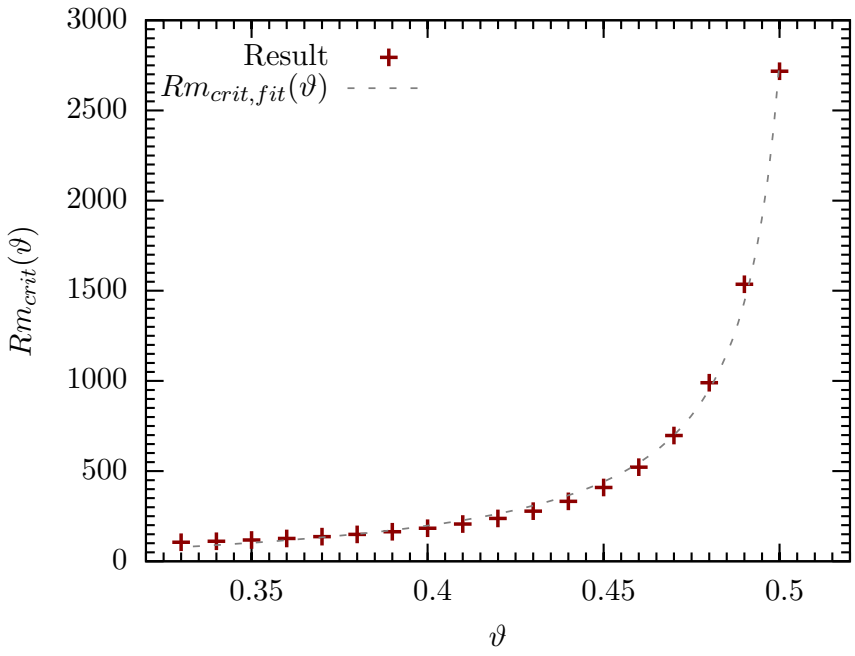

Figure 8.5: The dependence of the critical magnetic Reynolds number Rm_{crit} from the slope of the turbulent velocity spectrum ϑ. The dashed line is an empirical fit through our results.

with $a(\vartheta) \equiv 5/6 - 79/30\ \vartheta + 157/30\ \vartheta^2$ and $b(\vartheta) \equiv 14/15\ \vartheta - 103/60\ \vartheta^2$.
Now we can evaluate the eigenvalue condition (7.33) for this $p(y)$ at the "ground state" $n = 0$:

$$\int_{y_{0_1}}^{y_{0_2}} \sqrt{p(y)} \frac{\mathrm{d}y}{y} = \frac{\pi}{2}, \tag{8.9}$$

in which the additional y comes from the substitution $y = r/L = e^x/L$. The limits of the integral are the roots of $p(y)$. There is only one real and positive root of $p(y)$, which we label y_1. For the upper limit we have to realise that the potential (7.26) changes for $y > 1$ to $2\eta/(yL)^2$, which is clearly always positive. Furthermore, also the diffusion coefficient $\kappa_{\mathrm{diff}} = \eta + T_{\mathrm{L}}(0) > 0$ for $y > 1$. With U and κ_{diff} being positive $p(y)$ is negative in this range, which means that $p(y)$ needs to go through zero during this transition. So we have our second root at roughly $r \approx L$ and $y_2 = 1$. We can solve equation (8.9) numerically for the critical magnetic Reynolds number Rm_{crit} if we put in a fixed value of ϑ. Recall, that ϑ was defined in the inertial range of the turbulence via the relation $v(\ell) \propto \ell^{\vartheta}$. Results for common models in the literature can be found in Table 8.1. In Figure 8.5 we show how the critical magnetic Reynolds number depends on ϑ. Here one can see that the critical magnetic Reynolds number increases rapidly, as ϑ gets closer to its maximum value of 1/2. An empirical fit $Rm_{\mathrm{crit,fit}}(\vartheta)$ through this data in the range $0.33 < \vartheta < 0.5$ is

$$Rm_{\mathrm{crit,fit}}(\vartheta) = 88 \cdot (\tan(2.68\vartheta + 0.2) - 1)\,. \tag{8.10}$$

Model/Reference	ϑ	$Rm_{\rm crit}$	$\bar{\Gamma}$ $(Pm \to \infty)$
Kolmogorov [10]	1/3	≈ 107	$37/36\ Re^{1/2}$
intermittency of Kolmogorov turbulence (She and Leveque [67])	0.35	≈ 118	$0.94\ Re^{0.48}$
driven supersonic MHD-turbulence (Boldyrev et al.[68])	0.37	≈ 137	$0.84\ Re^{0.46}$
observation in molecular clouds (Larson [17])	0.38	≈ 149	$0.79\ Re^{0.45}$
solenoidal forcing of the turbulence (Federrath et al. [18])	0.43	≈ 227	$0.54\ Re^{0.40}$
compressive forcing of the turbulence (Federrath et al. [18]), observations in molecular clouds (Ossenkopf and Mac Low [69])	0.47	≈ 697	$0.34\ Re^{0.36}$
Burgers [12]	1/2	≈ 2718	$11/60\ Re^{1/3}$

Table 8.1: The critical magnetic Reynolds number $Rm_{\rm crit}$ and the normalised growth rate of the small-scale dynamo $\bar{\Gamma}$ in the limit of infinite magnetic Prandtl numbers. We show our results for different types of turbulence, which are characterised by the exponent ϑ of the slope of the turbulent velocity spectrum, $v(\ell) \propto \ell^{\vartheta}$. The extreme values of ϑ are 1/3 for Kolmogorov turbulence and 1/2 for Burgers turbulence.

Furthermore, we collect the results for common turbulence models in the literature in Table 8.1. The two extrema of turbulence are Kolmogorov turbulence [10], i.e. incompressible turbulence, with $\vartheta = 1/3$ and Burgers turbulence with $\vartheta = 1/2$, which describes highly compressible turbulence with vanishing rotational component [12]. Between those extreme values we choose values of ϑ from observations of molecular clouds, like $\vartheta \approx 0.38$ from Larson [17] and $\vartheta \approx 0.47$ from Ossenkopf and Mac Low [69]. Furthermore, we give $\vartheta \approx 0.35$ as an example for a theoretical model of intermittency [67]. Numerical experiments give $\vartheta \approx 0.37$ for driven supersonic MHD-turbulence [68] and $\vartheta \approx 0.43$ and $\vartheta \approx 0.47$ for solenoidal and compressive forcing of the turbulence [18]. Notice, however that the mean values of ϑ from observations and simulations have a typical uncertainty of ten percent.
We find that the small-scale dynamo is more easily excited in the case of a purely rotational turbulent velocity field, i.e. for Kolmogorov turbulence, where we find $Rm_{\rm crit} \approx 110$. The critical magnetic Reynolds number for a turbulent field with a vanishing rotational component, i.e. Burgers turbulence, is roughly 2700.

8.2.2 Discussion of the Critical Magnetic Reynolds Number

From these results we see that for all types of turbulence a high magnetic Reynolds number needs to be exceeded for small-scale dynamo action. In astrophysical objects we often find very high magnetic Reynolds numbers (see compilation in [62]). The core of Jupiter, for example, has a $Rm \approx 10^6$, the solar convection zone has $Rm \approx 10^8$ and the solar corona already $Rm \approx 10^{12}$. In the interstellar medium we find $Rm \approx 10^{17}$ and in a typical galaxy about 10^{19}. Consequently, the critical magnetic Reynolds number is exceeded by far in nature and we expect that the small-scale dynamo operates in typical astrophysical objects.
Recent high-resolution numerical studies confirm the existence of a critical magnetic Reynolds number for small-scale dynamo action. Haugen et al. [70] find $Rm_{\mathrm{crit}} \approx 35$ for subsonic turbulence and $Rm_{\mathrm{crit}} \approx 70$ for supersonic turbulence at a magnetic Prandtl number of about unity. In numerical simulations, the magnetic Reynolds number can be estimated by $Rm \approx (\lambda/\ell_{\mathrm{c}})^{\vartheta+1}$, where λ is the typical size of turbulent structures and ℓ_{c} is the cut-off scale of the turbulence. The latter can be estimated with the minimal resolved size in a simulation Δx by $\ell_{\mathrm{c}} \approx 0.5\ \Delta x$ [71]. In resolution studies, Sur et al. [72] and Federrath et al. [21] find that the typical length of a turbulent fluctuation needs to be resolved with at least 30 grid cells in magnetohydrodynamical simulations of self-gravitating gas (see Figure 8.6). Only then the magnetic field is amplified exponentially, which is explained by the action of the small-scale dynamo.
For a physical interpretation of this result it is useful to take the *stretch-twist-fold-dynamo* as a toy-model of the turbulent dynamo, which is described in Section (6.3.3). This process works best in a purely solenoidal turbulent velocity field. Therefore, we expect the dynamo to be more easily excited in Kolmogorov turbulence. In order to see this process in simulations, one needs to resolve the stretching, twisting and folding of the field lines, which leads to the required high resolution.
The determination of the critical magnetic Reynolds number is, moreover, the first step to understand the saturation of the small-scale dynamo. If the magnetic field in a system increases, back reactions from the gas become more important. Then processes like the Lorentz force or ambipolar diffusion can change the properties of the gas and the magnetic Reynolds number can decrease. If the magnetic Reynolds number gets smaller than the critical magnetic Reynolds number, the magnetic field stops growing and the small-scale dynamo is saturated.

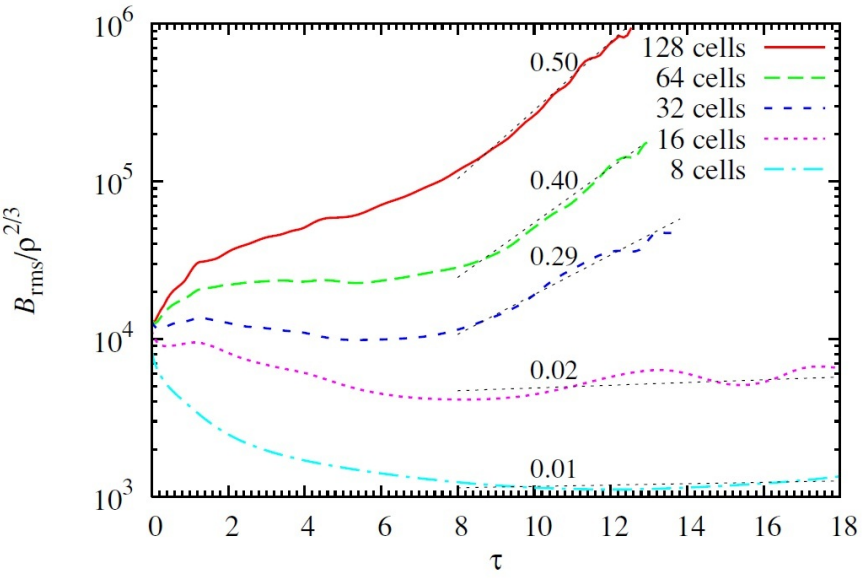

Figure 8.6: The growth of the magnetic field as a function of time in a numerical simulation from Federrath et al. [21]. As the effect due to gravitational compression is corrected, the pure dynamo growth is shown. The magnetic field only grows for resolutions higher that about 30 cells.

8.3 Growth Rate of the Small-Scale Magnetic Field

8.3.1 Derivation of the Growth Rate

Growth Rate in the Limit $Pm \to \infty$

In this paragraph we derive a general analytic solution for the growth rate Γ for an arbitrary slope of the turbulent velocity spectrum, in the limit of infinite magnetic Prandtl numbers.
As the potential has its minimum in the small-scale range, i.e. the dissipation range of the turbulence (see Figure 8.3), the growth rate, which is the eigenvalue of the Kazantsev equation, takes its maximum value there. So we expect the fastest growing mode to be in the small-scale range.
In order to have scale-independent equations, we introduce the substitution

$$z \equiv \left(\frac{V\sqrt{Re}}{3L\eta}\right)^{1/2} r = \left(\frac{Re^{3/2}Pm}{3}\right)^{1/2} y, \tag{8.11}$$

where the magnetic Prandtl number is $Pm = Rm/Re$.
The p-function in z-space, see (7.30) and (8.11), for the general turbulence spectrum

(3.19) in the dissipation range is

$$p(z) = \frac{A_0 z^4 - B_0 z^2 - 45 Re^{(3+7\vartheta)/(2+2\vartheta)}}{20 Re^{1/2} \left(Re^{(1+3\vartheta)/(2+2\vartheta)} + Re^{1/(1+\vartheta)} z^2\right)^2} \tag{8.12}$$

with the definitions

$$A_0 = Re^{(5+\vartheta)/(2+2\vartheta)} (163 - 304\vartheta) - \frac{20}{3} Re^{5/2} \bar{\Gamma}, \tag{8.13}$$

$$B_0 = (304\vartheta - 98)\, Re^2 + \frac{20}{3} Re^{(2+8\vartheta)/(1+\vartheta)} \bar{\Gamma}. \tag{8.14}$$

and the normalised growth rate $\bar{\Gamma}$ (8.3). In the limit of large Prandtl numbers z is large, too, and we can neglect the constant terms. We obtain

$$p(z) = \frac{Re^{-(5+\vartheta)/(2+2\vartheta)}}{20} \frac{A_0 z^2 - B_0}{z^2}. \tag{8.15}$$

The one real and positive root of this function is $z_1 = \sqrt{B_0/A_0}$. At the cut-off scale of the turbulence the p-function changes its sign. We take this as our second root and so have $z_2 = \sqrt{Pm/3}\; Re^{(3\vartheta-1)/(4\vartheta+4)}$. So we get for the general eigenvalue condition

$$\frac{Re^{-(5+\vartheta)/(4+4\vartheta)}}{2\sqrt{5}} \int_{z_1}^{z_2} \sqrt{\frac{A_0 z^2 - B_0}{z^4}} \mathrm{d}z = \frac{\pi}{2}, \tag{8.16}$$

resulting in the analytical solution of the integral

$$\frac{Re^{-(5+\vartheta)/(4+4\vartheta)}}{2\sqrt{5} z} \left[\sqrt{A_0} \ln\left(2\left(\sqrt{A_0} z + \sqrt{A_0 z^2 - B_0}\right)\right) - \sqrt{A_0 z^2 - B_0}\right]\Bigg|_{z_1}^{z_2} = \frac{\pi}{2}. \tag{8.17}$$

For $z_2 \gg 1$ this becomes

$$\frac{Re^{-(5+\vartheta)/(4+4\vartheta)}}{2\sqrt{5}} \sqrt{A_0} \left[1 - \ln\left(4\sqrt{A_0} z_2\right) + \frac{1}{2} \ln\left(4 B_0\right)\right] = \frac{\pi}{2}. \tag{8.18}$$

A zero-order iterative solution for $\bar{\Gamma}$ gives us

$$\bar{\Gamma} = \frac{163 - 304\vartheta}{60} Re^{(1-\vartheta)/(1+\vartheta)} - \left(\sqrt{5}\pi \frac{Re^{(5+\vartheta)/(4+4\vartheta)}}{\left[1 - \ln\left(4\sqrt{A_0} z_2\right) + 1/2 \ln\left(4 B_0\right)\right]}\right)^2, \tag{8.19}$$

which becomes for large Prandtl numbers

$$\bar{\Gamma} = \frac{163 - 304\vartheta}{60} Re^{(1-\vartheta)/(1+\vartheta)}. \tag{8.20}$$

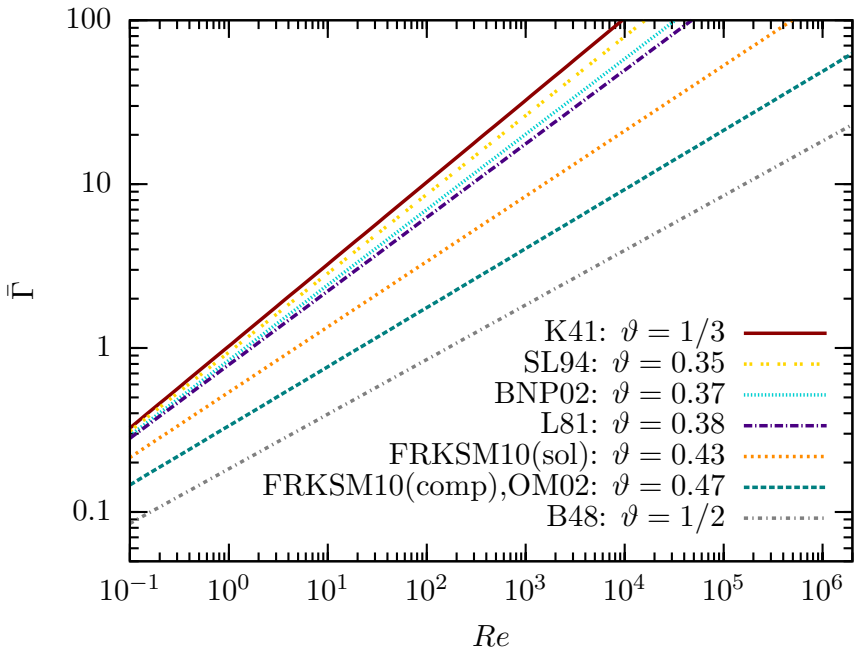

Figure 8.7: The normalised growth rate of the small-scale dynamo in the limit of infinite magnetic Prandtl numbers, depending on the Reynolds number, Re. For the slopes of the turbulent velocity spectrum ϑ we choose common values from the literature: K41 [10], SL94 [67], BNP02 [68], L81 [17], FRKSM10 [18] (sol: solenoidal forcing, comp: compressive forcing), OM02 [69], B48 [12].

As a result we get for the absolute growth rate Γ for a general slope of the turbulent velocity spectrum

$$\boxed{\Gamma = \frac{(163 - 304\vartheta)}{60} \frac{V}{L} Re^{(1-\vartheta)/(1+\vartheta)}} \tag{8.21}$$

in the limit $Pm \to \infty$.
In Figure 8.7 we show the dependency of the normalised growth rate $\bar{\Gamma}$ on the Reynolds number for different types of turbulence. One extreme case is incompressible turbulence, i.e. Kolmogorov turbulence, with $\bar{\Gamma} \propto Re^{1/2}$. In the other extreme case, highly compressible turbulence, i.e. Burgers turbulence, the growth rate increases only with $Re^{1/3}$. Altogether we find that the growth rate increases faster with the Reynolds number when the compressibility is lower.

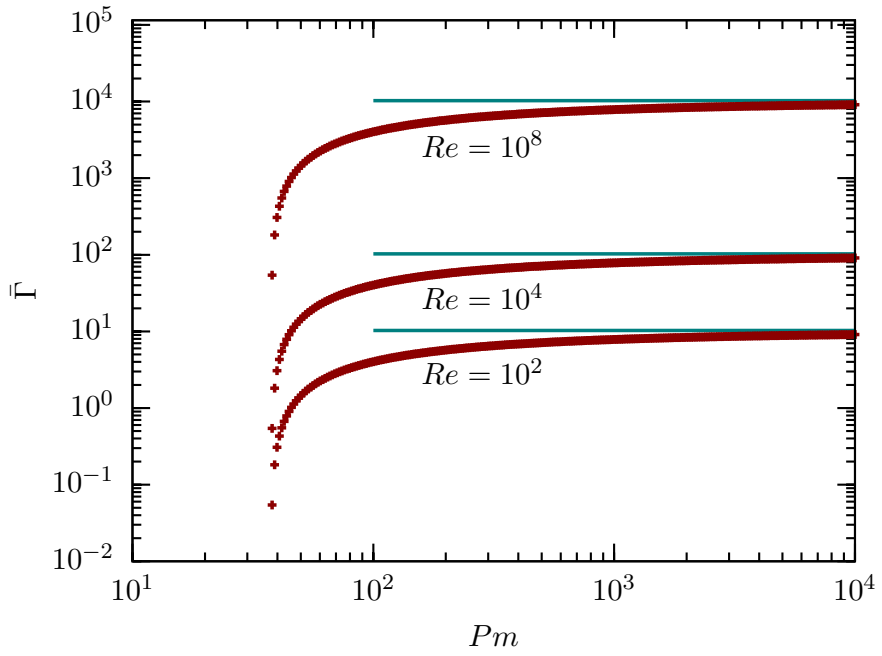

Figure 8.8: The normalised growth rate of the small-scale dynamo, depending on the magnetic Prandtl number, Pm, for Kolmogorov turbulence. We choose different values of the Reynolds number. Notice that in the limit $Pm \to \infty$ the normalised growth rates are $\bar{\Gamma} = 10.28$ for $Re = 10^2$, $\bar{\Gamma} = 102.78$ for $Re = 10^4$ and $\bar{\Gamma} = 10277.78$ for $Re = 10^8$. These limits are indicated in the plot as vertical lines.

Growth Rate as a Function of the Prandtl Number

In this section we discard the assumption of infinite Prandtl numbers. In this case we have to solve the full equation resulting from the WKB-method (7.33)

$$\int \frac{\sqrt{p(z)}}{z} \mathrm{d}z = \frac{\pi}{2}, \tag{8.22}$$

with $p(z)$ from (8.12). There is no analytical solution of this integral equation.
The numerical results of the normalised growth rate are shown in Figure 8.8 for Kolmogorov turbulence and in Figure 8.9 for Burgers turbulence. We plot the normalised growth rate depending on the Prandtl number for different values of the Reynolds number.

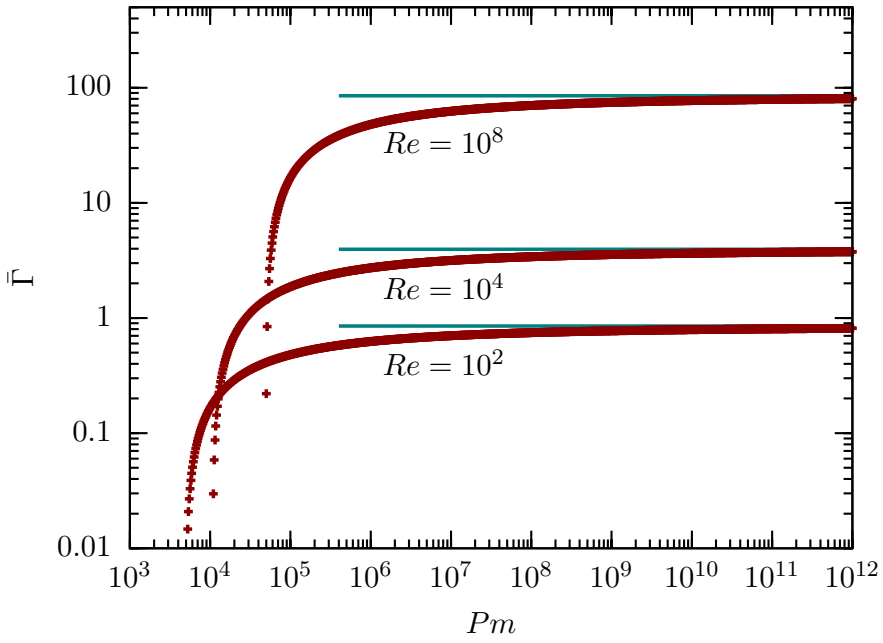

Figure 8.9: The normalised growth rate of the small-scale dynamo, depending on the magnetic Prandtl number, Pm, for Burgers turbulence. We choose different values of the Reynolds number. Notice that in the limit $Pm \to \infty$ the normalised growth rates are $\bar{\Gamma} = 0.85$ for $Re = 10^2$, $\bar{\Gamma} = 3.95$ for $Re = 10^4$ and $\bar{\Gamma} = 85.1$ for $Re = 10^8$. These limits are indicated in the plot as vertical lines.

8.3.2 Discussion of the Growth Rate

Our results show that the growth rate is proportional to the velocity V of the largest eddy divided by its length L. The ratio V/L is one over the turnover time of an eddy. Thus, the growth rate increases with decreasing turnover time, and the smallest modes grow at the highest rate. This is expected, because smaller turnover times lead to a faster tangling of the magnetic field lines.
Furthermore, the growth rate increases with increasing hydrodynamical Reynolds number for all types of turbulence, characterised by $v(\ell) \propto \ell^{\vartheta}$. In order to achieve the same growth rate for Kolmogorov and Burgers turbulence we have to provide a larger Reynolds number in the latter case. Assuming a different Reynolds numbers in both cases, Re^{K} and Re^{B}, the growth rate of the two different turbulence types are the same for $Re^{\mathrm{K}} \approx 0.18(Re^{\mathrm{B}})^{3/2}$. This fact can again be motivated with the stretch-twist-fold model (see Section 6). We need solenoidal modes, i.e. divergence-free modes, of the turbulence for this process [73], which explains that incompressible turbulence amplifies the magnetic field more effectively.
There are recent high-resolution numerical simulations that model the turbulent dynamo. The two limiting ways of driving the turbulence are solenoidal, i.e. divergence-

free, forcing and compressive, i.e. rotation-free, forcing. These simulations show, in agreement with our study, that solenoidally driven turbulence leads to larger growth rates of the small-scale dynamo. Waagan et al. [74] find, using a Reynolds number of about 1500[1] and a magnetic Prandtl number of about 1, for totally solenoidal forcing of the turbulence $\bar{\Gamma}^{\mathrm{sol}} = 0.60$ and for totally compressive forcing $\bar{\Gamma}^{\mathrm{comp}} = 0.28$. These values of the growth rate are in comparison with our model (with $Re = 1500$), $\bar{\Gamma}^{\mathrm{sol}} = \bar{\Gamma}^{\vartheta=0.43} \approx 10.07$ and $\bar{\Gamma}^{\mathrm{comp}} = \bar{\Gamma}^{\vartheta=0.47} \approx 4.73$, about a factor of 17 lower. This can be explained by the fact that the simulations have a very low magnetic Prandtl number of about 1. However, our result for the growth rate in Table 8.1 has been derived with the assumption of infinite Prandtl numbers. We have also explored the range of smaller Prandtl numbers. The result is presented in Figures 8.8 for Kolmogorov turbulence and in Figure 8.9 for Burgers turbulence. But with our model, we can make no predictions for Prandtl numbers around unity, because in this range the WKB-approximation is no longer applicable (see Appendix 8.1). However, the trend is that the growth rate decreases for smaller Prandtl numbers, which can explain the lower growth rates from simulations. Yet the ratio of the growth rate of turbulence driven by solenoidal and compressive forcing is in both cases about 2 (our model: $\bar{\Gamma}^{\mathrm{sol}}/\bar{\Gamma}^{\mathrm{comp}} \approx 2.1$, Waagan et al. [74]: $\bar{\Gamma}^{\mathrm{sol}}/\bar{\Gamma}^{\mathrm{comp}} \approx 2.1$), which shows that incompressible turbulence is more efficient in amplifying a magnetic field by the small-scale dynamo.
Furthermore, Federrath et al. [73] have presented a study of the Mach number dependence of the growth rate of the small-scale dynamo, where they compare solenoidal with compressive forcing of the turbulence. They find that, for low Mach numbers, the ratio of the growth rate of turbulence driven by solenoidal and compressive forcing is about 30 (for Mach number $M = 0.1$: $\bar{\Gamma}^{\mathrm{sol}} \approx 1.2$, $\bar{\Gamma}^{\mathrm{comp}} \approx 0.04$). However, for higher Mach numbers their calculations also result in a ratio of $\bar{\Gamma}^{\mathrm{sol}}/\bar{\Gamma}^{\mathrm{comp}} \approx 2$ (for Mach number $M = 10$: $\bar{\Gamma}^{\mathrm{sol}} \approx 0.7$, $\bar{\Gamma}^{\mathrm{comp}} \approx 0.3$), which is in agreement with our results. The lower growth rates in the simulation again may come from low Prandtl numbers in the simulations of order of unity. However, a great uncertainty is the Reynolds number in numerical simulations, which is only a crude estimate.

[1] Waagan et al. [74] give a magnetic Reynolds number of about 200. However, these ideal MHD-simulations were later calibrated with resistive non-ideal MHD-simulations in Reference [73] showing that the Reynolds number is about 1500.

9 Small-Scale Dynamo in Primordial Star Formation

As an application for the amplification of magnetic fields via the small-scale dynamo we consider primordial star formation. We start with a presentation of the most important issues on primordial star formation. Then we estimate the different microscopic and macroscopic properties of primordial gas, like viscosity, magnetic diffusivity and the Reynolds numbers. With these quantities we can determine the growth rate of the small-scale dynamo during primordial star formation, and finally the evolution of the magnetic field strength during the early phase of the collapse.

9.1 Primordial Star Formation

9.1.1 Star Formation in General

Stars form in the interstellar medium within overdense gas clouds [11]. In principle, there are two important forces in a cloud, the gravitational force, which leads to contraction of the cloud, and the pressure, which leads to expansion. In hydrodynamical equilibrium those two forces are equal,

$$\frac{\mathrm{d}p(r)}{\mathrm{d}r} = -G\frac{\rho(r)M(r)}{r^2}, \tag{9.1}$$

where $M(r)$ is the enclosed mass. As soon as the gravitational force is stronger than the pressure force, the cloud becomes unstable and collapses.
The two forces act on different timescales. The pressure changes in the time a sound waves needs to cross the could with a diameter d,

$$T_\mathrm{s} = \frac{d}{c_\mathrm{s}}, \tag{9.2}$$

where c_s is the sound speed. On the other hand, gravity acts on the free-fall time scale, which is

$$T_\mathrm{ff} = \frac{1}{\sqrt{G\rho}}, \tag{9.3}$$

where ρ is the density of the cloud. At a critical diameter of the cloud

$$\boxed{L_\mathrm{J} \equiv \frac{c_\mathrm{s}}{\sqrt{G\rho}}}, \tag{9.4}$$

called the *Jeans length*[1] [75], these two timescales are equal. Now we imagine that the cloud is perturbed and starts contracting. If the timescale of the pressure T_s is larger than the free-fall time, the pressure will not have enough time to compensate and the gravity predominates. Thus, the cloud collapses, if

$$T_\mathrm{s} > T_\mathrm{ff}, \tag{9.5}$$

which means

$$d > L_\mathrm{J}. \tag{9.6}$$

A very important quantity in this context is the *Jeans mass*, which is defined by

$$M_\mathrm{J} \equiv \frac{4\pi}{3}\rho\left(\frac{L_\mathrm{J}}{2}\right)^3. \tag{9.7}$$

Substitution of the Jeans length (9.4) leads to

$$\boxed{M_\mathrm{J} \equiv \frac{\pi}{6}\frac{c_\mathrm{s}^3}{G^{3/2}\rho^{1/2}}}. \tag{9.8}$$

With this definition, a cloud collapses if its mass M is larger than the Jeans mass, i.e.

$$M > M_\mathrm{J}. \tag{9.9}$$

Thus, gravitational collapse happens easiest, if the Jeans mass is small. This is the case for low temperatures, as the sound speed increases with temperature. These are ideal conditions for star formation.
As the equation of state changes from an isothermal to an adiabatic one, the collapse slows down. When the gas reaches a density of about 1 g cm^{-3}, the temperature becomes roughly 10^7 K and nuclear fusion sets in. This provides an additional force acting against gravity and the system gets into equilibrium. In this way a new star is born.
This is of course a very idealised picture. We assumed here a spherical gas cloud with a homogeneous density. External influences like large scale flows and shocks have not been included. Furthermore, we have not taken care of additional physical processes. Rotation and magnetic fields act against the collapse. Also turbulence changes the collapse as it provides an additional pressure.

9.1.2 Primordial Star Formation

The first stars mark an important transition in the Universe. Before their formation, the Universe was homogeneous, rather simple and, except for the cosmic microwave photons, dark. In this section we present the ideas of primordial star formation following mainly the review of Bromm and Larson [76].
At redshifts between 20 and 30 the first stars, also called Population III stars, formed in dark matter halos of a typical mass of 10^6 $\mathrm{M}_\odot$[2]. The main difference

[1] A proper derivation from the hydrodynamical equations leads to $L_\mathrm{J} \equiv \pi c_\mathrm{s}/\sqrt{G\rho}$.
[2] $M_\odot$ is the mass of the Sun, which is about 2×10^{33} g.

to present day star formation is the composition of the gas and related to this the cooling mechanisms. Primordial gas consists of roughly 75% hydrogen and 25% helium in terms of mass fraction. There is no dust, which is the main coolant in present-day star formation. The virial temperature of the dark matter halos is about 1000 K, which excludes cooling by hydrogen lines[3]. At these temperature cooling is possibile via rotational-vibrational transitions of H_2. Thus, the formation of molecular hydrogen is very important. Numerical simulations show that during the collapse of a primordial halo almost all hydrogen is converted to H_2 via different chemical reactions. In primordial star formation H_2 is the most important coolant. For a long time calculations showed that the first stars were extremely massive and no multiple systems formed. For example Abel et al. [77] show in their three-dimensional hydrodynamical simulations that the mass of the first stars was larger than 100 $M_\odot$. Stars of these masses would have lived only for a very short time, before they exploded in an extremely high-energy supernova explosion. On the other side, newer simulations of Clark et al. [78], which follow the evolution of protostellar disks, result in very tight systems of many first stars with lower masses.
The first stars themself produced a negative feedback in the form of soft UV-photons, which destroy the molecular hydrogen via photodissociation. This affects the cooling mechanism. Furthermore, the first stars enriched the gas with heavy elements by supernova explosions. This leads to the transition to Population II stars.
Many questions on primordial star formation remain unanswered. For example the initial mass function is unclear. Furthermore, the effect of magnetic fields has often been neglected.

9.2 Properties of Primordial Gas

9.2.1 Composition of Primordial Gas

Primordial gas at a redshift of about 800 consists mostly of atomic hydrogen, which makes up about 75% of the total mass. Most of this hydrogen is neutral, but roughly 0.25% is singlely ionised. Almost all the remaining mass of the primordial gas, i.e. 25%, is helium. The main helium isotope is ^{4}He, but there is also a small fraction of ^{3}He, while ionised helium plays no role. The primordial gas also includes some deuterium, which has a fraction relative to hydrogen of $D/H \approx 2.5 \times 10^{-3}$. There is also a low fraction of D^+. Besides, there is also a trace of lithium, which makes up a ratio of $Li/H \approx 5 \times 10^{-10}$. Most of the lithium is singly ionised [79].
In the further evolution of the Universe these species produce secondary species due to chemical reactions. We use the chemistry code of Glover and Savin [80] to calculate the abundances of the different species during the collapse of a primordial halo, including a treatment relating the collapse time to the equation of state from Schleicher et al. [81]. The numerical code determines the thermal and chemical evolution of the gas in a one-zone model. The density evolves according to a

[3]The threshold for hydrogen line cooling is roughly 10^4 K.

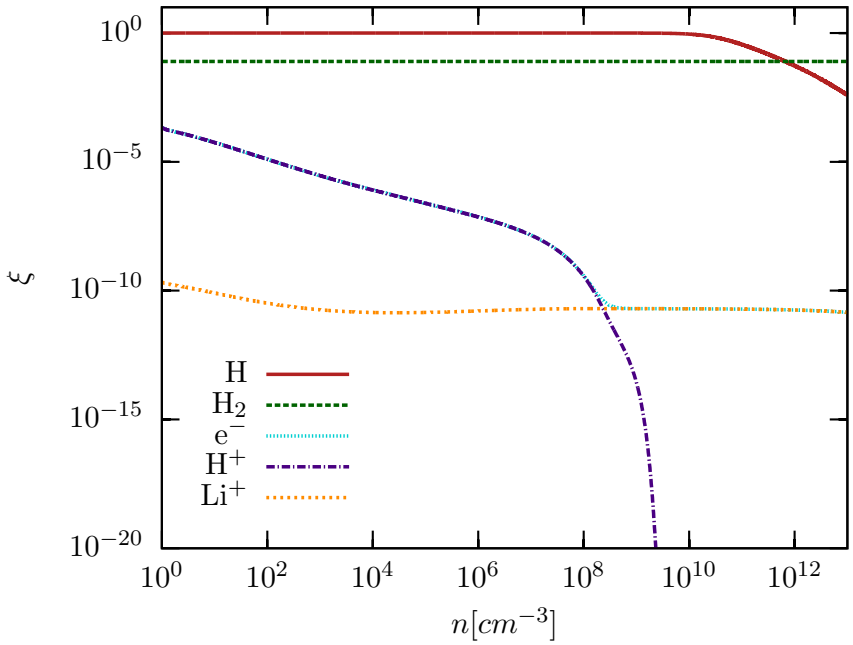

Figure 9.1: The abundances of different chemical species as a function of the density.

free-fall collapse and the temperature is calculated by solving the energy equation. Glover and Savin model the chemistry with a chemical network including around 400 reactions and 30 different atomic and molecular species. They take the full time-dependent non-equilibrium chemistry into account for many species. The initial fractional abundances relative to hydrogen are 0.083 for helium, 2.6×10^{-5} for deuterium and 4.3×10^{-10} for lithium. The initial density is 1 cm^{-3} and the initial temperature 1000 K.

9.2.2 Estimate of Physical Properties

The goal of this section is to estimate different microscopic and macroscopic properties of primordial gas.

Viscosity The kinematic viscosity ν can be estimated as

$$\nu \approx V(\ell_c)L(\ell_c), \tag{9.10}$$

where $V(\ell_c)$ is the typical velocity on the viscous scale ℓ_c and $L(\ell_c)$ the typical length on that scale. For the latter we use the mean free path λ. Thus, we set

$$L(\ell_c) \approx \lambda = \frac{1}{\sigma n}, \tag{9.11}$$

where we insert the geometrical cross section $\sigma \approx \pi d^2$. Here, $d = \sum_i \xi_i d_i$ is the mean particle diameter with the Van-der-Waals diameter d_i of the different species

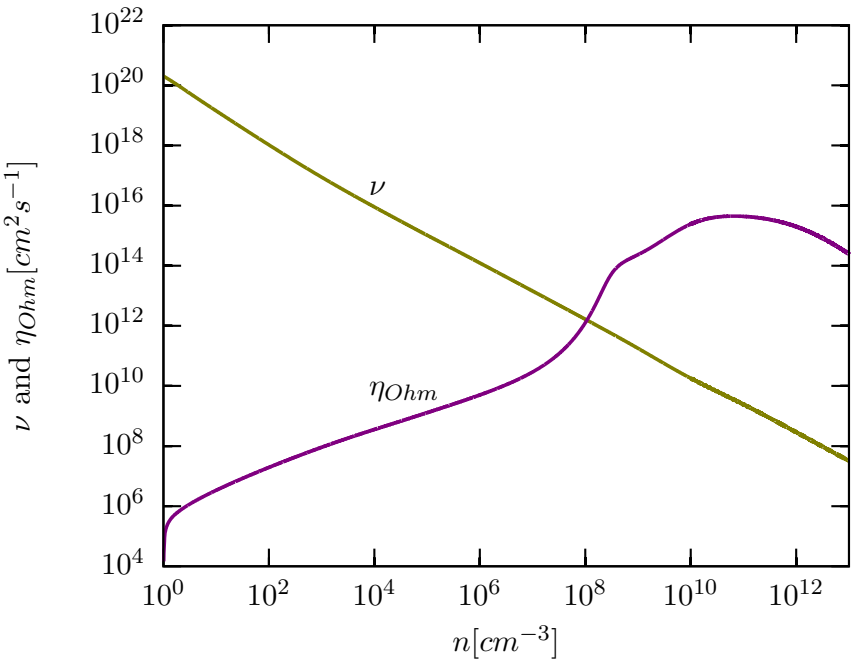

Figure 9.2: The viscosity and the Ohmic diffusivity as a function of the density.

of normalised fraction ξ_i. The typical velocity of the gas on small scales is the thermal velocity $v_{\rm therm}$. With $m/2\ v_{\rm therm}^2 = 3/2\ kT$ we find

$$V(\ell_{\rm c}) \approx v_{\rm therm} = \left(\frac{3kT}{m}\right)^{1/2}. \tag{9.12}$$

Here, k is Boltzmann constant and T the temperature. Moreover, $m = \sum_i \xi_i m_{\rm i}$ is the mean particle mass, with the masses of the different species m_i and the relative abundances ξ_i. The temperature as well as the abundances of the individual species depend on the density. We take these quantities from the chemistry code of Glover and Savin [80]. Thus, we find for the kinematic viscosity

$$\nu = \left(\frac{3kT}{m}\right)^{1/2} \frac{1}{\pi d^2 n}. \tag{9.13}$$

We show the resulting viscosity as a function of the density in Figure (9.2).

Diffusivity For the magnetic diffusivity η we use the Ohmic resistivity $\eta_{\rm Ohm}$ as derived by Pinto et al. [82],

$$\eta_{\rm Ohm} = \frac{c^2}{4\pi\sigma_{||}}. \tag{9.14}$$

The parallel conductivity $\sigma_{||}$ for a neutral species n is calculated by

$$\sigma_{||,n} = \frac{c}{B}\sum_{\rm s} n_{\rm s} q_{\rm s} \beta_{\rm ns}. \tag{9.15}$$

The sum is taken over the different charged species s, which carry the charge q_s. The Hall parameters β_ns are given as

$$\beta_\mathrm{ns} = \frac{q_\mathrm{s} B}{m_\mathrm{s} c} \frac{m_\mathrm{s} + m_\mathrm{n}}{m_\mathrm{n} \xi_\mathrm{n} n \langle \sigma v \rangle_\mathrm{sn}}. \tag{9.16}$$

Here m_n and m_n are the masses of the neutral and the charged particles, ξ_s is the fraction of the species s and $\langle \sigma v \rangle_\mathrm{sn}$ the momentum transfer rate coefficient. We take these coefficients, which are functions of the temperature, from Pinto and Galli [83], where we use the polarisation approximation for Li^+.
We use the most important neutral species H, He and H_2 and the charged species H^+, e^- and Li^+. For each neutral species we calculate the Ohmic resistivity, $\eta_{\mathrm{Ohm},n} = c^2/(4\pi\sigma_{||,n})$. Notice that the final expression does not depend on the magnetic field strength B. Finally, the total Ohmic magnetic diffusivity η_Ohm is

$$\eta_\mathrm{Ohm} = \frac{1}{\sum_n \eta_\mathrm{Ohm,n}^{-1}}. \tag{9.17}$$

Reynolds Numbers The hydrodynamic and magnetic Reynolds numbers are defined as

$$Re \equiv \frac{VL}{\nu} \tag{9.18}$$

$$Rm \equiv \frac{VL}{\eta}, \tag{9.19}$$

where L is the length of the largest turbulent fluctuations and V the typical velocity on that scale.
For the typical velocity of the largest fluctuations we use the sound speed c_s, as the Mach number in a primordial halos is roughly one [84]. With the assumption of ideal gas we get

$$V \approx c_\mathrm{s} = \sqrt{\frac{\gamma k T}{m}}. \tag{9.20}$$

Here γ is the adiabatic index defined as $\gamma = 1 + \mathrm{dlog}T/(\mathrm{dlog}\rho)$, which we take from the chemistry code [80].
We estimate the length of the largest turbulent fluctuations as the Jeans length (9.4), which is the typical length scale of a collapsing cloud, i.e.

$$L \approx \frac{c_\mathrm{s}}{\sqrt{Gmn}}, \tag{9.21}$$

where G is the gravitational constant.
The resulting Reynolds numbers are shown in Figure 9.3 as a function of the density. The critical magnetic Reynolds number, which we derived in Chapter 8, is also indicated for the two extreme types of turbulence.

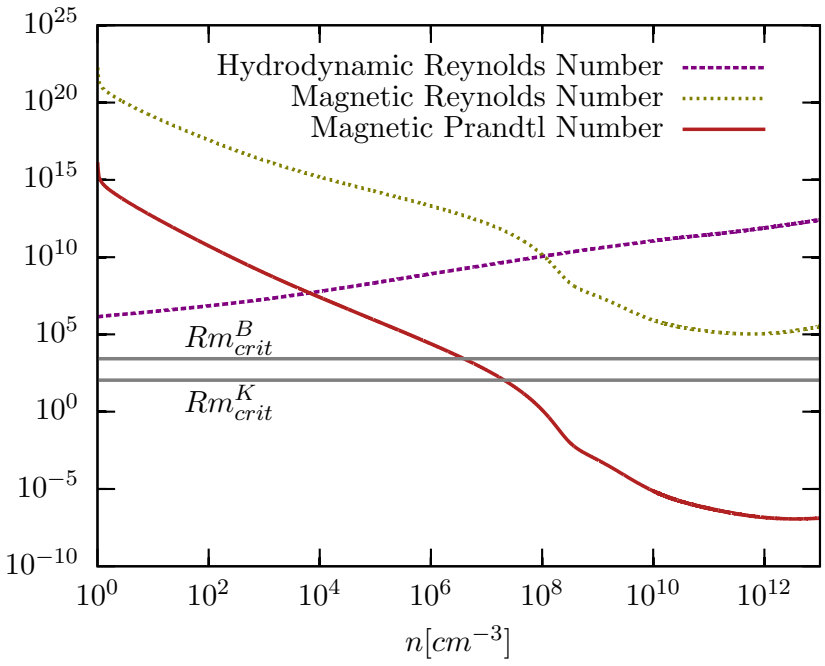

Figure 9.3: The hydrodynamic and magnetic Reynolds numbers as well as the magnetic Prandtl numbers as a function of the density. The two horizontal lines indicate the critical magnetic Reynolds number for Kolmogorov and Burgers turbulence.

Magnetic Prandtl Number The definition of the magnetic Prandtl number is

$$Pm \equiv \frac{Rm}{Re} = \frac{\nu}{\eta}. \tag{9.22}$$

We can calculate this quantity easily by using the equations (9.13) and (9.17). In Figure 9.3 the density dependency of the magnetic Prandtl number is shown.

9.3 The Small-Scale Dynamo in Primordial Star Formation

9.3.1 Validity of our Approximation

In Figure 9.3 the magnetic Prandtl number Pm is shown as a function of the density. During the whole collapse its value changes over 25 orders of magnitude. At the beginning of the collapse $Pm \approx 10^{15}$, which is very high. With increasing density Pm decreases rapidly. We assume the approximation of large magnetic Prandtl numbers to be valid until a particle density of about 10^3 cm^{-3}, when $Pm \approx 10^9$. Compare this to our results in Section 8.1.
This means we can use the formula (8.21) safely to calculate the growth rate of the small-scale dynamo up to densities of roughly 10^3 cm^{-3}. For larger densities the growth rate decreases. However, this decrease is strong only for rather low Pm, depending on the turbulence model and the hydrodynamical Reynolds number (see Figures 8.8 and 8.9).

9.3.2 Small-Scale Dynamo Action during the Collapse

Critical Magnetic Reynolds Number In Section 8.2 we found that the critical magnetic Reynolds number for small-scale dynamo action $Rm_{\rm crit}$ is roughly 110 for Kolmogorov turbulence and 2700 for Burgers turbulence. The dependence of the magnetic Reynolds number on the density is shown in Figure 9.3 together with the two extreme cases of $Rm_{\rm crit}$. We can see that the magnetic Reynolds number is larger than $Rm_{\rm crit}$ for all densities. This means that the small-scales dynamo can operate at all densities, unless, of course, it is already saturated.

Growth Rate of Magnetic Fields With the quantities determined in the last section, we can calculate the growth rate of the small-scale dynamo. We use our result from equation (8.21),

$$\Gamma = \frac{(163 - 304\vartheta)}{60} \frac{V}{L} Re^{(1-\vartheta)/(1+\vartheta)}, \tag{9.23}$$

and analyse the two extreme types of turbulence, Kolmogorov with $\vartheta = 1/3$ and Burgers turbulence with $\vartheta = 1/2$. We find

$$\begin{aligned} \Gamma^{\rm K} &= \frac{37}{36} \frac{V}{L} Re^{1/2}, \\ \Gamma^{\rm B} &= \frac{11}{60} \frac{V}{L} Re^{1/3}. \end{aligned} \tag{9.24}$$

For the typical velocity of the gas V we again use the sound speed $c_{\rm s}$ from equation (9.20) and for the typical length L we use the Jeans length (9.21). Figure 9.4 shows

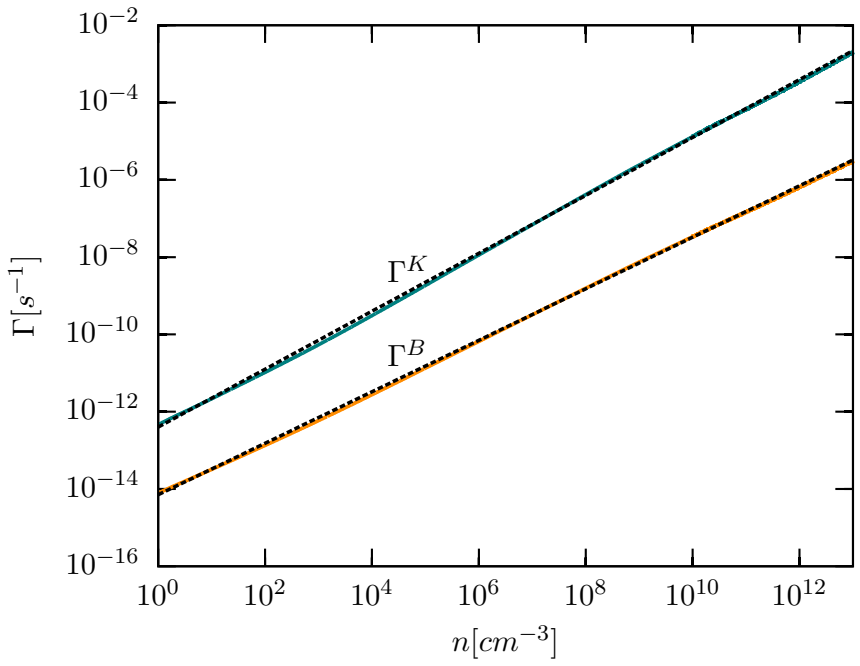

Figure 9.4: The growth rate of the magnetic field for Kolmogorov and Burgers turbulence as a function of the density. The black dashed lines are power-law fits.

the growth rates for the two extreme cases of turbulence as a function of the density. We fit the growth rates with a simple power law

$$\Gamma(n) = a\ n^b, \tag{9.25}$$

where n is in units of cm^{-3}. For Kolmogorov turbulence we find the fit parameters $a^{\mathrm{K}} = 4.00 \times 10^{-13}$ s^{-1} and $b^{\mathrm{K}} = 0.75$. In the case of Burgers turbulence we find $a^{\mathrm{B}} = 7.10 \times 10^{-15}$ s^{-1} and $b^{\mathrm{B}} = 0.67$. We estimate the time scale of the magnetic field amplification by the small-scale dynamo by

$$T_{\mathrm{dynamo}} = \frac{1}{\Gamma} \tag{9.26}$$

and compare it to the free-fall time

$$T_{\mathrm{ff}} = \sqrt{\frac{1}{Gmn}}. \tag{9.27}$$

The result is shown in Figure 9.5. In our model the magnetic field on the fastest growing scale growths one to three orders of magnitude faster than the halo collapses. Note, however, that the dynamo growth is exponential in time. This means that one e-folding in density corresponds to 10 e-foldings in the growth rate for Burgers turbulence, which is roughly 10^4, and 1000 e-foldings for Kolmogorov turbulence, which is roughly 10^{434}!

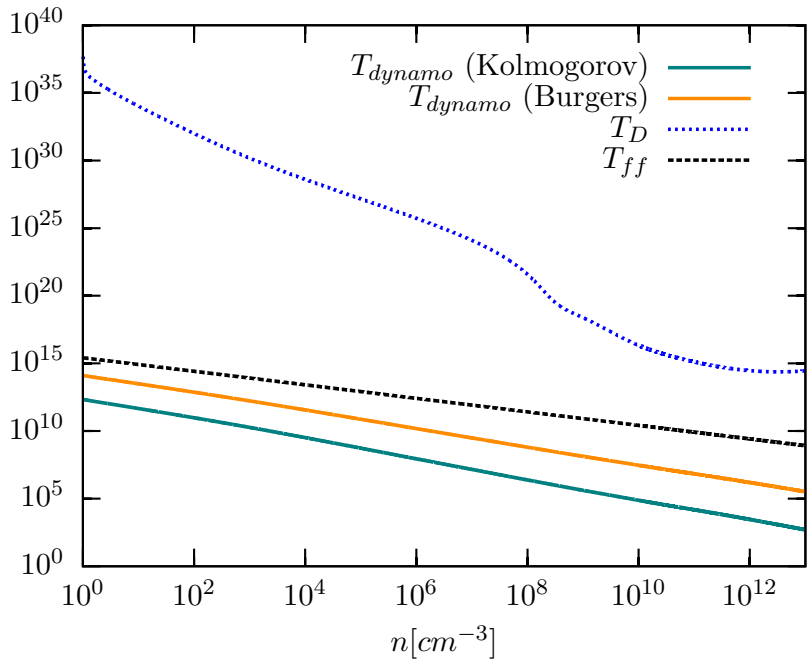

Figure 9.5: Comparison of different timescales. The timescales for dynamo growth is green for Kolmogorov turbulence and orange for Burgers turbulence. The decay timescale of the magnetic energy is blue and the free-fall time black.

Dissipation of Magnetic Energy The magnetic energy can be dissipated again. The dissipation term in the induction equation (5.6) is $\eta_{\rm Ohm}\nabla^2\mathbf{B}$. We approximate this by $\eta_{\rm Ohm}B/L^2$ and $\partial B/\partial t$ by $B/T_{\rm D}$. We then get

$$\begin{aligned} \frac{B}{T_{\rm D}} &\approx \eta_{\rm Ohm}\frac{B}{L^2} \\ \Leftrightarrow \mathrm{T_D} &\approx \frac{L^2}{\eta_{\rm Ohm}}, \end{aligned} \tag{9.28}$$

where $T_{\rm D}$ is the typical timescale for dissipation of magnetic energy and we use the Jeans length for L.
We show the comparison of the dissipation timescale, the free-fall time and the dynamo timescales in Figure 9.5. For low densities the dissipation timescale is many orders of magnitude higher than the other timescales. This means that it has a minor influence on the magnetic field during the collapse. With increasing density the dissipation timescale decreases, but even at a density of 10^{15} cm^{-3} it is still 5 orders of magnitude larger than the free-fall time. This behavior may change if we include besides the Ohmic resistivity also the ambipolar diffusivity.
We define the dissipation rate $D_{\rm Ohm}$ as

$$\mathrm{D_{Ohm}} = \frac{B^2/(8\pi)}{T_{\mathrm{D_{Ohm}}}} \approx \frac{\eta_{\rm Ohm}}{8\pi}\frac{B^2}{L^2}. \tag{9.29}$$

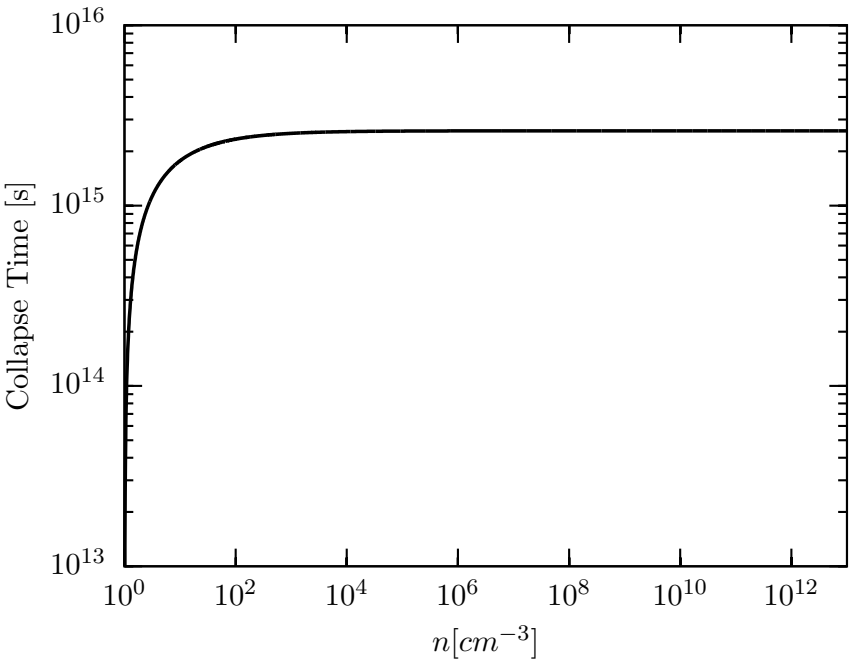

Figure 9.6: The collapse time $t_{\rm coll}$ as a function of the density.

The Resulting Magnetic Field The magnetic field is generated by the small-scale dynamo with a growth rate Γ as we have seen in this section. At the same time a part of the magnetic field decays again with $D_{\rm Ohm}$. Thus, the evolution of the magnetic energy $E_{\rm B} = B^2/(8\pi)$ is described by the differential equation

$$\frac{{\rm d}E_{\rm B}}{{\rm d}t} = \Gamma E_{\rm B} - D_{\rm Ohm}. \tag{9.30}$$

However, the timescale for dissipation is very high, as shown in Figure (9.5). Hence we can neglect $D_{\rm Ohm}$,

$$\frac{{\rm d}E_{\rm B}}{{\rm d}t} = \Gamma E_{\rm B}. \tag{9.31}$$

For the time t we use what we call the "collapse time" from now on,

$$t_{\rm coll} = \frac{1}{\sqrt{Gm_0n_0}} - \frac{1}{\sqrt{Gmn}}. \tag{9.32}$$

This is the time that starts from the beginning of the collapse, when the gas has a density $n_0 = 1$ cm^{-3} and a mean particle mass of $m_0 = 2.2 \times 10^{-24}$ g, to an arbitrary point of the collapse, when the gas has a density n. Figure 9.6 visualises this time. One can see, that the collapse is very slow in the beginning and becomes very fast in the end. The total time of the collapse is roughly 2.6×10^{15} s $= 8.2 \times 10^7$ yr.

With the collapse time we can rewrite equation (9.31) in terms of the density with

$$\frac{\mathrm{d}n}{\mathrm{d}t} = \frac{Gm}{(Gmn)^{3/2}} \tag{9.33}$$

and find

$$\frac{\mathrm{d}E_\mathrm{B}}{\mathrm{d}n} = \frac{Gm}{(Gmn)^{3/2}}\Gamma(n)E_\mathrm{B}. \tag{9.34}$$

For the dependence of the growth rate on the density we use the power-law fit from equation (9.25). Then the solution of equation (9.33) is

$$E_\mathrm{B}(n) = E_{\mathrm{B},0}\,\exp\left(\frac{a}{\sqrt{Gm}(b-1/2)}\left(n^{b-1/2} - n_0^{b-1/2}\right)\right). \tag{9.35}$$

The equation for the evolution of the magnetic field strength is

$$B(n) = B_0\,\exp\left(\frac{a}{2\sqrt{Gm}(b-1/2)}\left(n^{b-1/2} - n_0^{b-1/2}\right)\right), \tag{9.36}$$

with $B(n_0) \equiv B_0$. Equation (9.36) tells us how the magnetic field grows due to small-scale dynamo action. If we include the effect of amplification due to spherical gravitational compression (see Section 6.3.1), we get an additional factor of $(n/n_0)^{2/3}$. In total, the magnetic field strength is

$$\boxed{B(n) = B_0\,\exp\left(\frac{a}{2\sqrt{Gm}(b-1/2)}\left(n^{b-1/2} - n_0^{b-1/2}\right)\right)\cdot\left(\frac{n}{n_0}\right)^{2/3}}. \tag{9.37}$$

A natural upper limit of the magnetic field is given by equipartition with the turbulent kinetic energy. With $B_\mathrm{max}^2/(8\pi) = 1/2\rho V^2$ we find the maximum magnetic field strength

$$B_\mathrm{max} = \sqrt{4\pi\rho V^2}. \tag{9.38}$$

Using the thermal velocity v_therm (9.12) for a typical turbulent velocity, we find

$$\boxed{B_\mathrm{max} = \sqrt{12\pi kT}}. \tag{9.39}$$

As the magnetic field strength can never be larger than the saturation field strength (9.39), we have

$$\boxed{B(n) = \min\left\{B_0\,\exp\left(\frac{a}{2\sqrt{Gm}(b-1/2)}\left(n^{b-1/2} - n_0^{b-1/2}\right)\right)\cdot\left(\frac{n}{n_0}\right)^{2/3}, B_\mathrm{max}\right\}}. \tag{9.40}$$

In Figure 9.7 we show the resulting growth of the field strength. As an initial field strength B_0 we use 10^{-20} G, which is a typical field generated by a Biermann battery. The field strength grows extremely fast with the density during the dynamo growth. For Kolmogorov turbulence the saturation value is obtained already at a density of about 1.08 cm^{-3}. The collapse time at this density is roughly 9.9×10^{13} s $\approx 3.1 \times 10^6$ yr. For Burgers turbulence the dynamo is saturated at roughly 16 cm^{-3}, which refers to a collapse time of roughly 2.0×10^{15} s $\approx 6.2 \times 10^7$ yr.

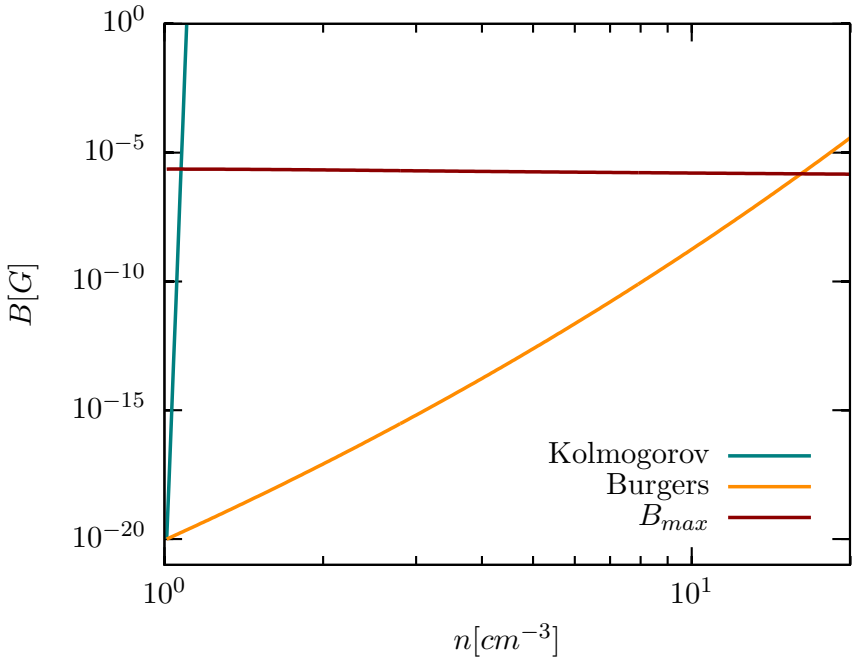

Figure 9.7: The magnetic field strength as a function of the density. The green line is the field generated by the small-scale dynamo with Kolmogorov turbulence, the orange line indicates the field in case of Burgers turbulence. The red line is the maximum magnetic field strength. The total field strength is the minimum of the dynamo generated field and the saturated field.

9.4 Effects of Magnetic Fields in Star Formation

We have seen in this chapter, that there may have been reasonably strong magnetic fields in the primordial gas generated by the small-scale dynamo. These fields could have affected the formation of the first stars in different ways.
An important effect of magnetic fields in star formation is the magnetorotational instability (MRI, see 6.3.2). Maki and Susa [85] find in their simulation of the collapse and the accretion phase of primordial star formation, that the magnetic flux is frozen into the gas during the whole evolution. This is the precondition for the MRI, which takes place in the accretion disk. Silk and Langer [86] explored the MRI in protostellar disks. They find that with magnetic fields, generated by MRI, primordial star formation can take place at any metallicity by regulating angular momentum transfer, fragmentation, accretion and magnetic feedback. Furthermore, they argue that the initial mass function (IMF) is a consequence of magnetic feedback and suggest that the IMF might be closer to the present-day IMF.
Magnetic fields can suppress the fragmentation of a cloud. Hennebelle et al. [87] find in their high resolution MHD-simulations of 100 $M_\odot$ clouds with turbulence and magnetic fields that the fragmentation is reduced by a factor of 1.5 to 2 in comparison to simulations without magnetic fields. Furthermore, they show that the angular momentum in the inner part of the cloud can be reduced by magnetic braking (see also Banerjee and Pudritz [88]). These two effects lead to stars with higher final masses.
In addition the condition of flux freezing leads to the formation of jets. Machida et al. [89] simulate a slowly rotating spherical cloud in an initially uniform weak magnetic field. They find that protostars with masses of 10^{-3} $M_\odot$ formed with a magnetic field strength of 10^6 G. This leads to the formation of jets, which blow off 3-10 % of the total accreting matter. This way the final mass of the stars can be significantly reduced. Moreover, the shocks provided by the jets can change the chemistry in the ISM, which influences the formation of the following generation of stars.
Magnetic fields influence also the final stages of star formation [90]. On the one hand, the fields control the kinematics of the in-falling gas from the circumstellar disk. On the other hand, they launch and collimate outflows of the star. When the magnetic field couples with the disk, the rotational evolution of the star can be influenced strongly. Also planet formation in the disk is sensitive to magnetic fields. Magnetic winds influence the migration of planets and the disk chemistry, which sets the initial conditions for planet formation.

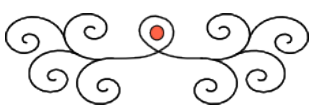

10 Summary and Conclusions

10.1 Summary of our Results

In the first part of this work, we presented an analytical treatment of the small-scale dynamo, using the Kazantsev theory. For this purpose we modelled the correlation function of the turbulent velocity field, depending on the slope of the turbulent velocity spectrum ϑ in $v(\ell) \propto \ell^{\vartheta}$. With this model, we solved the Kazantsev equation in the WKB-approximation and tested the validity of this approximation. We determined the critical magnetic Reynolds number for the small-scale dynamo and its growth rate in the case of infinite and finite magnetic Prandtl numbers.
The main results of our work are:

- The critical magnetic Reynolds number Rm_{crit} for the small-scale dynamo increases as the exponent ϑ increases (see Figure 8.5). For Kolmogorov turbulence ($\vartheta = 1/3$) $Rm^{\mathrm{K}}_{\mathrm{crit}} \approx 110$ and for Burgers turbulence ($\vartheta = 1/2$) $Rm^{\mathrm{B}}_{\mathrm{crit}} \approx 2700$.

- The growth rate of the magnetic field energy in the limit of infinite magnetic Prandtl numbers is

$$\Gamma = \frac{(163 - 304\vartheta)}{60} \, \frac{V}{L} \, Re^{(1-\vartheta)/(1+\vartheta)} \tag{10.1}$$

  (see also Figure 8.7).

- For decreasing magnetic Prandtl number the growth rate decreases. The details of this drop depend on the type of turbulence (see Figures 8.8 and 8.9).

- A validity test shows that the WKB-approximation gives exact solutions in the limit of infinite magnetic Prandtl numbers. The approximation breaks down at a Prandtl number of around unity (see Figures 8.1 and 8.2).

We applied these results to the magnetic fields during primordial star formation. We estimated, based on a detailed chemistry network, typical quantities of primordial gas, like kinematic viscosity and magnetic diffusivity of the gas, and the growth rate of magnetic field. Finally, we determined the magnetic field strength as a function of the density.
We found:

- The magnetic Reynolds number during the collapse always exceeds the critical magnetic Reynolds number for small-scale dynamo action (Figure 9.3).

- The magnetic Prandtl number is very large up to densities of rougly 10^3 cm^{-3} (Figure 9.3).
- The dynamo timescale in primordial star formation is shorter than the free-fall time (Figure 9.5).
- The dissipation timescale of the magnetic field is longer than the free-fall time (Figure 9.5).
- The magnetic field grows very quickly for all types of turbulence. With an initial Biermann field of 10^{-20} G and an initial density of 1 cm^{-3}, the dynamo saturates for Kolmogorov turbulence at a density of 1.08 cm^{-3} and for Burgers turbulence at 16 cm^{-3} (Figure 9.7).

10.2 Implications of this Work

With these results we are able to make predictions about the first magnetic fields in the Universe. We found that, during the collapse of a primordial halo a magnetohydrodynamical dynamo can amplify the magnetic field, at least on small scales, almost instantly up to saturation. For that reason there might already have been high magnetic field strengths even before the formation of the first stars, the first galaxies and the first galaxy clusters.
Turbulence and magnetic fields are key ingredients of current star formation theory [11, 91, 92]. Magnetic fields drive jets and outflows from young stars. Stellar winds and supernova explosions, which end the lives of massive stars, enrich the interstellar medium with heavy elements forged in the stellar interior. These processes are crucial for the chemical composition of the Universe, determining cooling and heating processes in the gas. This, in turn, is very important for the formation of the next generation of stars. The momentum from jets and outflows around accreting protostars may disperse some of the envelope material that otherwise will fall onto the central star. Thus, they are important ingredients for our understanding of the physical origin of the observed distribution of stellar masses [93].

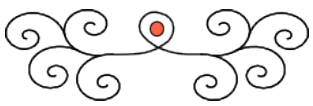

Appendix

A Acknowledgments

Writing this diploma thesis would not have been possible without the help and support of many people.

In the first place I want to thank my supervisor Ralf Klessen, who provided me this highly interesting topic. He came up with many fantastic physical ideas for my work and also let me follow my own interests. Ralf encouraged me to publish my results soon and give talks on them for example on the annual meeting of the "Astronomische Gesellschaft". He also made it possible for me to visit Dominik Schleicher in Leiden and Göttingen. Dominik was one of those who founded this project. As an expert on magnetic fields and the primordial Universe he was a perfect contact person. I am grateful to him for constantly proposing me new ideas and for many discussions about my work. Furthermore, I wish to thank Christoph Federrath. He provided me, always instantly, with detailed corrections of my paper and I could learn a lot from his comments. I am thankful to him for sharing his ideas with me and teaching me many facts about turbulence. In addition, I want to thank Robi Banerjee for his comments on our paper. The application on primordial star formation would not have been possible without the help of Simon Glover. I like to thank him for providing me his chemistry code and the discussions about the results.
In this place let me also thank my colleague Philipp Girichidis, who helped me solving many technical problems I had during writing this thesis. The whole "Arbeitsgruppe Sternentstehung" from the Institut für Theoretische Astrophysik in Heidelberg is to be thanked for supporting me. I am grateful that I can continue my work in this group as a Ph.D. student. Working in this familiar and productive atmosphere really is a joy.

Personally, I owe my deepest gratitude to my boyfriend Nicolai Christiansen, who has been a great help for me during my whole studies. He always stood on my side, which was important especially in the times of exams. As a physicist fellow he also was a scientific help and partner for countless discussions of physical problems. Furthermore, I wish to thank all my fellow students and friends in Heidelberg. Studying and spending free time with them was a pleasure right from the beginning. Moreover, I am thankful to my friends at home.
I want to thank my grandparents, Erika and Paul Hess, who gave me my first telescope at my tenth birthday and by this provided the basic for my passion for astrophysics. Furthermore, I wish to thank my grandmother Johanna Rodemich, my sister Carolin Schober and the rest of my family for their constant support.

Finally, I want to thank my parents, Monika Hess-Schober and Andreas Schober, whom I dedicate this thesis. They supported my interest in science not only during my studies in Heidelberg, but already during my school time. Without their financial and logistical help this work would not have been possible.

Thank you all very much!

Jennifer Schober
Heidelberg, November 2011

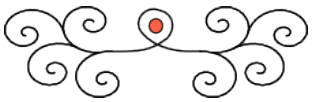

B Tables of Definitions and Constants

cgs-unit	SI-unit	Meaning
1 cm	1 m $= 10^2$ cm	distance
1 s	1 s	time
1 g	1 kg $= 10^3$ g	mass
1 dyn $= 1$ cm g s^{-2}	1 N $= 10^5$ dyn	force
1 erg $= 1$ cm^2 g s^{-2}	1 J $= 10^7$ erg	energy
1 esu $= 1\ \sqrt{\text{erg cm}}$	1 C $= 3.336 \cdot 10^{10} \sqrt{\text{erg cm}}$	electric charge
1 G	1 T $= 10^4$ G	magnetic field strength

Table B.1: Different unit systems: cgs verses SI.

Symbol	Value (cgs-units)	Name
c	2.998×10^{10} cm s^{-1}	speed of light
G	6.673×10^{-8} cm^3 s^{-2} g^{-1}	Gravitational constant
e	$4.803 \times 10^{-10}\ \sqrt{\text{erg cm}}$	elementary charge
k	1.38×10^{-16} erg K^{-1}	Boltzmann constant
m_{u}	1.661×10^{-24} g	atomic mass unit
m_{e}	9.109×10^{-28} g	electron mass
$M_\odot$	1.99×10^{33} g	mass of the Sun
pc	3.086×10^{18} cm	parsec

Table B.2: Table of physical constants.

Name	Definition	Physical Meaning
n		particle density
m		mass
ρ	$\rho = mn$	mass density
μ		dynamic viscosity
ν	$\nu \equiv \frac{\mu}{\rho}$	kinematic viscosity
θ		turbulence index
ω	$\omega = \nabla \times \mathbf{v}$	vorticity
Re	$Re = \frac{VL}{\nu}$	hydrodynamical Reynolds number
T^{ij}	$T_{ij}\delta(t-s) \equiv \langle \delta v_i(\mathbf{x},t)\delta v_j(\mathbf{y},s)\rangle$	correlation function of the turbulent velocity field
T_{L}		longitudinal correlation function of the turbulent velocity field
T_{N}		transversal correlation function of the turbulent velocity field
ℓ_{c}	$\ell_{\mathrm{c}} = L\ Re^{-1/(\vartheta+1)}$	cut-off scale of turbulence
$\mathbf{B}$		magnetic field
$\mathbf{E}$		electric field
$\mathbf{j}$		electric current density
σ		electric conductivity
r		distance coordinate
η	$\eta \equiv \frac{c^2}{4\pi\sigma}$	magnetic diffusivity
Rm	$Rm \equiv \frac{VL}{\eta}$	magnetic Reynolds number
M_{ij}	$M_{ij} \equiv \langle \delta B_i(\mathbf{x},t)\delta B_j(\mathbf{y},t)\rangle$	correlation function of the turbulent magnetic field
M_{L}		longitudinal correlation function of the turbulent magnetic field

M_{N}		transversal correlation function of the turbulent magnetic field
x	$x(r) \equiv \ln(r)$	distance coordinate
y	$y(r) \equiv \dfrac{r}{L}$	distance coordinate
z	$z(r) \equiv \left(\dfrac{Re^{3/2}Pm}{3L^2}\right)^{1/2} r$	distance coordinate
$\psi(r)$	$M_{\mathrm{L}} \equiv \dfrac{1}{r^2\sqrt{\kappa_{\mathrm{diff}}}}\psi(r)\mathrm{e}^{2\Gamma t}$	eigenfunction of the Kazantsev equation
$\theta(x)$	$\psi(x) \equiv \mathrm{e}^{x/2}\theta(x)$	eigenfunction of the Kazantsev equation
$p(x)$	$p(x) \equiv -\dfrac{(\Gamma + U(x))\mathrm{e}^{2x}}{\kappa_{\mathrm{diff}}(x)} - \dfrac{1}{4}$	"p-function" (in Kazantsev equation)
Γ		growth rate
$\bar{\Gamma}$	$\bar{\Gamma} \equiv \dfrac{L}{V} \cdot \Gamma$	normalised growth rate
κ_{diff}		diffusion coeffient
U		"potential" in Kazantsev equation
c_{s}		sound speed
T_{ff}	$T_{\mathrm{ff}} \equiv (G\rho)^{-1/2}$	free-fall time
L_{J}	$L_{\mathrm{J}} \equiv \dfrac{c_{\mathrm{s}}}{\sqrt{G\rho}}$	Jeans length
M_{J}	$M_{\mathrm{J}} \equiv \dfrac{4}{3}\pi\left(\dfrac{L_{\mathrm{J}}}{2}\right)^3$	Jeans mass
η_{Ohm}		Ohmic diffusivity
T_{dynamo}	$T_{\mathrm{dynamo}} \equiv \Gamma^{-1}$	dynamo timescale
t_{coll}	$t_{\mathrm{coll}} \equiv T_{\mathrm{ff}}(n_0) - T_{\mathrm{ff}}(n)$	collapse time

Table B.3: Table of frequently used definitions.

C Lists

C.1 List of Figures

C.2 List of Tables

D Bibliography

[1] E. N. Parker. *Cosmical magnetic fields: Their origin and their activity*. Oxford, Clarendon Press; New York, Oxford University Press, 1979.

[2] J. H. Piddington. On the origin and structure of stellar magnetic fields. *Astrophys. & Sp. Sci.*, 90:217–230, February 1983.

[3] S. Mereghetti. The strongest cosmic magnets: soft gamma-ray repeaters and anomalous X-ray pulsars. *Astron. & Astrophys. Rev.*, 15:225–287, July 2008.

[4] W. D. Cotton, B. S. Mason, S. R. Dicker, P. M. Korngut, M. J. Devlin, J. Aquirre, D. J. Benford, S. H. Moseley, J. G. Staguhn, K. D. Irwin, and P. Ade. 90 GHz Observations of M87 and Hydra A. *Astrophys. J.*, 701:1872–1879, August 2009.

[5] R. Beck. Galactic and Extragalactic Magnetic Fields. *Space Science Rev.*, 99:243–260, October 2001.

[6] T. H. Greif, S. D. M. White, R. S. Klessen, and V. Springel. The Delay of Population III Star Formation by Supersonic Streaming Velocities. *Astrophys. J.*, 736:147, August 2011.

[7] A. R. Choudhuri. *The Physics of Fluids and Plasmas: An Introduction for Astrophysicists*. Cambrigde University Press, December 1998.

[8] G. I. Taylor. Statistical Theory of Turbulence. *Royal Society of London Proceedings Series A*, 151:421–444, September 1935.

[9] George K. Batchelor. *The theory of homogeneous turbulence*. Cambridge monographs on mechanics and applied mathematics. Cambridge University Press, Cambridge, 1953.

[10] A. Kolmogorov. The Local Structure of Turbulence in Incompressible Viscous Fluid for Very Large Reynolds' Numbers. *Akademiia Nauk SSSR Doklady*, 30:301–305, 1941.

[11] Mordecai-Mark Mac Low and Ralf S. Klessen. Control of star formation by supersonic turbulence. *Rev. Mod. Phys.*, 76(1):125–194, Jan 2004.

[12] J.M. Burgers. *A Mathematical Model Illustrating the Theory of Turbulence*, volume 1 of *Advances in Applied Mechanics*. Elsevier, 1948.

[13] W. Schmidt, C. Federrath, M. Hupp, S. Kern, and J. C. Niemeyer. Numerical simulations of compressively driven interstellar turbulence. I. Isothermal gas. *Astron. & Astrophys.*, 494:127–145, January 2009.

[14] S. I. Vainshtein. A theory for small-scale magnetic fields. *Zhurnal Eksperimental noi i Teoreticheskoi Fiziki*, 83:161–175, July 1982.

[15] K. Subramanian. Dynamics of fluctuating magnetic fields in turbulent dynamos incorporating ambipolar drifts. *ArXiv Astrophysics e-prints*, August 1997. arXiv:astro-ph/9708216.

[16] E. A. Spiegel. A Generalization of the Mixing-Length Theory of Turbulent Convection. *Astrophys. J.*, 138:216, July 1963.

[17] R. B. Larson. Turbulence and star formation in molecular clouds. *Mon. Not. R. Astron. Soc.*, 194:809–826, March 1981.

[18] C. Federrath, J. Roman-Duval, R. S. Klessen, W. Schmidt, and M.-M. Mac Low. Comparing the statistics of interstellar turbulence in simulations and observations. Solenoidal versus compressive turbulence forcing. *Astron. & Astrophys.*, 512:A81, March 2010.

[19] M. Korpi, A. Brandenburg, and I. Touminen. Driving Galactic Turbulence by Supernova Explosions. *Studia geoph. et deod.*, 42:410–418, 1998.

[20] R. S. Klessen and P. Hennebelle. Accretion-driven turbulence as universal process: galaxies, molecular clouds, and protostellar disks. *Astron. & Astrophys.*, 520:A17+, September 2010.

[21] C. Federrath, S. Sur, D. R. G. Schleicher, R. Banerjee, and R. S. Klessen. A New Jeans Resolution Criterion for (M)HD Simulations of Self-gravitating Gas: Application to Magnetic Field Amplification by Gravity-driven Turbulence. *Astrophys. J.*, 731:62, April 2011.

[22] M. R. Krumholz and C. F. McKee. A General Theory of Turbulence-regulated Star Formation, from Spirals to Ultraluminous Infrared Galaxies. *Astrophys. J.*, 630:250–268, September 2005.

[23] J. D. Jackson. *Classical Electrodynamics*. John Wiley & Sons, 1962.

[24] H. Alvén. *Ark. f. Mat. Astro. o. Fysik*, 1942.

[25] R. Beck, A. Brandenburg, D. Moss, A. Shukurov, and D. Sokoloff. Galactic Magnetism: Recent Developments and Perspectives. *Ann. Rev. Astron. Astrophys.*, 34:155–206, 1996.

[26] R. Beck. Magnetic Fields in Galaxies. *Space Science Rev.*, page 135, May 2011.

[27] C. G. T. Haslam, W. E. Wilson, D. A. Graham, and G. C. Hunt. A further 408 MHz survey of the northern sky. *Astron. and Astrophys. Sup.*, 13:359, March 1974.

[28] K. Beuermann, G. Kanbach, and E. M. Berkhuijsen. Radio structure of the Galaxy - Thick disk and thin disk at 408 MHz. *Astron. & Astrophys.*, 153:17–34, December 1985.

[29] A. Neronov and I. Vovk. Evidence for Strong Extragalactic Magnetic Fields from Fermi Observations of TeV Blazars. *Science*, 328:73–, April 2010.

[30] F. Tavecchio, G. Ghisellini, L. Foschini, G. Bonnoli, G. Ghirlanda, and P. Coppi. The intergalactic magnetic field constrained by Fermi/Large Area Telescope observations of the TeV blazar 1ES0229+200. *Mon. Not. R. Astron. Soc.*, 406:L70–L74, July 2010.

[31] A. M. Taylor, I. Vovk, and A. Neronov. Extragalactic magnetic fields constraints from simultaneous GeV-TeV observations of blazars. *Astron. & Astrophys.*, 529:A144+, May 2011.

[32] A. Fletcher, R. Beck, A. Shukurov, E. M. Berkhuijsen, and C. Horellou. Magnetic fields and spiral arms in the galaxy M51. *Mon. Not. R. Astron. Soc.*, 412:2396–2416, April 2011.

[33] D. G. Yamazaki, K. Ichiki, T. Kajino, and G. J. Mathews. Constraints on the Evolution of the Primordial Magnetic Field from the Small-Scale Cosmic Microwave Background Angular Anisotropy. *Astrophys. J.*, 646:719–729, August 2006.

[34] D. Grasso and H. R. Rubinstein. Revisiting nucleosynthesis constraints on primordial magnetic fields. *Physics Letters B*, 379:73–79, February 1996.

[35] D. R. G. Schleicher and F. Miniati. Primordial magnetic field constraints from the end of reionization. *ArXiv e-prints*, August 2011.

[36] D. R. G. Schleicher, D. Galli, S. C. O. Glover, R. Banerjee, F. Palla, R. Schneider, and R. S. Klessen. The Influence of Magnetic Fields on the Thermodynamics of Primordial Star Formation. *Astrophys. J.*, 703:1096–1106, September 2009.

[37] P. P. Kronberg, M. L. Bernet, F. Miniati, S. J. Lilly, M. B. Short, and D. M. Higdon. A Global Probe of Cosmic Magnetic Fields to High Redshifts. *Astrophys. J.*, 676:70–79, March 2008.

[38] M. L. Bernet, F. Miniati, S. J. Lilly, P. P. Kronberg, and M. Dessauges-Zavadsky. Strong magnetic fields in normal galaxies at high redshift. *Nature*, 454:302–304, July 2008.

[39] Michael S. Turner and Lawrence M. Widrow. Inflation-produced, large-scale magnetic fields. *Phys. Rev. D*, 37(10):2743–2754, May 1988.

[40] G. Sigl, A. V. Olinto, and K. Jedamzik. Primordial magnetic fields from cosmological first order phase transitions. *Phys. Rev. D*, 55:4582–4590, April 1997.

[41] F. Miniati and A. R. Bell. Resistive Magnetic Field Generation at Cosmic Dawn. *Astrophys. J.*, 729:73, March 2011.

[42] L. Spitzer. *Physics of Fully Ionized Gases*. Interscience, 1956.

[43] L. Biermann. Über den Ursprung der Magnetfelder auf Sternen und im interstellaren Raum (mit einem Anhang von A. Schlüter). *Zeitschrift Naturforschung Teil A*, 5:65, 1950.

[44] R. M. Kulsrud and E. G. Zweibel. On the origin of cosmic magnetic fields. *Reports on Progress in Physics*, 71(4):046901, April 2008.

[45] A. G. G. M. Tielens. *The Physics and Chemistry of the Interstellar Medium*. Cambridge University Press, September 2005.

[46] H. Xu, B. W. O'Shea, D. C. Collins, M. L. Norman, H. Li, and S. Li. The Biermann Battery in Cosmological MHD Simulations of Population III Star Formation. *Astrophys. J. Lett.*, 688:L57–L60, December 2008.

[47] R. Schlickeiser and P. K. Shukla. Cosmological Magnetic Field Generation by the Weibel Instability. *Astrophys. J. Lett.*, 599:L57–L60, December 2003.

[48] P. K. Shukla, N. Shukla, and L. Stenflo. Generation of magnetic fields by the ponderomotive force of electromagnetic waves in dense plasmas. *Journal of Plasma Physics*, 76:25, 2010.

[49] D. A. Frank-Kamenezki. *Vorlesungen über Plasmaphysik*. Verlag deutscher Wissenschaften, 1967.

[50] E. P. Velikhov. Stability of an Ideally Conducting Liquid Flowing Between Cylinders Rotating in a Magnetic Field. *Soviet Physics JETP*, 1959.

[51] S. Chandrasekhar. The Stability of Non-Dissipative Couette Flow in Hydromagnetics. *Proceedings of the National Academy of Science*, 46:253–257, February 1960.

[52] J. E. Pringle. Accretion discs in astrophysics. *Ann. Rev. Astron. Astrophys.*, 19:137–162, 1981.

[53] S. A. Balbus and J. F. Hawley. A powerful local shear instability in weakly magnetized disks. I - Linear analysis. II - Nonlinear evolution. *Astrophys. J.*, 376:214–233, July 1991.

[54] G. E. Hale. On the Probable Existence of a Magnetic Field in Sun-Spots. *Astrophys. J.*, 28:315, November 1908.

[55] G. E. Hale, F. Ellerman, S. B. Nicholson, and A. H. Joy. The Magnetic Polarity of Sun-Spots. *Astrophys. J.*, 49:153, April 1919.

[56] E. W. Maunder. Note on the distribution of sun-spots in heliographic latitude, 1874-1902. *Mon. Not. R. Astron. Soc.*, 64:747–761, June 1904.

[57] E. N. Parker. The Formation of Sunspots from the Solar Toroidal Field. *Astrophys. J.*, 121:491, March 1955.

[58] E. N. Parker. Hydromagnetic Dynamo Models. *Astrophys. J.*, 122:293, September 1955.

[59] M. Steenbeck, F. Krause, and K.-H. Rädler. Berechnung der mittleren Lorentz-Feldstärke für ein elektrisch leitendes Medium in turbulenter, durch Coriolis-Kräfte beeinflußter Bewegung. *Zeitschrift Naturforschung Teil A*, 21:369, April 1966.

[60] J. Love. Reversals and excursions of the geodynamo. *Astronomy and Geophysics*, 40:14, December 1999.

[61] A. Brandenburg and K. Subramanian. Astrophysical magnetic fields and nonlinear dynamo theory. *Phys. Rep.*, 417:1–209, October 2005.

[62] Stephen Childress and Andrew D. Gilbert. *Stretch, twist, fold: the fast dynamo*. Number 37 in Lecture notes in physics : New series m, monographs ; 37 ; Lecture notes in physics / New series M. Springer, Berlin ; Heidelberg [u.a.], 1995. Literaturverz. S. 381 - 396.

[63] A. P. Kazantsev. Enhancement of a Magnetic Field by a Conducting Fluid. *Soviet Journal of Experimental and Theoretical Physics*, 26:1031, May 1968.

[64] H. A. Kramers. Wellenmechanik und halbzahlige Quantisierung. *Zeitschrift für Physik*, 39:828–840, October 1926.

[65] L. Mestel and K. Subramanian. Galactic dynamos and density wave theory. *Mon. Not. R. Astron. Soc.*, 248:677–687, February 1991.

[66] J. Schober, D. Schleicher, C. Federrath, R. S. Klessen, and R. Banerjee. Amplification of Magnetic Fields by Small-Scale Dynamo Action: Dependence on Turbulence Models, Reynolds and Prandtl Numbers. *in prep.*, 2011.

[67] Zhen-Su She and Emmanuel Leveque. Universal scaling laws in fully developed turbulence. *Phys. Rev. Lett.*, 72(3):336–339, Jan 1994.

[68] S. Boldyrev, Å. Nordlund, and P. Padoan. Scaling Relations of Supersonic Turbulence in Star-forming Molecular Clouds. *Astrophys. J.*, 573:678–684, July 2002.

[69] V. Ossenkopf and M.-M. Mac Low. Turbulent velocity structure in molecular clouds. *Astron. & Astrophys.*, 390:307–326, July 2002.

[70] N. E. Haugen, A. Brandenburg, and W. Dobler. Simulations of nonhelical hydromagnetic turbulence. *Phys. Rev. E*, 70(1):016308, July 2004.

[71] Roberto Benzi, Luca Biferale, Robert T. Fisher, Leo P. Kadanoff, Donald Q. Lamb, and Federico Toschi. Intermittency and Universality in Fully Developed Inviscid and Weakly Compressible Turbulent Flows. *Phys. Rev. Lett.*, 100:234503, Jun 2008.

[72] S. Sur, D. R. G. Schleicher, R. Banerjee, C. Federrath, and R. S. Klessen. The Generation of Strong Magnetic Fields During the Formation of the First Stars. *Astrophys. J. Lett.*, 721:L134–L138, October 2010.

[73] C. Federrath, G. Chabrier, J. Schober, R. Banerjee, R. S. Klessen, and D. R. G. Schleicher. Mach Number Dependence of Turbulent Magnetic Field Amplification: Solenoidal versus Compressive Flows. *Phys. Rev. Lett.*, 107:114504, Sep 2011.

[74] K. Waagan, C. Federrath, and C. Klingenberg. A robust numerical scheme for highly compressible magnetohydrodynamics: Nonlinear stability, implementation and tests. *Journal of Computational Physics*, 230:3331–3351, May 2011.

[75] J. H. Jeans. The Stability of a Spherical Nebula. *Royal Society of London Philosophical Transactions Series A*, 199:1–53, 1902.

[76] V. Bromm and R. B. Larson. The First Stars. *Ann. Rev. Astron. Astrophys.*, 42:79–118, September 2004.

[77] T. Abel, G. L. Bryan, and M. L. Norman. The Formation of the First Star in the Universe. *Science*, 295:93–98, January 2002.

[78] P. C. Clark, S. C. O. Glover, R. J. Smith, T. H. Greif, R. S. Klessen, and V. Bromm. The Formation and Fragmentation of Disks Around Primordial Protostars. *Science*, 331:1040–, February 2011.

[79] S. Glover. The Chemistry of the Early Universe. In *IAU Symposium*, volume 280 of *IAU Symposium*, May 2011.

[80] S. C. O. Glover and D. W. Savin. Is H^+_3 cooling ever important in primordial gas? *Mon. Not. R. Astron. Soc.*, 393:911–948, March 2009.

[81] D. R. G. Schleicher, D. Galli, S. C. O. Glover, R. Banerjee, F. Palla, R. Schneider, and R. S. Klessen. The Influence of Magnetic Fields on the Thermodynamics of Primordial Star Formation. *Astrophys. J.*, 703:1096–1106, September 2009.

[82] C. Pinto, D. Galli, and F. Bacciotti. Three-fluid plasmas in star formation. I. Magneto-hydrodynamic equations. *Astron. & Astrophys.*, 484:1–15, June 2008.

[83] C. Pinto and D. Galli. Three-fluid plasmas in star formation. II. Momentum transfer rate coefficients. *Astron. & Astrophys.*, 492:1–1, December 2008.

[84] T. H. Greif, J. L. Johnson, R. S. Klessen, and V. Bromm. The first galaxies: assembly, cooling and the onset of turbulence. *Mon. Not. R. Astron. Soc.*, 387:1021–1036, July 2008.

[85] H. Maki and H. Susa. Dissipation of Magnetic Flux in Primordial Star Formation: From Run-away Phase to Mass-Accretion Phase. *Pub. of the Astron. Soc. of Japan*, 59:787–797, August 2007.

[86] J. Silk and M. Langer. On the first generation of stars. *Mon. Not. R. Astron. Soc.*, 371:444–450, September 2006.

[87] P. Hennebelle, B. Commerçon, M. Joos, R. S. Klessen, M. Krumholz, J. C. Tan, and R. Teyssier. Collapse, outflows and fragmentation of massive, turbulent and magnetized prestellar barotropic cores. *Astron. & Astrophys.*, 528:A72, April 2011.

[88] R. Banerjee and R. E. Pudritz. Massive Star Formation via High Accretion Rates and Early Disk-driven Outflows. *Astrophys. J.*, 660:479–488, May 2007.

[89] M. N. Machida, K. Omukai, T. Matsumoto, and S.-i. Inutsuka. The First Jets in the Universe: Protostellar Jets from the First Stars. *Astrophys. J. Lett.*, 647:L1–L4, August 2006.

[90] S. G. Gregory, M. Jardine, C. G. Gray, and J.-F. Donati. The magnetic fields of forming solar-like stars. *Reports on Progress in Physics*, 73(12):126901, December 2010.

[91] C. F. McKee and E. C. Ostriker. Theory of Star Formation. *Ann. Rev. Astron. Astrophys.*, 45:565–687, September 2007.

[92] B. G. Elmegreen and J. Scalo. Interstellar Turbulence I: Observations and Processes. *Ann. Rev. Astron. Astrophys.*, 42:211–273, September 2004.

[93] G. Chabrier. Galactic Stellar and Substellar Initial Mass Function. *Pub. Astron. Soc. Pac.*, 115:763–795, July 2003.

Erklärung:

Ich versichere, dass ich diese Arbeit selbstständig verfasst habe und keine anderen als die angegebenen Quellen und Hilfsmittel benutzt habe.

Heidelberg, den 24.11.2011 .....